Characterization of two new mouse models of neurodegenerative diseases

Francesca Achilli

Department of Neurodegenerative Disease,

Institute of Neurology, Queen Square,

London WC1N 3BG, UK

Submitted to the University of London

in fulfilment of the requirements of the PhD Degree

August 2007

ProQuest LLC
789 East Eisenhower Parkway
P.O. Box 1346
Ann Arbor, MI 48106-1346

Abstract

The aim of this study was to phenotypically and genotypically characterize two new neurological mouse mutants arising from the Harwell ENU Mutagenesis Programme.

GENA 201 and 202 mice are siblings. Heterozygous mice show poor grip strength and have a dominantly inherited phenotype. Homozygotes show compromised hind limb movement resulting in a more severe phenotype. Histopathology data from 15 days old GENA201 and 202 homozygotes showed a significantly reduced dorsal column in thoracic spinal cord sections.

To identify the mutant gene underlying the GENA201 and 202 phenotypes, mutant backcross progeny were genotyped with a panel of markers spanning the genome. Both GENA 201 and 202 mutations were localised to a 5Mb region on chromosome 6 suggesting they are allelic. A point mutation (T>C transition in exon 5) was identified in the glycyl tRNA synthetase gene in both mouse lines, which charges tRNA with glycine.

Glycyl tRNA synthetase mutations have been identified in two hereditary motor and sensory neuropathies, Charcot Marie Tooth 2D and distal spinal muscular atrophy type V, thus the gene plays a role in neurological diseases. GENA 201 and 202 mutants are therefore interesting animal models that could provide new insights in the understanding of new biological pathways involved in hereditary motor and sensory neuropathies.

To investigate the possible functional impact of the mutation, a protein assay was carried out. No loss of glycyl tRNA activity was observed by comparing *Gar* $^{C201R/+}$ with wild type littermates. However, a reduction in activity was observed in *Gar* $^{C201R/C201R}$ mice compared to wild type and *Gar* $^{C201R/+}$ littermates suggesting that the possible molecular mechanisms of pathology for the Gars^{C201R} mutation might be some loss of function.

In addition to GENA 201 and 202 lines, the BHV7 mouse line was also characterised. BHV7 heterozygote mice are significantly lighter than wild types and show an ataxic gait with retropulsion. Histopathology data from 6 month old BHV7 mutant mouse brain also revealed cerebellar defects characterized by loss of Purkinje cells.
BHV7 is of potential interest for the study of ataxia. Genotyping of BHV7 mutants localised the mutation to a 26 Mb interval on chromosome 3.

The two mutations are valuable additions to the scientific community and may be useful in the better understanding of the genetic basis of neurodegenerative diseases.

Dedicato ai miei genitori, Lorenzo e Antonia Achilli, per il grandissimo ruolo che hanno avuto nell'aiutarmi a diventare chi sono oggi. Il loro costante amore e incoraggiamento, mi ha permesso di rischiare nella vita, di volare alto ed esplorare i miei limiti, sempre consapevole del fatto che loro sarebbero stati pronti ad aiutarmi e supportarmi.

Dedicated to my parents, Lorenzo and Antonia Achilli.Their constant love has allowed me to take risks in life, to aim high and to explore my limits, sure of the fact that they would always be there to support me and encourage me.

Acknowledgements

This work would not have been possible without the contributions of several people to whom I am deeply grateful. I would like to thank my supervisor Prof. Elizabeth Fisher for her guidance and constructive criticism throughout this project. My sincere thanks to Dr Pat Nolan who always gave me valuable advice to help solve various problems I encountered and to Prof Jo Martin for the many hours spent helping me interpret various results and explaining anatomy and histology.

I am also grateful to Hazel Williams for the important role she played in the optimization of the aminoacylation assay, to Carole Nickols and Graham McPhail at the Royal London Hospital for the helping me in the preparation of various tissues for histological analysis, to Zuzanna Tymowska-Lalanne and Debra Brooker for teaching me how to perform genome scans an sequencing, to Sara Wells and Rachel Kendall and the many animal technicians who were involved in the maintenance of healthy mouse colonies, cage changes and weaning of litters over the last three years.

I would also like to express my appreciation to all my friends and rest of the family for their encouragement and for being always there. Thank you to the Fisher's lab for the constant support: Gaia, Ruth, Marie, Paresh and Simon you always showed me a way out when I was lost. Thank you!

Finally, many thank to the Motor Disease Association for funding the study and giving me the great opportunity to carry out a project of this nature.

Contents **Page**

List of tables **Page**

List of figures **Page**

List of Appendices **Page**

Abbreviations used in the text

DAB	3,3'-diaminobenzidine
A	adenine
ABC	avidin and biotinylated horseradish peroxidase complex
ATP	adenosine tri-phosphate
Bp	base pairs
BCA	bicinchoninic acid
C	cytosine
cAMP	cyclic adenosine monophosphate
cDNA	complementary DNA
Chr	chromosome
cM	centimorgan
DMSO	dimethyl sulfoxide
DNA	deoxyribonucleic acid
dNTP	deoxyribonucleoside triphosphate
DTT	dithiothreitol
EDTA	ethylenediaminetetraacetic acid
EMMA	European Mouse Mutant Archive
ENU	*N*-ethyl-*N*-nitrosourea
F1	first generation
Fig	figure
G	guanine
G2	second generation
hr	hour
IMMC	International Mouse Mutagenesis Consortium
IVF	*in vitro* fertilization
kb	kilobases
kDa	KiloDaltons
M	molar
Mb	megabases
MgAc	magnesium acetate
Min	minutes
MIT	Massachusetts Institute of Technology

MRC	Medical Research Council
mRNA	messenger RNA
ng	nanogram
nm	nanometer
NTPs	nucleoside triphosphates
PBS	phosphate buffered saline
PCR	polymerase chain reaction
Pi	inorganic phosphate
PPi	inorganic pyrophosphate
Rcf	relative centrifugal force
RNA	ribonucleic acid
RNAse	ribonuclease
Rpm	revolution per minute
SD	standard deviation
SDS	sodium dodecyl sulphate
Sec	seconds
T	thymidine
TBE	tris/borate/EDTA
TBS	tris-buffered saline
TCA	trichloric acid
µM	micromolar
µl	microlitre
Vol	volume
WR	working reagent

1. Chapter 1: Introduction

1.1 Mouse genetics

1.1.1 A brief history

The domestication of mice dates back to classical times. During the 19th century, mice were selectively bred for unusual (fancy) traits in China and Japan (Sage 1981). At the beginning of the 20th century, Miss Abbie Lapthrop, an experimental mouse breeder, began to supply stocks of "fancy" mice to the research laboratories of William Castle and Leo Loeb at the University of Pennsylvania (Morse 1978). William Castle soon realized the potential advantage of genetically homogenous inbred lines of mice to demonstrate the genetic basis of diseases. In 1909, Clarence Cook Little, founder of the Roscoe B. Jackson Memorial Laboratory in Bar Harbor (Maine, USA) began to breed the first inbred line which resulted in the DBA strains.

A wide variety of inbred lines were soon developed which played a crucial role in all areas of biomedical and genetic research because they allowed scientists to perform experiments on the same genetic material and to compare their results. Over 450 inbred strains are available today (Beck et al. 2000). Early experiments in mouse genetics did not only confirm the dominant and recessive inheritance pattern expected from Mendel's laws but also explained phenomena such as epistatic interactions between unlinked genes, the existence of more than two alleles per locus and recessive lethal alleles (Silver 1995). In addition, the most significant medical advances, including insights in the immune system and cancer, can be directly attributed to inbred mouse strains (Festing & Fisher 2000).

Oak Ridge Laboratory in Tennessee, the Medical Research Council Radiobiology Unit at Harwell in Oxfordshire and the Jackson Laboratory in Maine soon became the world leader laboratories in mouse genetics.

The research programs in Harwell and Oak Ridge were set up following the Second World War to study the effect of radiation on mice as a model for understanding the effect of nuclear radiation on humans. Researchers realised the potential of mutagenised mice to study gene function in mammals and mouse mutagenesis programs were soon established culminating in the development in mid-1980s of the ultimate tool of genetic engineering known as targeted mutagenesis which combines embryonic stem cell culture and homologous recombination technologies (Capecchi 1989; Smithies 1993).

1.1.2 The human and mouse genomes

The human genome was published in 2001 (Lander et al. 2001; Venter et al. 2001). The implications of such an achievement in biological science, which included the prospect of functionally understanding all our genes and unravelling the genetic code of our species, were enormous and promised to revolutionise medical science and the way we see ourselves.

The human genome consists of an estimated 3.2 billion base pairs which code for 30,000 genes. It was soon realised that comparative genomics would help to understand the functions and interactions of human genes in biology and disease (Boguski 2002). The mouse was one of the five experimental organisms (*Escherichia coli, Saccharomyces cerevisiae*, *Caenorhabditis elegans* and *Drosophila melanogaster*) anticipated to offer useful insight for such an aim.

In 1999 the Wellcome Trust, Sanger Institute, the Whitehead Center for Genome Research and the Washington University Sequencing Center, collectively known as the "Mouse Genome Sequencing Consortium" initiated the first concerted effort to sequence the mouse genome (Waterston et al. 2002). A physical map of the mouse genome was published in August 2002 (Gregory et al. 2002) followed shortly by a

high-quality draft sequence and analysis of the genome of the C57BL/6J mouse in December 2002 (Waterston et al. 2002). The mouse genome is about 14% smaller than the human genome, consisting of ~ 2.5 billion base pairs estimated to code for less that 30,000 genes (Waterston et al. 2002). 40% of the human and mouse genomes can be directly aligned at the nucleotide level. 99% of mouse genes have a homologue in the human genome. For 96% the homologue lies within a similar conserved syntenic interval in the human genome (Waterston et al. 2002). The encoded proteins are thought to have a median amino acid identity of 78.5% (Boguski 2002) which reflects the relatively recent divergence of mice and humans (75 million years ago) (Paigen 1995).

Despite valuable similarities between mice and humans, several differences need to be considered. Mice have 20 pairs of chromosomes whereas humans have 23 pairs. Most mice chromosomes are acrocentric whereas in humans chromosomes are metacentric (except the five acrocentric chromosomes encoding rRNAs).
Due to evolutionary gene duplication and loss, variation in the number of genes in certain gene families and occasional differences in gene distribution, organization and expression have occurred (Waterston et al. 2002). For example, the mouse genome is 14% smaller than the human genome and the difference probably relates to the high rate of deletion in the mouse lineage.

Since the two species diverged, the neutral substitution rate has been roughly half a nucleotide per site, with about twice as many of these substitutions having occurred in the mouse compared to human.

Dozens of local gene family expansions have occurred in the mouse lineage compared to humans. Most of these seem to involve genes related to reproduction, immunity and olfaction, suggesting that these physiological systems have been under positive selection in rodents, which drives rapid evolution. An illustrative example is the expansion of four subfamilies of cytochrome P450 (CYP) genes in mice compared

with humans. These genes encode enzymes that function in drug metabolism, and biologically are part of a 'sensory system' for chemical compounds in the environment. In the pharmaceutical industry, one stage of drug development includes studies of the absorption, distribution, metabolism, excretion and toxicology of drug candidates. Mice and humans have been exposed to different types and amounts of environmental substances (including toxins) during their evolutionary divergence, and one might expect natural selection to have altered the numbers and activities of these enzymes in the two species (Boguski 2002). Indeed, humans and rodents do often have different responses to drugs and other chemicals.

Despite such differences, mice and humans are still ten times more closely related than either of them is to flies or nematodes (Silver 1995) which makes the mapping of the mouse a more valuable resource than mapping other model organisms.

1.1.3 Mouse models of human disease

The study of spontaneous and induced mutations in mice has been central to our current understanding of genetic diseases (Cox & Brown 2003). Mouse mutants are suitable for modelling human disease conditions because they have a similar genetic makeup to humans. The products of orthologous genes are generally involved in the same physiological and cell biological pathways.

In addition the advantages of using mice in medical research are several. Mice are small and easy to maintain. They are sociable and thrive in the environment of controlled matings. Complex breeding programmes can be arranged to establish recombinant inbred strains and congenic strains because they can breed so easily (Silver 1995). Mice can breed from about 2 months of age, have a short gestation time, generate large litters (between 5 and 10 pups depending on strain) and

have a short lifespan (up to 2 years) (Fisher 1997). Our ability to manipulate their genetic makeup through transgenic technology and gene targeting make the mouse a powerful tool in studies of gene function and expression (Meisler 1996). Finally, the short gestation time and life-span of mice facilitates studies monitoring the effect of transmitting a pathogenic mutation through several generations (Fisher 1997).

1.1.4 Role of mice in the post genomic era

The use of the mouse in the post-genomic era has shifted to the study of gene function and expression. The International Mouse Mutagenesis Consortium (IMMC) aims to produce a least one heritable mutation in every gene in the mouse genome in an attempt to identify every gene that affects key traits of biomedical interest (Nadeau et al. 2001). The growing mouse mutant archive is a valuable resource for the identification of novel genes underlying various human diseases (Brown & Hardisty 2003).

The European Mouse Mutant Archive (EMMA) aims to collect, archive and distribute European mouse mutant strains that are essential for basic biomedical research (www.emma.rm.cnr.it). A vast collection of mutant mice identified on various mutagenesis programs are already available to the scientific community (see for example www.mgu.har.mrc.ac.uk; www.jax.org, www.gsf.de, www.gsf.riken.go.jp).

EUMORPHIA is an integrated research programme aiming to develop and standardise approached in mouse phenotyping techniques, mutagenesis and informatics. The program began in 2002 and has already improved characterization of mouse models for the understanding of human disease and allows for better comparison of

results between various research institutions across Europe (www.eumorphia.org).

1.2 Mutations and mice: ENU mutagenesis

1.2.1 The mutagenic action and success of ENU

The laboratory synthesised compound *N*-ethyl-*N*-nitrosourea (ENU) (Fig 1.1) was first used in the mouse in the late seventies when it was demonstrated to be one of the most powerful mutagens in the mouse (Russell et al. 1979). The chemical acts directly by alkylation of nucleic acids and predominantly causes point mutations (Shibuya & Morimoto 1993).

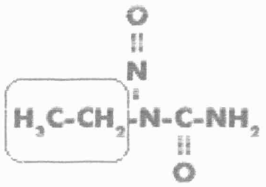

Fig 1.1 Molecular structure of *N*-ethlyl-*N*-nitrosourea (ENU) with its transferable ethyl group underlined in red.

The ethyl group of ENU can be transferred to oxygen or nitrogen radicals at a number of reactive sites. The transferred ethyl groups do not constitute a mutation. Their presence, however, can result in mistaken identity of the ethylated base during replication that results in mismatching (Noveroske et al. 2000) .

ENU preferentially modifies A/T base pairs and its action is estimated to involve 44% A/T to T/A transversions, 38% A/T to G/C transitions, 8% G/C to A/T transitions, 3% G/C to C/G transversions, 5% A/T to C/G

transitions and 2% G/C to T/A transitions (Justice et al. 1999). Its main targets are the spermatogonial stem cells, from which mature sperm are derived.

Hitotsumachi *et al* (Hitotsumachi et al. 1985) found that a dose of 400mg ENU/kilogram body weight to (101 X C3H) F1 males delivered a mutation rate of 1.5 X 10^{-3} per locus / gamete. They also found that multiple administrations of lower doses of ENU increase the mutagenic effectiveness of ENU while maintaining survival and fertility. Although, ENU mutagenesis can give rise to offspring carrying more than one point mutation, phenotypic traits which can be isolated through backcrossing of affected offspring, are likely to be the consequence of a single point mutation (Nolan et al. 2002).

Manipulation of mammalian genes by ENU mutagenesis has proved to be very useful in accelerating our understanding of gene function. For example, the circadian rhythm gene clock (King et al. 1997; Vitaterna et al. 1994) was identified in an ENU mutagenesis screen and has proved important to understand the molecular basis of biological rhythm. Recently, Godinho et al. 2007 by screening N-ethyl-N-nitrosourea-mutagenized animals for alterations in rhythms of wheel-running activity, identified a mouse mutation, after hours (Afh). The mutation, a Cys (358) Ser substitution in *Fbxl3*, an F-box protein with leucine-rich repeats, results in long free-running rhythms of about 27 hours in homozygotes. Circadian transcriptional and translational oscillations are attenuated in Afh mice, suggesting a central and new role for Fbxl3 in mammalian circadian timekeeping (Godinho et al. 2007).

Successful examples of the potential of ENU in associating abnormal phenotypes with previously uncharacterised genes include mutations in dynein which have been associated with motor neuron degeneration (Hafezparast et al. 2003), a mutation in *Af4,* a gene previously implicated in leukaemogenesis, results in a cerebellar ataxia with associated cerebellar purkinje cell degeneration (Isaacs et al. 2003). In addition, a

recent ENU screen has identified a novel function of the transcription factor Evi1 in the genetic predisposition to Otitis media (Parkinson et al. 2006). Furthermore, ENU mutagenesis was used to successfully identify a mouse with low plasma alkaline phosphatase (ALP) activity, identified by a clinical chemistry screen. These mice provide for the first time animal model of late onset hypophosphatasia (HPP) that will be valuable in future functional studies and for the evaluation of therapies such as those aimed at HPP (Hough et al. 2007).

In addition, ENU point mutations can potentially display a range of mutant effects including dominant negative, gain of function, complete loss-of-function and partial loss-of-function that mouse null mutations would not necessarily display as they would only relay information about the most severe phenotypes (Justice et al. 1999). Allelic mutation of a gene of interest can convey information about regions of the gene involved in regulation of its expression as well as functionally important domains of the proteins it codes for. For example, three peripheral myelin protein 22 (pmp22) mouse mutant lines, named tr-m1H, tr-m2H and tr-m3H, provide an allelic series of mutants on a common genetic background for gene function analysis (Isaacs et al. 2000; Isaacs et al. 2002). Mutations in PMP22 in humans are associated with many peripheral neuropathies. Comparison of the phenotype of each mutant line using behavioural and pathological assessment allowed the mutants to be clearly distinguished in terms of severity of disease, which in turn can be correlated with a unique pattern of PMP22 intracellular localization.

Finally, ENU mutagenesis can provide a useful complement to other techniques of genetic manipulation, such as transgenesis and gene targeting.

1.2.2 Phenotypic and genotypic driven ENU mutagenesis screens

ENU mutagenesis is primarily based on phenotype-driven approach due to its potential to associate abnormal phenotypes with previously uncharacterized genes. Phenotype-based screens make no assumption about the nature of the genes that cause a specific phenotype. They employ appropriate screens on mutagenised animals to identify mice with a phenotype of interest.

There are several approaches to generate ENU mutant mice depending on whether one is interested in acquiring new recessive or dominant phenotypes. The most complex genetic strategies are associated with the recovery of recessive mutations. Recessive genome-wide screens involve three generation crosses. However, recessive screens can be targeted to recover recessive mutations in particular regions of the genome covered by deletions or inversions. These screens can involve only two generations of crosses and have the added advantage that the identified mutations are already pre-localised to defined regions of the genome in which candidate gene searches can immediately begin. Published figures indicate that up to 30% of lines from a three generation recessive screen will carry heritable mutant phenotypes (Herron et al. 2002).

Screens for dominant genome-wide mutations are simple a very efficient mode for generating new mutant phenotypes. Mutagenised males are crossed and the progeny are immediately entered into the appropriate phenotype screen. Published figures for major dominant genome-wide screens underway over the last few years, indicate that up to 2% of progeny carry a heritable mutant phenotype (Hrabe de Angelis et al. 2000; Nolan et al. 2000).

Lastly, ENU can be used to undertake sensitised or modifier screens. In sensitised screens, mutagenised males are mated to mice carrying mutations in specific genes that may sensitise the mice while not necessarily generating an overt phenotype. The aim is to identify mutations that interact to generate the relevant phenotype and thus help to elaborate a genetic pathway. For modifier screens, mutagenised males are mated to mice carrying mutations (possibly transgenic or knock-out in origin) that demonstrate an overt phenotype that may be expected to be amenable to enhancement or suppression. Again the purpose is to identify modifying genetic loci that interact with the mutation. These strategies have exciting potential for the elaboration of the genetic pathways involved with disease (Brown & Hardisty 2003).

Following the isolation of such animals, test breeding is used to confirm the genetic nature of the trait. Genetic and molecular tools of positional cloning are then used to isolate and identify the mutated gene. The power of phenotype-driven mutagenesis lies in the possibility of screening for any phenotype for which an assay can be developed. This can include for example blood-based abnormalities, neurological, developmental and immunological defects.

Via the dominant screens, a large number of new deafness mutations were identified and the phenotypes characterised and the underlying genes cloned (Parkinson & Brown 2002). Importantly, many of the new mutations mapped to regions of the mouse genome where deafness phenotypes had not previously been reported indicating that they represented novel disease phenotypes. A large number of mutants were identified that affect the development or patterning of the hair cells in the inner ear. A number of the mutants have been cloned including the Slalom (Tsai et al. 2001) and Headturner (Kiernan et al. 2001) mutants that show an aberrant organisation of hair cells in the inner ear as well as abnormalities of the semi-circular canals in the vestibular apparatus. Both mutants are encoded by the *Jag1* ligand, identifying a novel function for the Jagged1 signalling molecule in the patterning of the inner

ear. *JAG1* mutants in humans result in Alagille syndrome that presents with a number of features including semi-circular canal abnormalities

A major screen has been undertaken for new models of ocular disease (Thaung et al. 2002). Utilising slit-lamp observation and indirect ophthalmoscopy, a large number of new anterior segment and retinal phenotypes were recovered. Eighteen new dominant inherited phenotypes were recovered. Mapping indicated that eight of these represented novel mutant phenotypes. Four novel mutants were identified that demonstrate phenotypes similar to a number of human syndromes with dilated pupils or iris dysgenesis. For two of these human syndromes, Axenfeld–Rieger Anomaly, AXA (an iridogoniodysgenesis anomaly) and the related Rieger syndrome, the genes have been cloned—*FOXC1* and *PITX2*, respectively. However, there are a number of iris dysplasia or hypoplasia diseases in the human population for which the genetic basis is still unknown, and these new mutants can be expected to shed light on the genetic pathways involved (Brown & Hardisty 2003).

The screen also uncovered a number of additional alleles of known genetic loci, particularly the PAX6 locus which causes aniridia in humans (Thaung et al. 2002). Three new missense alleles were recovered, one of which alters a conserved argenine in the paired-box domain known to be involved with DNA binding. An identical mutation has been found in humans, but intriguingly, these patients have a mild phenotype with no anterior segment defects in contrast to the mouse (Oda et al. 1997).

Several ENU screens have focused on the identification of new recessive lethal phenotypes representing defects at various stages of development. One recent recessive screen focused on identifying abnormalities in organogenesis at embryonic day 18.5 (Herron et al. 2002). Many of these mutations might be expected to survive to term and thus represent potential models of human birth defects. Fifteen mutants were identified from the analysis of 54 lines and the mapping

and complementation testing of several of these lines indicated that they represented novel phenotypes. Several of these novel mutant phenotypes indicated that they may be potential new models for human malformation syndromes. For example, the *shorty* mutation that demonstrates abnormal ribs, vertebrae and post-natal lethality may represent a model of Jeune asphyxiating thoracic dystrophy (Brown & Hardisty 2003).

Genotype-driven approaches involve screening for mutations in a known gene of interest. This requires the establishment of a DNA archive obtained from the progeny of ENU mutagenised mice. As ENU introduces point mutations this approach has the potential to deliver allelic mutation representative of the full range of functional mutations (Cox & Brown 2003). A successful example of such approach was the identification of mutations in the gene (*Gjb2*) encoding connexin 26, using archives established from the UK ENU mutagenesis program (Coghill et al. 2002).

1.2.3 ENU mutagenesis programmes

Various research centres across the world have invested in large-scale mouse ENU mutagenesis programmes which specialize in different area of research.

The MRC Harwell, UK, concentrates on diseases such as diabetes, neurological / neurobehavioral and bone disorders (http://www.har.mrc.ac.uk/).

The Institute of Mammalian Genetics, Neuherberg, Germany, aims to elucidate questions related to development and homeostasis (http://www.gsf.de/ieg/).

The Jackson Laboratory, Bar Harbour, Maine, USA, leads research in six major areas which include cancers (bone, cervical, leukaemia, liver, lymphoma, mammary, ovarian), development and aging-related: birth defects (Down syndrome, osteoporosis), immune system and blood disorders (AIDS, anemia, autoimmunity, immune system disorders, tissue transplant rejection), metabolic diseases (atherosclerosis, diabetes, gallstones, hypertension, obesity) and neurological and sensory disorders (blindness, cerebellar disorders, deafness, epilepsy, glaucoma, macular degeneration, neurodegenerative diseases) (http://www.jax.org/).

The Centre for Modelling Human Disease, Toronto, Canada, has developed a range of sophisticated phenotyping tools which provide an invaluable resource in the characterization of mutants in areas of diabetes, hematology, bone mineralization, cardiovascular and renal function, behaviour, learning and memory, and embryonic development (http://www.cmhd.ca/).

The Riken Institute, Yokohama City, Japan aims to establish specific mutant line to research auto-immune or allergic disease model animals (http://www.riken.go.jp/engn/index.html).

The Baylor College of Medicine, Houston, Texas, USA is producing new mutants to represent models of human diseases such as birth defects, patterning defects, growth and endocrine defects, neurological anomalies, and blood defects (www.bcm.edu/).

The Medical Genome Centre, Australia's research focuses on infectious diseases, cancer, diabetes, autoimmune disease and mental illness, with a major interest being the immune system (http://www.acrf.com.au/page/medical_genome_centre_australian_national_university.html).

1.3 The Harwell ENU mouse mutagenesis programme

The ENU mutagenesis program at MRC Harwell started as a consortium set up between the MRC Harwell Mammalian Genetics Unit, SmithKline Beecham Pharmaceuticals (now GlaxoSmithKline Pharmaceuticals), Imperial College London and Queen Mary and Westifield College London (now Queen Mary University College London) (www.mgu.har.mc.ac.uk/mutabase).

The programme consists of large genome-wide screen for dominant mutations. ENU-treated BALB/cAnN males are mated with wild type C3H/HeH females and the F1 progeny undergoes intensive phenotyping.

DNA from the F1 progeny is collected for archiving that allows the confirmation of mutations cloned in the backcross offspring. In addition, sperm samples are also collected from all the F1 males that allows for rederivation of male mutants identified by the phenotyping screen via *in vitro* fertilization (IVF) (Thornton et al. 1999). The DNA and sperm archives are also available for detection of the additional mutants via the genotype-driven approach. Selected cohorts of mice are aged and retested at age 6 months or 1 year in an attempt to identify late–onset phenotypes.

1.3.1 Phenotype analysis

1.3.1.1 Visual screen

All F1 litters are screened for visible anomalies at birth and weaning (3 weeks). Mice are then marked with ear punches for identification and housed in groups of up to 5 per cage.

At 5 weeks of age mice are subject to the SHIRPA protocol (Rogers et al 1997;wwww.mgu.har.ac.uk/mutabase/shirpa) which consists of a battery

of 40 semi-quantitative tests based on earlier screens developed by Irwin (Irwin 1968) to classify the various effects of drugs on wild type animals.

The SHIRPA screen can indicate deficits in muscle and lower motor neuron, spinocerebellar, sensory, neuropsychiatric and autonomic function. This approach mimics the diagnostic process of general, neurological and psychiatric examination in humans. The standardized protocol involves three stages, the first two give a detailed general phenotype assessment, and the tertiary stage provides a specialised screen primarily tailored to neurological deficits (Rogers et al. 1997).

The primary screen provides a behavioural and functional profile by observational assessment of mice. This test will indicate defects in gait or posture, motor control and co-ordination, changes in excitability and aggression, salivation, lacrimation, piloerection, defaecation, muscle tone and temperature. It also provides a gross measure of analgesia. All parameters are scored to provide a quantitative assessment which enables comparison of results both over time and between different laboratories.

The secondary screen involves a comprehensive behavioural and functional screening battery and pathological analysis. This includes measurement of spontaneous locomotor activity in the horizontal and vertical planes, and during these tests, food and water intake is also monitored. Tests of motor performance are carried out to confirm and quantify effects observed in the behavioural profile. Balance and co-ordination is quantified with an accelerating rota-rod which measures the ability of the mice to remain on a rotating drum (Jones & Roberts 1968). The effects on the perception of pain are measured with the mouse hot plate test (O'Callaghan & Holtzman 1975), a well established test of nociception.

In addition, histopathological analysis of animals is carried out, and biochemical studies to measure serum urea, electrolyte and blood glucose levels are performed to identify major metabolic deficits. These tests are carried out in conjunction with mass spectroscopic analysis of dried blood spot samples to screen for amino acid and intermediate metabolism defects.

The tertiary screening stage concentrates on the analysis of neurological mutants and is suitable for the assessment of existing or potential models of neurological disease, as well as the assessment of phenotypic variability which may be the result of known or uncharacterised genetic influences (Rogers et al. 1997).

1.3.1.2 Behavioural and neurological screening

At 6 weeks of age the F1 mice are subject to behavioural screens. Several tests are used to identify different phenotypes. Locomotor activity is assessed using the open field to identify potential models of anxiety disorder and abnormally high activity levels. The open field is the most standardized general measure of spontaneous activity and locomotor abnormalities are seen in many mutants. Measurement of locomotor activity, for example, gives data regarding the integrated function of cortical arousal, cerebral locomotor control, and neuromuscular function. This test can be taken alone as a coarse functional indicator, but when it forms part of a screening panel including tests of motor strength and neural control, such as grip strength and limb tone, it helps to define specific deficits. Thus it may become apparent that a poor performance in locomotor activity tests reflects a muscular weakness in the absence of central nervous system dysfunction.
For example, mutations in SNAP-25 (synaptosomal-associated protein-25 KDa) cause an extreme hyperactive behaviour in the *coloboma* mouse (Hess et al. 1992) and hyperactivity is seen in the *weaver* mouse, which displays dopamine deficiency (Schmidt et al. 1982).

The rotarod test measures balance and motor coordination in rodents. Rotarod deficits characterized in R6/2 mice helped to establish R6/2 mice as a model of Hungtinton disease (Carter et al. 1999).

Deficits in motor neuron function are assessed by using grip strength and wire manoeuvre, which measure neuromuscular function by sensing the amount of force an animal applies in grasping either on a pull bar or on a metal wire. Null mutant mice deficient in calbindin D28k, a calcium binding protein expressed in the dopaminergic nigrostiatal pathway, show poor grip strength (Airaksinen et al. 1997) and knockout mice deficient in fibroblast growth factor receptor-3 (FGFR-3), a receptor expressed at high levels in cartilage and mediator of bone ossification, have major motor deficits on the wire manoeuvre.

Acoustic startle responses and prepulse inhibition of acoustic startle response (PPI) are a neurophysiological and behavioural measure of sensorimoter gating (Swerdlow et al. 2006). Assessment of acoustic startle responses and PPI are used to detect further behavioural disorders such as schizophrenia (Swerdlow et al. 1990).

Learning and memory models use the Morris water maze (Morris 1981) in which mice have to locate a submerged platform using distal cues.

This comprehensive assessment is complemented by electromyography, electroencephalography, nerve conduction and magnetic resonance imaging techniques which employ well established methods in the analysis of structural and functional abnormalities of the nervous system.

Additional screens to identify neurological and neuromuscular mutants, vision mutants, deafness and vestibular mutants, motor mutants, hair loss mutants, ethanol preference mutants and connective tissue mutants have also been carried out. Cohorts of females aged to 6 months and males aged to 1 year have also been screened in an attempt to identify late onset phenotypes.

1.3.2 Inheritance testing

Once an abnormal phenotype is identified, the mutant is backcrossed to C3H/HeH strain. 20 backcross 1 (G2) progeny are then assessed for the abnormality at the same age that the parent F1 animal was found to be abnormal. If the phenotype is dominantly inherited, then 50% of the backcross progeny should also express the phenotype. If the classification of certain phenotypes becomes difficult in mice backcrossed to the C3H strain, mice are backcrossed to C57BL/6 strains. The prefix "GENA" followed by a breeding lines number is assigned to selected lines with heritable phenotypes which are then subject to genetic mapping.

1.3.3 Positional cloning of mouse genes

1.3.3.1 Genetic mapping

Once DNA is extracted from the tails of affected mice, a rapid mapping strategy is employed to determine a low resolution mapping position. Briefly, equimolar samples of DNA from 13 affected offspring are genotyped with 72 biotinylated single nucleotide polymorphisms (SNPs) that span the mouse genome with an average spacing of 20-40 Mb. The selected markers are polymorphic between the BALB/c and C3H backgrounds strains.

Once an area of linkage has been identified, the region of interest can be narrowed down by genotyping the individual mutants for additional markers that lie within the critical region. Known genes within this region can then be considered for mutation detection or sequencing.

Alternatively, additional backcrossing may be needed to refine the map position. The larger the number of backcross progeny is, the smaller the minimal interval in which the gene responsible of the mutant phenotype

has to be located. With ~50 backcross mice, it is possible to map a mutation to a specific chromosome and locate the affected gene to an interval of 10cM to 20cM (Silver 1995). However, with 500-1000 backcross mice, the critical region can be narrowed to 1 cM interval. With about 2000 kb in 1 cM and 1 gene every 50 to 100kb, this may reduce the number of candidate genes to less than 100.

In vitro fertilization is used to speed up the production of backcrossed progeny alleviating the pressure of time and animal space. Sperm from the epididymides of mice is obtained and then used as either frozen or fresh to produce hundreds of offsprings in a single *in vitro* experiment (Glenister & Thornton 2000; Marschall et al. 1999).

1.3.3.2 Identification of candidate genes

Once the minimal interval of a mutation is established, the available mouse genome sequence can be scanned for any genes located in the interval. On the basis of expression data, human conserved synteny and known function, a list of candidate genes can be established. Although any gene in minimal interval initially qualifies as a candidate, the addition of further genetic, genomic, or biochemical data can be very useful to the prioritization of potential candidate genes (Balling 2001).

1.3.3.3 The success of the Harwell ENU mutagenesis programme

Aproximally 35,000 F1 progeny have been generated in 2002 and screened and 700 new mouse mutant lines with stably inherited single-gene dominant or semi dominant mutations have been identified (Nolan et al. 2000).To date more that 80 mutants have been mapped to within a 20cM region. The number of mutants identified by each part of the screen is summarized in Table 1.1.

	Number screened	Number of phenotypes	Observed phenotype rate	Number inheritance tested	Inherited mutation	Not inherited	Unknown
Growth	28,600	334	1 in 85	133	31	64	38
Pigment	28,600	140	1 in 204	41	21	14	6
Skin/hair	28,600	70	1 in 409	21	10	5	6
Tail	28,600	43	1 in 665	9	4	3	2
Cranifacial	28,600	148	1 in 193	37	12	17	8
Digits/limbs	28,600	24	1 in 1,192	14	3	8	3
Neurological/ behavioural	15,000	526	1 in 28	139	56	52	31
Clinical chemistry	2255	58	1 in 39	42	15	23	4
Vestibular	28,600	54	1 in 530	20	15	3	2
Deafness	15,000	28	1 in 536	14	6	2	6
Eye/vision	6,500	51	1 in 74	51	25	23	3

Table 1.1 Summary of the mutants identified in each screen (Nolan et al. 2002).

1.4 Neurological mouse mutants

1.4.1 Peripheral mouse mutants

Disorders of the peripheral nerves can be classified in terms of the component of the peripheral nervous system that is primarily affected. Neuropathies consist of conditions in which there is loss of neuron that contribute axons to the peripheral nerves. Axonopathies are characterized by the axonal degeneration but neuronal cell bodies survive. Conditions that affect the Schwann cells or myelin lead to a demyelinating neuropathy. Demyelination may also be a consequence of axonal disease (Thomas et al. 1996).

Charcot Marie Tooth (CMT) diseases are the most common genetic disorders of the peripheral nervous system (PNS) and have been

estimated to affect up to 1 in 2,500 people (Skre 1974).These heterogeneous neurodegenerative diseases display muscle weakness and distal muscle atrophy, impaired sensation and other features (Thomas et al. 1996). The CMTs are divided into two clinical types: type 1 patients have decreased motor nerve conductance velocity (MNCV) with demyelinating axons whereas type 2 patients have normal MNCV, no demyelination but show decreased amplitudes of evoked motor and sensory nerve responses (Antonellis et al. 2003).

Although many CMT genes still await discovery, to date 24 human mutations are known to cause CMT. Several CMT animal models have been created covering various CMT loci and have expanded our knowledge about protein function and the CMT disease mechanism (Robertson 2005; Sereda & Nave 2006).

Mutations in peripheral myelin protein 22kDa (*PMP22*) and myelin protein zero (*MPZ*) have been most intensively studied. The most common mutation causing CMT is a 1.4Mb duplication of human chromosome 17p12–p11.2 (subtype CMT1A) which encodes the *PMP22* gene (Szigeti et al. 2006). CMT1A patients exhibit approximately 1.7-fold PMP22 mRNA overexpression by Schwann cells (Yoshikawa et al. 1994), a peripheral demyelination, and secondary axon loss (Suter & Scherer 2003).

The transgenic mouse line (heterozygous C61) with a two fold *Pmp22* overexpression has been generated using yeast artificial chromosomes (Huxley et al. 1998). Phenotype analyses revealed weak motor impairments at an age of 2 months (Huxley et al. 1998). Histological data shows that these mice develop normal myelin that slowly degenerates. Nerve conduction velocities are reduced which is a typical sign of demyelinating peripheral neuropathy. The C61 mouse line represents a useful animal model of CMT1A (Sereda & Nave 2006) .

Reduction of the *Pmp22* overexpression has been obtained in a mouse line with a tetracycline- regulated *Pmp22* transgene which resulted in improved myelination (Perea et al. 2001). Perea et al. (Perea et al. 2001) demonstrated that peripheral demyelination due to *PMP22* overexpression is reversible if expression is normalized. They also suggested that novel treatment strategies could be aimed at lowering the *Pmp22* expression level.

Several other lines overexpressing *Pmp22* have been generated but they differ in many respects from human CMT1A (Robertson 2005). Animal models with several-fold Pmp22 overexpression, including CMT rats that are bred to homozygosity and mouse strains TgN248, My41, and C22, are severely dysmyelinated or remain amyelinated (Huxley et al. 1998). In these models nerve conduction velocities are massively reduced (Huxley et al. 1998). The lifespan is reduced to a few months (Robertson et al. 2002) unlike in patients with CMT1A (Shy 2005). Clinically they are better suited as models for Dejerine-Sottas neuropathy (DSN) (Roa et al. 1993).

Only 2.5 % of all CMT cases are due to point mutations in the *PMP22* gene (Szigeti et al. 2006). The phenotype in these mutants varies greatly in severity, and can be much more severe than in gene duplication cases (Lupski 2005) The Trembler and Trembler-J mutants of the mouse (Robertson 2005) carry *Pmp22* point mutations and model DSN. Abnormal protein aggregates that contain *PMP22* and ubiquitin cause upregulation of the endosomal–lysosomal pathway and the ubiquitin–proteasome pathway (Ryan et al. 2002) in Schwann cells of Trembler-J mice. The aggregates are found in nerves from Trembler-J mice (Ryan et al. 2002) as much as in *Pmp22* overexpressing cultured Schwann cells (Fortun et al. 2006; Notterpek et al. 1999). PMP22, when retained as a misfolded protein, appears to play a role in endoplasmic reticulum overload, leading later to a block of normal intracellular protein degradation, and increased cell death.

More than 100 different mutations have been identified in the gene for the major cell adhesion protein in peripheral myelin (myelin protein zero/P0/MPZ) in patients with CMT and related disorders (Shy 2006). The clinical picture varies widely in severity. Only few of the human mutations represent a true loss of function situation (Pareyson et al. 1999; Warner et al. 1996).

In mice, a heterozygous loss of *Mpz* expression leads to a mild, late onset neuropathy in the first CMT1B animal model (Martini et al. 1995). Homozygous mice with a null mutation have a severe DSN-like phenotype (Martini et al. 1995). The majority of human *MPZ* mutations, however, show both partial loss and abnormal gain of function effects that are difficult to model in mice.

CMT4B is caused by mutations in the gene encoding myotubularin related protein 2 (*MTMR2*) ,and its histological hallmarks are folded myelin sheaths and demyelination (Houlden et al. 2001). MTMR2 is a member of the family of phosphoinositide-3-phosphatases and hydrolyzes phosphatidylinositol 3-bisphosphate (PIP2) (Berger et al. 2002). PIP2, a second messenger lipid, is implicated in the regulation of intracellular membrane and protein trafficking (Michell et al. 2006). Recently, a Mtmr2-deficient mouse was generated by excising exon 4 of the *Mtmr2* gene (Bolino et al. 2004). When bred to homozygosity, mice exhibited gait abnormalities, reduced NCV, and myelin outfoldings characteristic of CMT4B (Bolino et al. 2004). To define whether loss of MTMR2 from neurons or Schwann cells is responsible, the gene was conditionally inactivated (using HB9-Cre and MPZCre mice) selectively in either cell type (Bolis et al. 2005). These experiments revealed that the *Mtmr2* elimination in Schwann cells (but not in motoneurons) is sufficient to cause a CMT4B-like peripheral neuropathy, including myelin outfoldings. The loss of phosphatase could perturb intracellular membrane trafficking, causing abnormal myelin growth.

More than 250 mutations in connexin-32 (*Cx-32*), also termed gap junction protein beta 1 (*GJB1*), have been identified in patients suffering from X-linked CMT disease (CMTX) (reviewed in (Suter & Scherer 2003). A progressive late-onset demyelinating neuropathy predominantly affecting motor fibres was observed in *Cx32*-null mice (Anzini et al. 1997). Transgenic expression of human *CX32* under the control of the rat *Mpz* promoter in *Cx32*- deficient mice rescued their neuropathic phenotype (Scherer et al. 2005). Mice transgenically expressing mutant *Cx32* (frameshift R142W) develop a late onset demyelinating neuropathy and suggest gain-of-function mechanisms in CMTX (Scherer et al. 1999).

The transcription factor early growth response 2 (EGR2), also termed Krox-20, regulates peripheral myelination (Topilko et al. 1994) and myelin gene expression in Schwann cells (Nagarajan et al. 2001). Mutations in the *EGR2* gene cause phenotypes ranging from severe congenital hypomyelination to demyelinating CMT1D (Vandenberghe et al. 2002). Homozygous *Egr2*-null mice show severe peripheral dysmyelination similar to human congenital hypomyelination while Schwann cell differentiation is arrested at a premyelination state (Topilko et al. 1994). Homozygous *Egr2*-null mice die shortly after birth while heterozygous mice show no reduced lifespan or abnormalities of myelination (Topilko et al. 1994). Low expression of a hypomorphic *Egr2* allele resulted in prolonged postnatal survival combined with arrested peripheral myelination (Nagarajan et al. 2002).

Periaxin is a cytoskeletal component of Schwann cells (Sherman et al. 2001) and has been suggested to mediate interaction of the cytoskeleton with the extracellular matrix (Sherman et al. 2001). Mutations in the gene have been associated with autosomal-recessive CMT4F (Boerkoel et al. 2001; Guilbot et al. 2001). Mice homozygous for a periaxin-null allele develop thickening of myelin sheath, myelin infoldings and progressive demyelination (Gillespie et al. 2000). Nerve conduction velocities are reduced and animals exhibit signs of thermal hyperalgesia and

mechanical allodynia (Gillespie et al. 2000) making them useful to study CMT4F and neuropathic pain.

Mutations in mitofusin 2 (*MFN2*) have been suggested as the most common cause for human CMT2 (Lawson et al. 2005; Reilly 2005). Mitofusin 2 coregulates mitochondrial fusion and fission (Chen et al. 2003; Neuspiel et al. 2005). No myelin defects have been demonstrated in heterozygously *Mfn2*-deficient mice (Zuchner et al. 2004) while homozygous null mice are not viable (Chen et al. 2003).

Mouse lines carrying mutations in the microtubule motor protein KIF1B (Zhao et al. 2001), in neurofilament light chain and lamin zA/C (De Sandre-Giovannoli et al. 2002) constitute models of some forms of axonal CMT2.

CMT-associated genes encode proteins that are involved in vital cellular processes, including mitochondrial function and endosomal trafficking. Mitochondrial dysfunction is known to be involved in various neurodegenerative diseases, including Parkinson's disease, Alzheimer's disease and neuromuscular disease.
Trafficking of vesicles, mitochondria and other membrane-encased organelles along microtubules in the axons of peripheral nerves is crucial for the functioning of neurons and impairment of transport results in neurodegeneration in the *loa* mouse (Hafezparast et al. 2003).
Some of the causative proteins have been the subject of molecular biology studies, but not necessarily in relation to the nervous system and detailed pathophysiological models are still lacking. Many CMT genes still wait to be discovered and the result of future studies promises to be highly relevant to the whole field of neurodegeneration by providing new powerful tools for identifying targets for future therapeutic intervention.

1.5 Project aims

Our understanding of the roles of genes is crucial to interpret the human genome which promises to revolutionise medical science and the way we see ourselves. The sequencing of the mouse genome will greatly enhance the understanding of gene function and expression in humans.

ENU mutagenesis is a useful technique to uncover new genes and to study the roles of known ones. The Harwell ENU mutagenesis programme employs a wide variety of phenotype screens to identify mice with phenotypes relevant to the study of human disease conditions.

As well characterized mouse mutants with clinically relevant phenotypes may be relevant to the study of a variety of human disease conditions , the aim of this project was to characterize two male F1(C3HxBALB/c) mice, MUTN/610.6d and MUTN/610.6c, identified during a routine ENU screen at the MRC Mammalian Genetics Unit, Harwell UK (Nolan et al. 2002) with deficits in grip strength, rotarod and wire manoeuvre when screened using the SHIRPA protocol at 6 weeks of age.

As the clinical phenotype of several diseases of the peripheral nerve includes distal weakness, atrophy and sensory disturbances more pronounced in the legs than in the arms, the two mutants identified in the Harwell screen were of potential interest as animals models of motor and sensory neuropathies and mapping the underlying mutation in such mice would broaden our understanding of the roles of various genes in these heritable disease conditions.

One primary target was to perform a longitudinal behavioural screen to further characterize phenotypically the mice and to establish whether the abnormal phenotype would be progressive. For in depth phenotyping four parameters were adopted: grip strength, rotarod, wire manoeuvre

and weight over a period of 1-15 months. In addition, a detailed histopathology analysis was carried out on the mice at different ages.

Sufficient numbers of backcross progeny were then generated for linkage analysis. Once an area of linkage had been established, candidate genes were identified and screened for mutations. Any mutation found was then investigated to determine if it is likely to cause a functional change.

Efforts were made to study the overall effect of any functional mutation on the stability of the mutant protein, to explain how the altered protein functions *in vitro*, how it selectively affects the nervous system and how it results in associated abnormal phenotype. The observed phenotype was then compared to the phenotype of humans with mutations in the human orthologous gene.

In addition, a third mouse line (BHV/7) identified during a routine ENU screen at the MRC Mammalian Genetic Unit. Harwell UK was characterized as it also showed an abnormal motor phenotype.

BHV/7 mutant mice showed a visible ataxic gait with retropulsion, suggesting that the mice could be of interest as potential models of human ataxia. For in depth phenotyping the same four parameters as GENA 201 and 202 were adopted: grip strength, rotarod, wire manoeuvre and weight. In addition, preliminary histopathology analysis was carried out on the mice.

Efforts were made to generate backcross progeny for linkage analysis and once an area of linkage had been established, an attempt to narrow down the critical interval to a small enough region to look for candidate genes was made.

2. Chapter 2: Materials and methods

2.1 Materials

2.1.1 General chemicals and reagents

3,3'-diaminobenzidine (DAB)	VWR
^{3}H-Glycine	Amersham Bioscience
^{3}H-Tryptophan	Amersham Bioscience
10x MegaBACE LPA Buffer	Amersham Bioscience
Absolute ethanol 100%	VWR
Absolute industrial methylated spirits	VWR
Acetic acid	VWR
Aqueous lithium carbonate	VWR
Aqueous cresyl violet	VWR
Araldite epoxy resin	Leica
Adenosine tri-phosphate (ATP)	Sigma
Avidin horseradish peroxidise	VWR
ß-mercaptoethanol	Sigma
Betaine	Sigma
Better Buffer	Microzone
Bovine serum albumin	Pierce
Canada Balsam	VWR
Dithiothreitol (DTT)	Fluka Biochemika
Dimethyl sulfoxide (DMSO)	Sigma
Electophoresis Grade Ultra Pure Agarose	Invitrogen
Eosin	VWR
Ethidium bromide	Sigma
Formal alcohol	VWR
Glycerol	Sigma
Glycine	Fluka Biochemika
Glycine tRNA synthetase	Bio S&T
Haematoxylin	VWR
Hyperladder I	Bioline
Hyperladder IV	Bioline

Hydrochloric acid	VWR
Iso-proply Alcohol (propan-2-ol 'analar')	VWR
Potassium Chloride	Ambion
Lead citrate	BHD
Luxol fast blue	VWR
Microclean	Microzone
Megamix Blue PCR Master Mix	Microzone
MegaBACE Loading Solution	Amersham Biosciences
MegaBACE ET400-R Size Standard	Amersham Biosciences
MegaBACE Long Read Matrix	Amersham Biosciences
Methanol	VWR
Magnesium acetate	Fluka Biochemika
Mouse DNA	MRC Mammalian Genetic Unit
Normal goat serum	BDH
NP40 detergent	Fluka Biochemika
Nuclei lysis solution	Promega
Oligonucleotide primers	Sigma Genosys
Paraformaldehyde	BHD
Phosphate Buffered Saline (PBS)	Sigma
Protein precipitation solution	Promega
Protease inhibitor	Ambion
Proteinase K	BDH
Reagent A	Pierce
Reagent B	Pierce
Restriction enzymes	Bioline
RNAse inhibitor	Ambion
Sagatal	Rhône Mérieux
Scintillation fluid Ultima Gold	PerkinElmer USA
Sodium dodecyl sulphate (SDS)	Sigma
Sodium acetate buffer	Sigma
Tris/Borate/EDTA (TBE) (x10)	National Diagnostic
Tris-buffered saline (TBS)	VWR
Toluene solution	VWR

Toludine blue	BDH
trichloric acid (TCA)	Sigma
tRNA (bovine liver)	Sigma
Tris	Sigma
Tryptophan	Fluka Biochemika
Uranyl acetate	BDH
Wax	VWR
Xylene	VWR

2.1.2 Equipment

0.5-10µl Multichannel Pipette	Anachem
5-50µl Multichannel Pipette	Anachem
25-200µl Multichannel Pipette	Anachem
0.5ml Screw Cap Microtubes	Sarstedt
10µl Sterile Filter Tips	ABgene
20µl Sterile Filter Tips	ABgene
200µl Sterile Filter Tips	ABgene
1000µl Sterile Filter Tips	ABgene
96-well plates	Abgene Ltd
Adhesive PCR Film	ABgene
1.5ml Screw Cap Microtubes	Sarstedt
6ml polyethylene vials	PerkinElmer USA
Aluminium Foil	Thamesmead
Autoclave Tape	VWR
Balance	Mettler
Bin Liners	Thamesmead
Blue Paper Rolls	Thamesmead
Centrifuge Allegra 25R	Beckman Coulter
Clinical Waste Sacks	Griffiths and Neilsen
Electrophoresis power packs	Amersham Pharmacia Biotech
Electrophoresis tanks	Life Technologies Inc

Gilson pipettes	Anachem Ltd
Glass slides	BDH
Glass slides (super frost)	VWR
Grip Strength machine	Bioseb
Hypercenter automatic processor	Thermo Shandon UK
Incubator shaker	Orbital Incubator S150
Incubator Raven	LTE Scientific
JEM1230 transmission electron microscope	JEOL
Light microscope	Leitz
Microcentrifuge	Eppendorf S415C
Microwave	Proline
Microtome	Leitz
Nalgene filters	Fisher Scientific
Non-Skirted Thermo-Fast Low Profile Plates	ABgene
Olympus BH2 light microscope	Olympus Optical Co Ltd
Purple Thermo-Fast 96 Skirted Plates	ABgene
P-1000 Pipetman	Gilson
P-200 Pipetman	Gilson
P-20 Pipetman	Gilson
P-10 Pipetman	Gilson
P-2 Pipetman	Gilson
Peltier Thermal Cycler PTC-225	MJ Research
Peristaltic pump	Merck Eurolab Ltd
Powder Free Latex Gloves	VWR
Pyrosequencer HS 96A	PyrosequencingAB
Rotarod	Ugo Basile
Sagatal	Rhone Merieux
Sigma Lab Centrifuge 6K15	Philip Harris
Scintillation counter	Beckam
Sunrise plate reader	Tecan
Gel Doc EQ UV-transilluminator	Bio-Rad Laboratories
Ultrospec2000 spectrophotometer	Pharmacia Biotech
Ultracut E ultra microtome	Leica
Water bath	Grant Instruments

Whatman paper (3MM)	Schleicher & Schull
Wire manoeuvre box	MRC Mammalian Genetic Unit
Video printer	Bio-Rad Laboratories

2.1.3 Commercial kits

Hotstart taq polymerase kit	Qiagen
ET-Dye Terminator Cycle Sequencing Kit	Amersham Biosciences
Big-Dye Terminator v1.1 Cycle Sequencing Kit	Applied Biosystems

2.1.4 Software

Pyrosequencing HS 96A Software v1.1	PyrosequencingAB
Sequence Analyser Version 3	Molecular Dynamics

2.2 Experimental animals

The animal experiments described in this thesis were carried out under the guidance issued by the Medical Research Council in "Responsibility in the use of animals for Medical Research"(July 1993) and Home Office Project licences No.30/7025. All mice were derived from stocks at the MRC Harwell. Mouse lines were maintained using the standard husbandry protocol of the MRC Harwell Mammalian Genetics Unit. Mice were housed in a controlled enviroment in the animal facility on site (Table 2.1).

Isolation and conditioning	Ventilated racking
Cage	Polycarbonate with stainless steel lids
Bedding	Grade 5, dust-free, autoclaved wood bedding (Datastand Diet Service, UK)
Diet	SDS Rat and Mouse no.3 (breeding diet) expanded (spezial diet services, UK)
Room temperature	19°C± 2°C
Room humidity	55%±15%
Ventilation	±20 air changes/hour
Lighting	16 hour light, 8 hour dark

Table 2.1 Controlled environment details in which mice were housed during study.

2.3 Behavioural screens

For the purpose of this neurological study, four parameters were chosen to phenotype the mice. They include grip strength, rotarod, wire manouvre and weight.

2.3.1 Grip strength

The grip strength test assessed objectively neuromuscular function by sensing the peak amount of force an animal applied in grasping a stainless steel pull bar (10cmx 8cm) (Bioseb Instruments). The instrument used an electronic digital force gauge. For forelimb grip strength measurements, the animal was held by the base of the tail and allowed to place its forepaws on the flat wire mesh of the pull bar connected to the force gauge. The animal was pulled away from the pull bar until it released it and peak tension recorded. Hind limb grip strength measurements were obtained in a similar way but allowing the animal to grasp the pull bar with both front and hind limb paws. The mean of 5 measurements was determined. Acquired data were transferred to Excel spreadsheets for analysis.

2.3.2 Rotarod

The rotarod test assessed balance and motor coordination in mice. The animal was to keep its balance on a rotating rod 5cm in diameter and 10cm in length made of hard and smooth plastic material (Compagnia). The apparatus was provided with magnetic plates to detect when a mouse falls off the rod. Each mouse was placed in the middle of the rotating rod with its anteroposterior axis perpendicular to the rotation axis and its head directed against the direction of rotation. A training phase was performed which consisted of 3 trials separated by 10 mins intervals. In training trial one, a maximum of four mice were placed on

the rod not moving for 60 secs. In training trials two and three, a maximum of four mice were place on the rod set at 4 rpm constant speed for 60 secs. If a mouse fell off the rod before 60 secs trial three was repeated. Following a 30 mins break between training phase and the test phase, 4 trials were performed, each separated by 15 mins brakes. In each trial, 4 mice were placed on an accelerating rod from 4rpm to 40rpm in 300secs. The test was effective in quantifying progressive impairments in motor coordination and balance. The latency to fall off the rod rotating under continuous acceleration was measured and used as an indication of motor coordination and balance. Data were transferred to Excel spreadsheets for analysis.

2.3.3 Wire manoeuvre

The capacity of mice to balance was evaluated in the wire manoeuvre test. The animal was held above a steel wire (50 cm long and 12 mm wide) by tail suspension and lowered to allow the forelimbs to grip the horizontal wire elevated 40 cm. Animal was held in extension and rotated around to the horizontal as it was released. The mean of 3 trials was analysed. The mouse received a score of 0 if it showed active grip with hind legs, 1 if it showed difficulty to grasp with hind legs struggling, 2 if it was unable to grasp with hind legs, 3 if it fell within seconds and 4 if it fell immediately. Data were transferred to Excel spreadsheets for analysis.

2.3.4 Weight

Body weights of males and females wild type and heterozygotes were recorded over a period of 1 to 15 months. Body weights of homozygotes were recorded at 15 days of age. Data were transferred to Excel spreadsheets for analysis. The student's *t* test was applied to the data obtained at each time point to check for any significant difference in body weight between the genotypes for each sex.

2.3.5 Identification of outliers

Mice from litters produced by backcrosses and through IVF were initially classed as mutant or wild type by behavioural testing. The test results from each test were were plotted on a XY scatter plot, the classes were determined as follows:

1) Mice with results within 1 SD of the C3H mean were classed as wild types
2) Mice with results beyond 3 SD of the C3H mean classed as mutants

Mice with test results between 1 and 3 SD from the F1 mean were excluded from initial genotyping.

2.4 Mapping mutations

2.4.1 DNA extraction

DNA was extracted from tail tissues or ear notches using genomic DNA extraction kits from Promega (Promega UK Ltd). 2mm of tail tip was taken from mice using ethyl chloride as local anaesthetic and potassium permanganate to achieve hamostasis. The biopsy was incubated overnight at 55°C in a CAMLAB microtherm incubator shaker in 600µl of a solution containing 0.5mM EDTA pH 8 , 20mg/ml proteinase K and a Promega nuclei lysis solution containing 0.5% sodium dodecyl sulphate (SDS), 0.1M NaOH and 50mM Tris pH 8. SDS lyses the cells and acts as a protein denaturant while Proteinase K degrades the proteins. 200µl Promega protein precipitation solution was added to remove degraded proteins, cellular debris and tail fur. The solution was mixed by inversion, placed at 4°C for 5 mins and then centrifuged for 10 mins at 4°C at 13000rpm. The supernatant was transferred to a new 1.5 ml eppendorf tube and 600µl isopropanol were added to the solution to precipitate DNA. The mixture was centrifuged in a microcentrifuge for 10 minute at 13000rpm to pellet the DNA. The isopropanol was pipetted off and 300µl 70% ethanol was added wash the DNA. The mixture was mixed by

inversion several times and then microfuged in a microcentrifuge for 5 mins at 13000rpm to repellet the DNA. The final DNA pellet was air dried and resuspended in 100µl sterile distilled water. The DNA was stored at 4°C in use and - 20°C for archiving.

2.4.2 Spectrophotometric analysis of DNA and RNA

The purity and quantity of recovered DNA was measured by reading the absorbance at 260nm, using an Ultrospec 2000, UV//Visible spectrophotometer (Pharmacia Biotech). A rough indication of the DNA content in each sample was given by using the absorbance at 260nm (A_{260}). DNA concentration can be calculated by using the following formula:

DNA concentration (µg/ml)= A_{260} x 50µg/ml x dilution factor

The purity of the DNA sample was assessed by the ratio of absorbance at 260 and 280nm. DNA of acceptable purity produced a ratio of > 1.8.

2.4.3 Genotyping

2.4.3.1 PCR for genotyping

Initial genoptyping was performed using 72 single nucleotide polymorphism (SNPs) developed by Novartis which provided coverage of 90% of the mouse genome at a spacing of 20-40 Mb (Appendix 1). Initial PCRs were performed on BALB/c, C3H, control F1 and 13 mutant DNA samples. PCR cycle were performed on a Peltier Thermal Cycler (MJ Research) using a Taq PCR Master Mix kit (Qiagen) and either the forward or reverse primer was biotinylated. 20µl reactions containing 2.5 units of Taq PCR Master mix, recommended amount of template and 0.2µlM of each primer were subject to the following conditions: 95°C for 1 min followed by 44 cycles of 95°C for 15 secs, 60°C for 30 secs, 72°C for 15 secs, and a final extension of 72°C for 5 mins.

2.4.3.2 Sample preparation for pyrosequencing

Pyrosequencing, a DNA sequencing technique that is based on the detection of released pyrophosphate (PPi) during DNA synthesis, was used to detect SNPs. Biotinylated PCR products were immobilized on streptavidin-coated Sepharose beads (Amersham Biosciences). 38µl binding buffer (PyrosequencingAB) and 30µl sterile double distilled water were added to 20ul PCR product. Then 2µl streptavidin-coated Sepharose beads were added and the mixture was vigorously mixed at room temperature for 5 mins. The streptavidin-coated Sepharose bead and PCR mixture was transferred to a filter plate (Amersham Biosciences) and the binding buffer was removed by vacuum. The biotinylated DNA attached to the streptavidin-coated Sepharose beads was washed in 180ml 70% ethanol for 5 mins, it was then denaturised in 120ml denaturation buffer (PyrosequencingAB) for 5 mins and finally washed in 180ml wash buffer (PyrosequencingAB). The 70% ethanol, the denaturation buffer and the washing buffer were removed by vacuum.

2.4.3.3 Pyrosequencing reaction

DNA was transferred to 96-well PSQ96 plate containing in each well 11.5µl annealing buffer (PyrosequencingAB) and 0.5µl 10mM sequencing primer. The sequencing primer was allowed to anneal on a heat plate set for 80°C for 2 mins. Samples are allowed to cool for 5 mins at room temperature. Once samples were cooled the plate was placed on the Pyrosequencer HS 96A and the Pyroseqencer HS 96A enzyme, substrate and dNTPs reagents (PyrosequencingAB) were added to the Pyroseqencer HS 96A cartridge (PyrosequencingAB). Genotyping was automatically designed using Pyrosequencer HS 96A software v1.1. Visible light was generated through a cascade of reactions that was proportional to the number of incorporated nucleotides (Fig 2.1). The cascade started with a nucleic acid polymerization reaction in which inorganic PPi was released as a result of nucleotide incorporation by

polymerase in a quantity equimolar to the amount of incorporated nucleotide. The released PPi was subsequently converted to ATP by ATP sulfurylase, which provides the energy to luciferase to oxidize luciferin and generate light. Because the added nucleotide was known, the sequence of the template could be determined. The light produced in the luciferase-catalyzed reaction was detected by a charge coupled device (CCD) camera and seen as a peak in a pyrogram. Each light signal was proportional to the number of nucleotides incorporated.

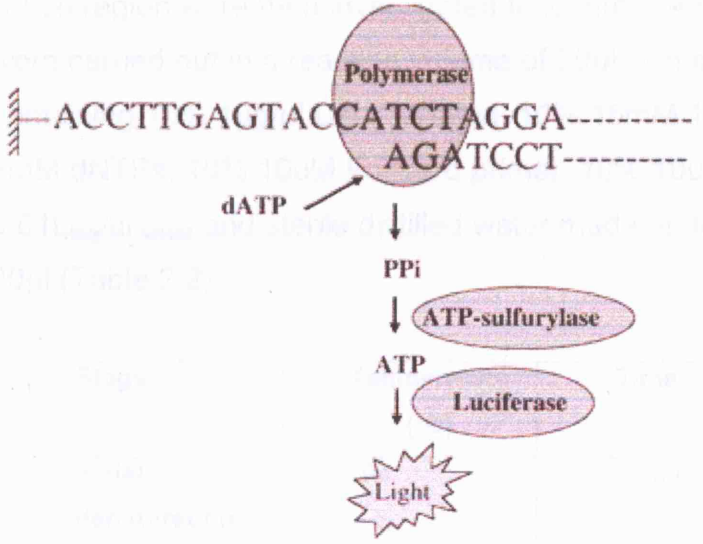

Fig 2.1 The four different nucleotides are added stepwise to the immobilized primed DNA template and the incorporation event is followed using the enzyme ATP sulfurylase and luciferase. After each nucleotide addition, a washing step is performed to allow interactive addition.

2.4.3.4 Linkage analysis

The use of inbred mouse strains simplified the linkage analysis of the backcross progeny. The founder animals (F1s) were BALB/cAnN x C3H/HeH. All progeny of F1 mice mated to C3H were obligate BALB/c x C3H heterozygotes at the mutation-affected locus. Recombination events and the presence of C3H homozygosity excluded unlinked areas. Once

linkage was found, microsatellite markers and more SNPs markers (Appendix 2) that spanned the critical region were genotyped to narrow down the region. Primer sequences and information regarding microsatellite marker polymorphisms between relevant mouse strains was obtained using the Mouse Genome Informatics genes and markers database (http://www.informatics.jax.org/). All primers were manufactured by Sigma-Genosys (http://orders.sigma-genosys.eu.com/index.php). DNA from individual mutant animals were used for PCR. Mouse genes in the linked region were then investigated to identify candidate genes. PCRs were carried out in a reaction volume of 20µl. A mix was prepared containing 10% 1µg/µl DNA solution, 10% 15mM 1x reaction buffer, 10% 2mM dNTPs, 10% 10uM Forward primer, 10% 10uM Reverse primer, 1% $0.01L_{taq}/ul_{water}$ and sterile distilled water made up to a final volume of 20µl (Table 2.2).

Stage	Temperature (°C)	Time	Number of cycles
Initial denaturation	94	15 mins	1
Denaturation	94	30 secs	34
Annealing	50-65	30 secs	
Extension	72	30-60 secs	
Final Extension	72	5 mins	1

Table 2.2 PCR parameters.

For scoring markers on an agarose gel, PCRs were carried out as described above. However, as primer annealing is dependent on melting temperature (T_m) of primers, alteration was made to the annealing temperature in order to optimise amplification of the desired product. The extension time was also varied depending on the expected size of the product assuming 1kb is amplified per minute.

2.4.3.5 PCR cloning: *Glycyl-tRNA synthetase*

The published genomic sequence (AC079183.5, *Mus musculus* clone RP23-258N2) and available information about intron-exon boundaries of *Gars* (http://www.ensembl.org/Mus_musculus/exonview?db=core;transcript=ENSMUST00000003572) were used to design oligonucleotides for the differential amplification of each exon (Appendix 3). Primers for PCR of genomic DNA (gDNA) were designed by hand following the general rules for primer designing. According to these rules the primers should ideally:

i) be 20-30 nucleotides long, to provide good specificity for unique target sequence.

ii) contain approximately equal GC/AT content.

iii) avoid repetitive sequences or regions containing stretches of the same nucleotide
as this can lead to slipping of the primer on the template.

iv) avoid runs of three or more G or C at the 3' end as this can lead to mispriming at GC rich region.

v) allow no secondary structures formation due to internal complementarities.

vi) have free 3' ends to avoid primer dimers.

vii) not hybridise elsewhere in genome such that unwanted product may form.

Oligonucleotides were designed to lie at least 30 base pairs into the intronic sequence (to incorporate the splice sites), be at least 20 base

pairs long, have an approximate GC to AT ratio of 1:1 and begin and end with G or a C base. Oligonucleotides were ordered from Sigma Genosys (http://orders.sigma-genosys.eu.com/index.php). The primers were designed based on known sequence available from Ensembl (http://www.ensembl.org/Mus_musculus/) and NCBI databases (https://www.ncbi.nlm.nih.gov/).

Following manufacturer's instructions freeze dried primers were resuspended in dH_2O to a dilution of 100µM. Details of relevant dH_2O volumes were provided. Primer stock solutions were stored at -20°C. For a PCR working stock a 1 in 10 dilution to 10µM in TE (i.e. 50µl DNA, 450µl TE) was made. Primer PCR working dilutions were stored at -20°C or 4°C dependent upon regularity of use to avoid degradation through unnecessary freeze-thawing. All primers were resuspended in a dilution of 10µM unless otherwise stated.

25µl reactions contained 15-30ng DNA, 10µM forward and reverse primers, 22µl Megamix Blue PCR Master Mix (Microzone). This mix was scaled up appropriately according to the number of samples in question, mixed well and pulsed using a microcentrifuge 5415C (Eppendorf). 24µl of the mix was aliquoted into each well of a 96-well non-skirted thermo-fast low profile plate (ABgene). 1µl DNA was added per well with one well per primer set assigned as a non-template, water control. The plate was sealed with an adhesive PCR film lid (ABgene) and centrifuged briefly using Allegra 25 R Centrifuge (Beckman and Coulter). The samples were then subjected to an appropriate thermal cycling program on a PTC-225 machine (MJ Research).

Stage	Temperature (°C)	Time	Number of cycles
Initial denaturation	94	15 mins	1
Denaturation	94	30 secs	34
Annealing	50-65	30 secs	
Extension	72	30-60 secs	
Final Extension	72	5 mins	1

Table 2.3 PCR parameters.

PCRs were carried out under the conditions described above. Primer annealing is dependent upon the melting temperature (T_m) of primers and so the annealing temperature was manipulated accordingly to optimise amplification of the target product. The extension step was also altered depending on the size of the amplicon and making the assumption that 1kb is amplified per minute. Cycle number was increased in cases where a previous PCR had amplified a weak product band on subsequent gel electrophoresis, the aim being to increase the amount of product amplified and generate a stronger signal. If PCR products proved difficult to amplify a gradient PCR program was employed in which an annealing temperature range of 50-65°C was used across a plate of identical samples to identify an optimum condition. In cases where GC rich regions were causing amplification problems 20% Betaine or 5% of dimethyl sulfoxide (DMSO) was used. Betaine is known to improve PCR amplification of GC-rich DNA regions by reducing the formation of the secondary structure they cause. DMSO has been shown to facilitate DNA strand separation in GC rich regions because it disrupts base pairing and has been shown to improve PCR efficiency. Upon completion of PCR plates were stored at 4°C.

2.4.3.6 Restriction enzyme digestion

HaeII and HhaI restriction enzymes used were purchased from New England Biolabs (NEB). Restriction digests of PCR product were carried out according to the manufacturer's instructions. At least 1U enzyme/µg of DNA was used for a minimum of 1hr.

The *Gars*^{201R} mutantation changed a restriction site for the enzymes HaeII and HhaI. A protocol was designed for routine genotyping by PCR followed by RFLP analysis.

Routine genotyping: PCR primers (forward: CACGTGCTTGCTCTAGCAAGA; reverse: GTCTACCACTGAACACAGTCC) that lay within intron 4 and intron 5 respectively, and thus spanned exon 5 of *Gars* were used to amplify a 422bp product. This amplicon was digested with HhaI to give fragments of 422bp (no restriction site, wildtype C3H and C57BL/6 *Gars* loci) and of 169bp and 253bp (*Gars*^{201R} mutant gene).

2.4.3.7 Agarose gel electrophoresis

Electrophoresis grade agarose and TBE buffer were obtained from Life Technologies. Agarose gels were electrophorized in horizontal Horizon 11.4 tanks from Life Technologies (30 samples, 2 markers). Agarose was melted in a microwave and allowed to cool. When warm to touch, 5ul 10mg/ml ethidium bromide was added per 100ml gel. The gel was poured in gel boxes and the appropriate size combs were added. The gels were then left to set for 30 min. The volume of sample loaded varied between 5 to 10µl PCR product and 2µl bromophenol blue loading buffer. Various DNAladders (2µl) were used depending on size of DNA under study.

Marker	Size	Supplier
Hyperladder I	500bp-100bp	Bioline
HyperladderV	12kb-100bp	Bioline

Table 2.4 Size Markers.

Gels were electrophoresed in 1x TBE at 90-120V/30cm for 30 to 120 minutes, depending on the size of the products being resolved, then visualised on a Bio-Rad UV transilluminator and digital imaging system.

2.5 Sequencing

2.5.1 PCR purification

PCR products were purified using *micro*CLEAN (Microzone), to remove reaction buffers, enzymes, primer dimers and unincorporated primers and dNTPs, following the manufacturer's protocol. Briefly, an equal volume of *micro*CLEAN was added to a 96-well plate containing PCR products and incubated at room temperature for 5 minutes. The plate was centrifuged at 3000 rcf for 40 mins and then inverted onto absorbent paper and pulsed at 100 rcf to discard the supernatant. The purified DNA pellet was then resuspended in 20µl sterile distilled water.

2.5.2 Sequencing reaction

Automated fluorescent sequencing was carried out with the BigDye Terminator Ready Reaction Kit (Applied Biosystems), DYEnamic ET Dye Terminator Kit (Amersham Pharmacia) and 1µM PCR primers. For the BigDye Terminator Ready Reaction Kit, a sequencing master-mix was made containing (per reaction) 1µl BigDye terminators, 5µl BetterBuffer (Microzone), 0.5µl forward/reverse primer (1µM), and 7µl sterile distilled water. A Gilson Distriman repeater-pipette was used to aliquot 13.5µl

BigDye master-mix into wells of a skirted 96-well plate, to which 1.5µl purified PCR products were added, for a total reaction volume of 15µl. Cycling conditions were 96°C for 30 secs, followed by 30 cycles of 50°C for 15 secs and 60°C for 3 mins and a final hold step of 15°C for 5 mins.

The DYEnamic ET Dye Terminator Kit sequencing master-mix contained, per reaction, 2µl ET terminators, 6µl BetterBuffer and 4µl forward/reverse primer (1µM). 12µl ET terminators master-mix was aliquoted into wells of a skirted 96-well plate, to which 8µl purified PCR products were added, for a total reaction volume of 20µl. Cycling conditions were 25 cycles of 95°C for 20 secs, 50°C for 15 secs and 60°C for 1 min, with a final hold step of 10°C for 10 mins.

2.5.3 DNA precipitation

Sequencing products were precipitated to remove reaction buffers and unincorporated terminators to avoid tall early peaks, often termed "terminator blobs". 55µl 100% absolute ethanol (Sigma-Aldrich) and 1µl 3M sodium acetate (Sigma-Aldrich) was added to 20µl reaction and the mixture was chilled on ice for 15 minutes. The plate was centrifuged at 3000 rcf for 45 minutes to pellet the DNA and the supernatant discarded by inverting onto absorbent tissue paper and pulse-centrifuging at 100 rcf for 1 minute. 150µl 70% ethanol was added to wash the pellets and the plate was centrifuged at 3000 rcf for 10 minutes. Again, the plate was inverted onto absorbent tissue paper, pulse-centrifuged at 100 rcf for 1 minute to remove the supernatant and the pellet was allowed to air dry for 10 minutes.

2.5.4 MegaBACE 1000 DNA analysis system

The automated MegaBACE 1000 DNA Analysis System (Amersham Pharmacia) was used to sequence DNA. The MegaBACE uses capillary array electrophoresis to perform fragment size separation of fluorescently labelled DNA samples with a confocal optical system to collect data. The manufacturer's guidelines and protocols were followed unless otherwise stated. Precipitated DNA with fluorescently labelled

terminators, was resuspended in 10µl MegaBACE Loading Buffer (Amersham Pharmacia), vortexed thoroughly to ensure the complete solublization of the DNA and then pulse-centrifuged to return the liquid to the bottom of the 96-plate wells.

MegaBACE Long Read Sequencing Matrix (Amersham Pharmacia) was used to pressure-fill the capillary array with sieving matrix to separate DNA fragments of varying sizes. Sequencing products were electrokinetically injected into the capillary array by a potential difference of 3kV for 40 seconds and electrophoresis was carried out in 1x LPA Buffer (Amersham Pharmacia) at 9kV for 100 minutes. Laser excitation of the fluorescently labelled samples yielded data as an electropherogram for each capillary/sample which were analyzed in forward and reverse directions using the Sequence Analyser v3.0 package (Molecular Dynamics), and inspected by eye.

2.5.5 Bioinformatics

Genomic DNA sequences were obtained from the Ensembl (http://www.ensembl.org/Mus_musculus/) and NCBI (https://www.ncbi.nlm.nih.gov/) databases. UNISTS markers positions were obtained using Broad Institute (http://www.broad.mit.edu/) and NCBI (https://www.ncbi.nlm.nih.gov/) databases.

2.6 Aminoacylation assay

2.6.1 Brain Extraction

Mice to be sacrificed were culled according to Home Office regulations. Brains were removed and flash frozen in liquid nitrogen. A reaction mix was prepared by adding 50mM Tris pH 7.5, 25 mM KCl, 1% NP40, 10%

Glycerol, 1 mM DTT, 10µl of protease inhibitor per ml buffer. 10mg of brain samples per ml buffer were homogenized using plastic mortar and then centrifuged in a microcentrifuge for 20 minute at 12,000rpm. Supernatant was aliquoted and stored at -80°C until used. Protein concentration of homogenates was determined using BCA (Pierce).

2.6.2 Protein Concentration assay using BCA (Pierce)

The BCA™ Protein Assay, a detergent-compatible formulation based on bicinchoninic acid (BCA) for the colorimetric detection and quantitation of total protein was used to asses protein concentration. This method combined the reduction of Cu^{+2} to Cu^{+1} by protein in an alkaline medium with the sensitive and selective colorimetric detection of the cuprous cation (Cu^{+1}) using a unique reagent containing bicinchoninic acid. A fresh set of protein standards was prepared by diluting a 2.0mg/ml bovine serum albumin (BSA) stock standard (stock) in the same diluent used in the brain samples. Table 2.5 shows the list of standard dilution. The BSA standard (1ml ampule of the 2.0mg/ml) was sufficient to prepare a set of diluted standards for either working range.

Vol. of BSA to add	Vol. of Dilute to add	Final BSA concentration
300µl of (stock)	0µl	2000µg/ml
375µl of (stock)	125µl	1500µg/ml
325µl of (stock)	325µl	1000µg/ml
175µl of (A)	175µl	750µg/ml
325µl of (B)	325µl	500µg/ml
325µl of (D)	325µl	250µg/ml
325µl of (E)	325µl	125µg/ml
100µl of (F)	400µl	25µg/ml

Table 2.5 Preparation of the diluted BSA standards.

The working reagent (WR) was prepared by mixing 50 parts of BCA reagent A with 1 part of BCA reagent B. When BCA reagent B was

initially added to BCA reagent A, a turbidity was observed that quickly disappears upon mixing to yield a clear green WR. Sufficient volume of WR was prepared based upon the number of tests to be done. 200µl of WR was added to the microwell plate wells followed by 25µl of each standard or unknown sample. 25µl of the diluent for the blank wells was used.The plate's wells were mixed on a shaker for 30 secs and the plate was then covered with aluminium foil and incubated for 30 mins at 37°C. Following incubation, the plate was cooled at room temperature and the absorbance was measured at 562 on a Sunrise plate reader (Tecan) A standard curve was prepared by plotting the average A(562) reading for each BSA standard vs its concentration in µg/ml and the protein concentration was determined for each unknown sample.

2.6.3 Aminoacylation

A reaction mix was prepared by adding the following reagents: 10µM Glycine, 50mM Tris pH 7.5, 25mM KCl, 2mM DTT, 10mM MgAc, 5mM ATP, 2 µl RNAse inhibitor (Ambion), 1µM ^{3}H-Glycine, 20µl total protein. Each sample was assayed in triplicate with three individual data points taken for each assay. Homogenates were assayed for both glycyl and tryptophan-tRNA synthetase activity.

The reaction was preincubated at 37°C for 20 mins. 80uM tRNA- bovine liver (Sigma) was added and the reaction was incubated for a further 5 min at 37°C. The reaction mix was spotted on 3MM Whatman filter paper and washed once in 10% TCA for 15 min, 3 times in 2.5% TCA for 15 min and once in 100% ethanol. The filter was then air dried and 5 ml of scintillation fluid (Ultima Gold, PerkinElmer USA) were added.The samples were then counted in a scintillator counter. No tRNA was added to the negative control

The scintillator counter reports the number of photons that it detects as counts per minute (cpm). The difference between cpm and disintegration per minute (dpm) is the efficiency (eff) of the counter in detecting the release of beta particles. To obtain dpm the mean of each sample count was divided by the efficiency of the assay. Dpms were converted to disintegration per second and then divided by the specific activity of the radioactive glycine to obtain pmoles. The result was normalized using the protein concentration to obtain picomoles per mg of protein per minute of time.

2.7 Perfusions

2.7.1 Preparation of solution

Roughly 120-130 ml PBS (Sigma) solution was prepared for each mouse. 4% paraformaldehyde solution was prepared by dissolving 4 g papraformaldehyde powder (BHD Laboratory) in 100ml PBS. The solution was mixed for 1-2 hours at 60°C using a heated magnetic stirrer. Suitable protective clothing was worn throughout the procedure. Preparation was conducted in a fume cupboard to avoid inhaliation of carcinogenic fumes. Once all the powder had dissolved the solution was allowed to cool down to room temperature and filtered (Nalgene filters, Fisher Scientific) using a vacuum pump. The solution was refrigerated at 4 °C until needed.

2.7.2 Procedure

A peristaltic pump (Watson Marlow series 101U/R, Merck Eurolab Ltd.) with a flow rate of roughly 10 ml/min was used to perform the perfusions. Mice were killed by an intra-peritoneal Sagatal (Pentobarbitone Sodium B.P. 60mg/ml Rhône Mérieux) overdose (0.3 ml). Once the heart stopped beating and all the relexes were absent, the abdominal and chest cavities were opened. The diaphragm was cut away to the side without pucturing the organs or rupturing any of the larger blood vessels.

The ribcage was flexed open to expose the heart. The needle at the end of the pump's outlet tube was carefully inserted into the left ventricle of the heart. A hole was snipped in the right atrium of the heart using a sharp pair of scissors. Each mouse was first flushed with 20-30ml PBS (or until only clear PBS flowed out of the right atrium). Roughly 100ml 4% paraformaldeyde solution was flushed through the mouse to fix the tissues. The whole carcass was then submerged in a container of formalin saline solution.

2.8 Histopathology

2.8.1 Preparation of mouse tissue for histological staining

All of the histopathological analyses for GENA 201 and 202 were conducted by Prof. Jo Martin, Ms Carole Nickols and Graham McPhail at the Royal London Hospital in Whitechapel, London, UK. Analysis was performed on GENA201 and 202 mice on a C3H background at 15 days old and 17 months old.

The organs and tissues dissected from parfused animals are listed in table 2.6. All reagents were manufactured by VWR unless otherwise stated. Samples were first processed on a Hypercenter automatic processor (Thermo Shandon, UK). The processing involved automatic rotation of the tissues through 10% formal alcohol (2 X $1^{1/2}$ hours) at room temperature, 10% formal alcohol (1 X 1 hour) at room temperature, absolute industrial methylated spirits (4 X 1 hour) at room temperature, toluene solution (3 X 1 hour) at room temperature and a first change of wax (1 X 2 hours) at 60°C under vacuum follwed by a second change of wax (1 X 2 and ½ hours) at 60°C under vacuum. Tissues were then embedded in wax on a Blockmaster III. A base sledge microtome (Leitz) was used to cut 3µm sections from the embedded tissues. Sections were floated out on a water bath (VWR) set at 52°C, picked un on super frost plus glass slides (VWR) and oven dried overnight at 37°C. Sections were

de-waxed in Xylene (2x 2 minutes) and rehydrated through graded series of alcohols and finally into water before staining. Slides were examined under Olympus BH2 light microscope fitted with a Colourview Soft Imaging System for capturing digital images (Olympus Optical Co Ltd.).

Thyroid/parathyroid	Kidneys	Spinal cord
Esophagus	Adrenal glands	Brain
Stomach	Heart	Cerebellum
Duodenum	Lungs	Pituitary
Ileum	Diaphragm	Triceps
Colon	Testis/Ovaris	Quadriceps
Pancreas	Fallopian	Gastrocnemius
Spleen	tubes/uterus	Sciatic nerve
Liver and gall	Bladder	
bladder	Skin	

Table 2.6 The organs and tissues dissected from mice for general histological investigations.

2.8.2 Histological staining

Haematoxylin and eosin

Tissues were subsequently stained with Gills haematoxylin (VWR) for 20 minutes, differentianted in 1% acid alcohol, stained with eosin (VWR) for 3 minutes, dehydrated through a graded series of alcohols, cleared in xylene (2 X 2minutes) and mounted in Canada Balsam (VWR).

Luxol-fast blue and cresyl violet

Section were stained with 0.1% luxol fast blue in methanol containing 0.0075M hydrochloric acid overnight at 56°C, differentiated in 0.05%

aqueous lithium carbonate and then stained with 0.5 % aqueous cresyl violet for 5 minutes, dehydrated through a graded series of alcohols of which the 90% ethanol contained a few drops of acetic acid to aid differentiation, and mounted.

2.8.3 Immunostaining of brain sections

Sections were blocked in 10% normal goat serum for 10 minutes, followed by incubation with the primary antibody. The specific conditions for each antibody, of which all used were raised in rabbits, are given in table 2.7. All antibodies underwent a heath mediated antigen retrieval and the endogenous peroxidise was blocked. Following three 5 minutes washes in TBS, detection was achieved by immunoperoxidase. A biotinylated secondary antibody (goat anti-rabbit, 1:300), to which a preformed Avidin and Biotinylated horseradish peroxidase complex (ABC) is added. The chromagenic peroxidase substrate 3,3'-diaminobenzidine (DAB) was used to visualise the complex. DAB is insoluble in alcohol, allowing dehydration of the specimen in a graded series of alcohols followed by mounting in Canada Balsam (VWR).

Primary antibody	Supplier	Dilution used	Incubation conditions	Detection method
Glial fibrillary acid protein immunohistochemistry (GFAP)	Dako	1:2000	1 hour at room temperature	ABC NGS goat and rabbitb
Parvalbumin immunohistochemistry (PV)	Novakastra	1:300	30 minutes at room temperature	MOM (Vector) technique *
Cholineaceytlytransferase immunohistochemistry (ChAT)	Chemicon	1:50	1 hour at room temperature	ABC NRS rabbit and goat

Table 2.7 List of specific conditions for each antibody
* MOM (mouse to mouse) technique was used because it was a mouse monoclonal antibody to be used on mice.

2.8.4 Electron microscopy of sciatic nerve

Sciatic nerve was fixed in a solution of 4 % paraformaldehyde at room temperature. Specimens were washed, stained with unbuffered aqueous 1% osmium tetroxide (BDH), dehydrated, and embedded in araldite epoxy resin (Leica). Semithin sections (0.5–1 μm) were cut on a on a Ultracut E ultra microtome (Leica) stained with 1% toludine blue (BDH), and examined under Dialux light microscope. Ultrathin sections (70–100 nm) were collected on copper grids, stained with uranyl acetate and lead citrate (BDH), and examined under a JEOL JEM1230 transmission electron microscope.

3. Chapter 3: Characterization of GENA 201 and 202

3.1 Introduction

Two male F1(C3HxBALB/c) mice, MUTN/610.6d and MUTN/610.6c, were identified during a routine screen in a large ENU mutagenesis project at the MRC Mammalian Genetics Unit, Harwell UK (Nolan et al. 2002).

The two founder animals were siblings produced by a G0 BALB/c mutagenised male crossed to a C3H female. They were part of an aged cohort tested at up to 1 year and were found to have deficits in grip strength, locomotor activity and rotarod when screened using the SHIRPA protocol at 6 weeks of age (data not included).

The first aim of the project was to perform a longitudinal behavioural screen on the progeny from these mice. This was done to further characterize phenotypically the mice, to confirm whether the abnormal phenotype was progressive and to score affected and unaffected animals for genetic mapping. For in depth phenotyping four parameters were adopted: grip strength, rotarod, wire manoeuvre and weight over a period of 1-15 months.

3.2 Phenotype of GENA 201 and 202

GENA 201 and 202 lines were maintained by in vitro fertilization and backcrossing mutant offspring to the C3H/HeH and C67BL/6 background. Based on the SHIRPA results of the founder siblings, for in depth phenotyping four parameters were used to assess the motor performance of progeny from the two animals. The parameters measured were (1) grip strength, (2) rotarod performance, (3) wire manoeuvre and (4) weight over a period of 2 to 15 months.

The aim of the behavioural screen was to be able to characterize affected and unaffected animals for positional cloning by combining the results of all the tests. Female and male data were analyzed separately to allow for any size differences in the parameter tested. Male and female means and standard devations were calculated in each test. Mice were classed as mutant or wild type by analysis of the tests results taken at 9 weeks. Means of 10 female and 10 male mice on a C3H and C57BL/6 background tested at 9 weeks were used as reference mean. The original F1 mean was not used as a reference mean as the apparatus used to test the two F1 progeny differed from the automated apparatus available when the project started. Mice with results within 1 SD of the C3H or C57BL/6 control mean at 9 weeks were classed as wild types. Mice with results beyond 3 SD of the C3H or C57BL/6 control mean at 9 weeks were classed as mutants.

3.2.1 Grip strength

19 GENA201 and 26 GENA202 N2 mice produced by in vitro fertilization on a C3H background underwent grip strength testing of the combined fore and hind limbs over 2 -15 months of age. A reduction in grip strength was observed in both male and female GENA 201 and 202 mice as early as 9 weeks. For example, in the C3H GENA 201 and 202 male cohort 4 paws, 10 animals out of a total of 21 were beyond 3 SD of the C3H control mean at 9 weeks and, in the C3H GENA 201 and 202 female cohort 4 paws, 11 animals out of a total of 23 mice were beyond 3 SD of the C3H control mean at 9 weeks (Fig 3.1). As GENA201 and 202 cohorts showed no significant differences from each other, the data were combined into "mutant" and one 'wild type littermate' control male and female cohort (Fig 3.2).

In addition, 80 GENA 201 and 79 GENA 202 N2 mice produced by in vitro fertilization on a C57BL/6 background were tested for grip strength at 3 months of age to have more genetic markers available for positional

cloning. GENA 201 and 202 grip strength data, 4 paws trials, on the C57BL/6 background also segregated in two distinct cohorts (Fig 3.3) adding a further genetic background in which the mutation was segregating.

It was apparent that GENA 201 and 202 male and female mice segregated in two distinct cohorts when they were tested with all four paws. However, when tested with two paws such clear distinction was lost in some cases. For example in Fig 3.3, male and female GENA 202, two paws trials, showed no clear distinction between the two cohorts. This might be due to the fact that the strength in the fore paws is less affected in GENA 202 than the hind limb strength or that the animals were more distressed when suspended by the base of the tail and allowed to place only its forepaws on the flat wire mesh rather than the all 4 paws.

The results were normalized to the weight of each animal and compared to age- and sex-matched littermates. No significant difference was observed between the raw data (force per grams) and the normalized data (force per grams/grams) (Fig 3.4). Thus, the raw data were used to score affected and unaffected animals.

A significant reduction in grip strength was seen in both male and female 201 and 202 mutant mice compared to wild type littermates from 1 to 15 months of age on both C3H (Fig 3.2) and C57BL/6 genetic backgrounds (Fig 3.5). For example, the grip strength mean of 3-month old mutant males (n=11) on the C3H background is 123.9±7.38 force per grams compared to 205.48±6.25 force per grams in littermate controls (n=10) an average reduction of 40%. However, the phenotype was considerably more pronounced on the C57BL/6 background than the C3H genetic background when we scored both cohorts at 3 months of age. At 3 months of age the grip strength mean of GENA 201 males (n=23) on the C57BL/6 background is 75.4±3.7 force per gram compared to 177.1±7.5 in wildtype littermates controls (n=14), a reduction of 57%. The grip

strength mean of mutant females on the C3H background is 111.2±3.2 force per grams (n=9) compared to 71.18±2.75 force per grams of mutant females (n=24) on the C57BL/6 background. Similarly that of mutant males on the C3H background 123.9±7.38 force per grams (n=11) compared to 75.36±3.69 force per grams of mutant males on the C57BL/6 background (n=23). This indicates that genetic modifiers segregating between the C3H and C57BL/6 backgrounds are having a pronounced effect.

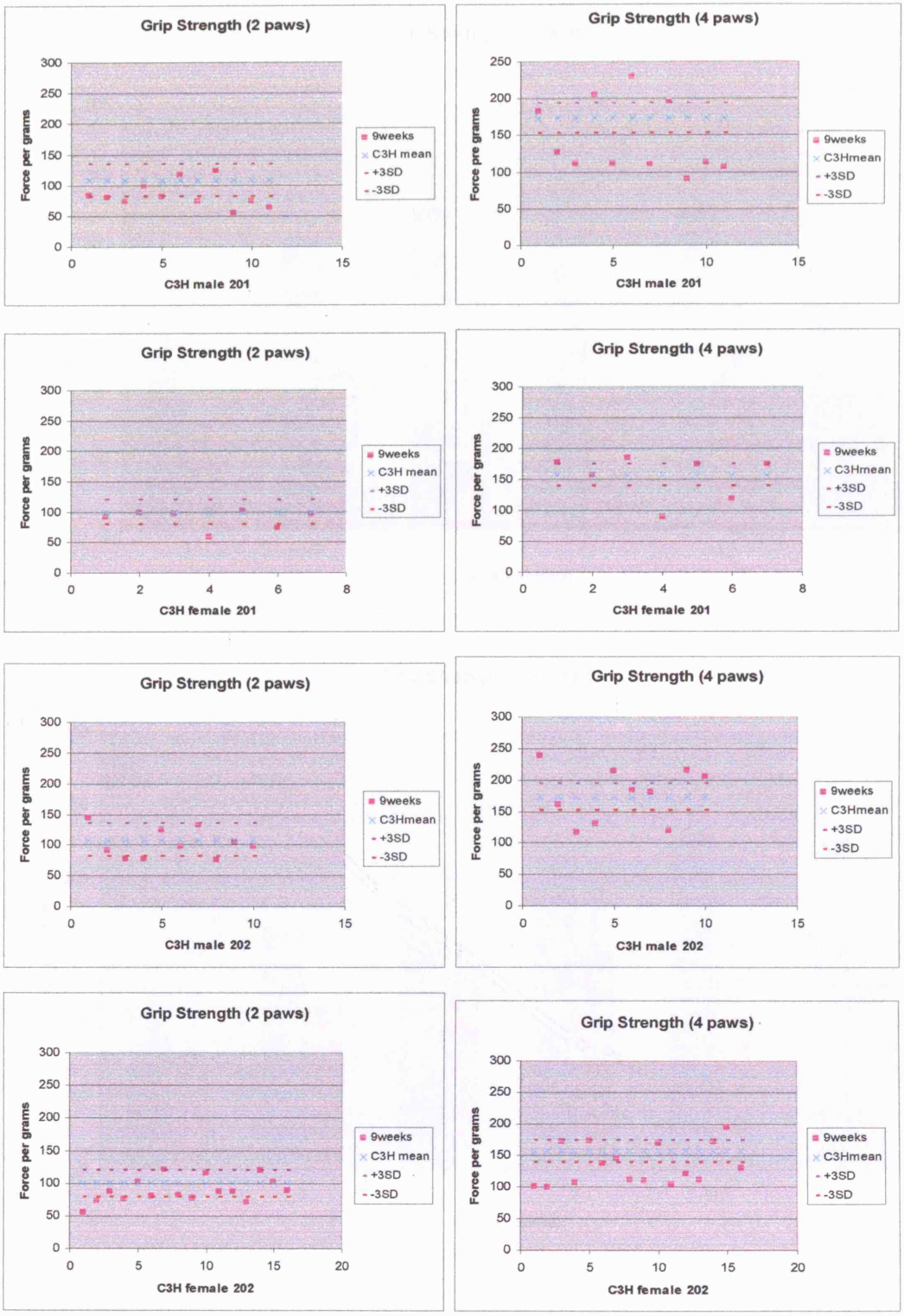

Fig 3.1 Grip strength performance of male and female GENA201 and GENA202 N2 individual mice at 9 weeks on a C3H genetic background. Each dot represents a mouse performance. The animals underwent 2 paws and 4 paws trials. The C3H mean control age was at 9 weeks. N. male 201=11, n. female 201=7,n. male 202=10, n. female 202=16.

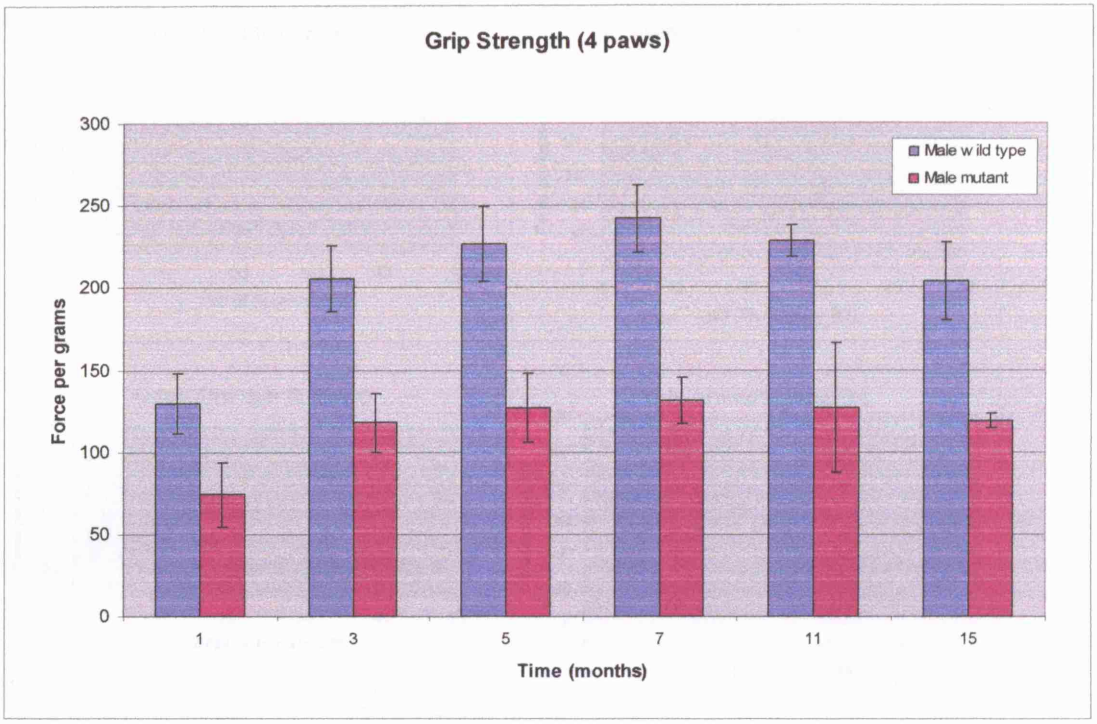

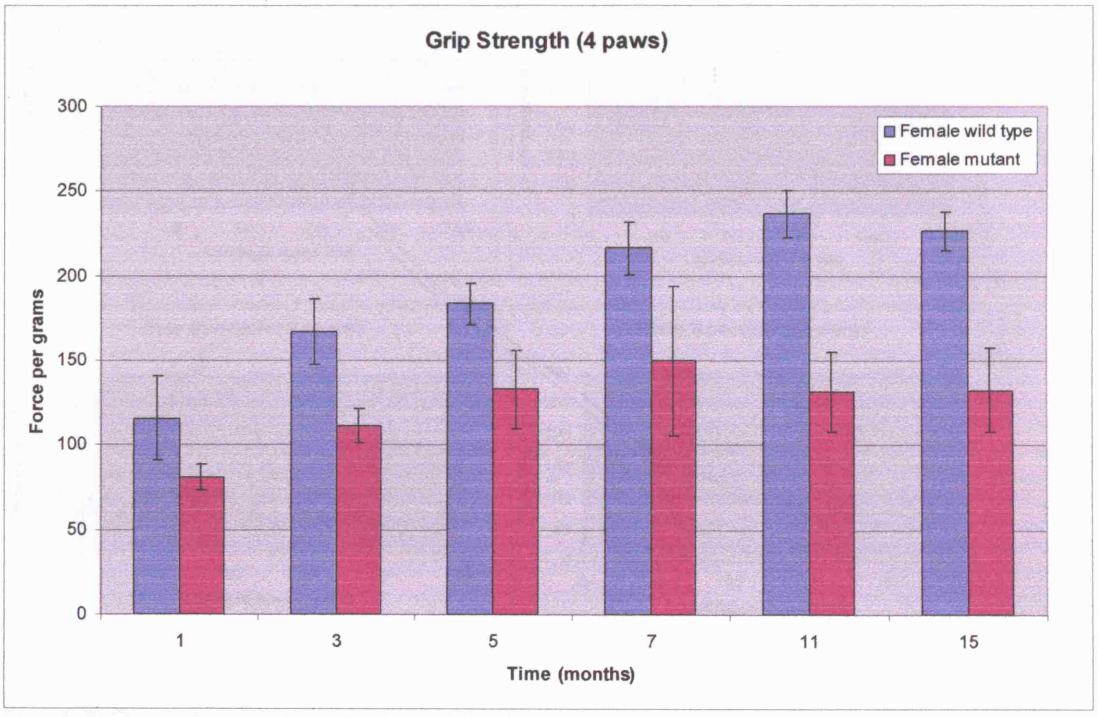

Fig 3.2 Grip strength of mutant male and female mice on C3H background compared to age-and sex-matched wild type littermates. N. of mice sampled varied with the time point: wild type n=3-7; mutant n=4-9 ($P<0.05$).

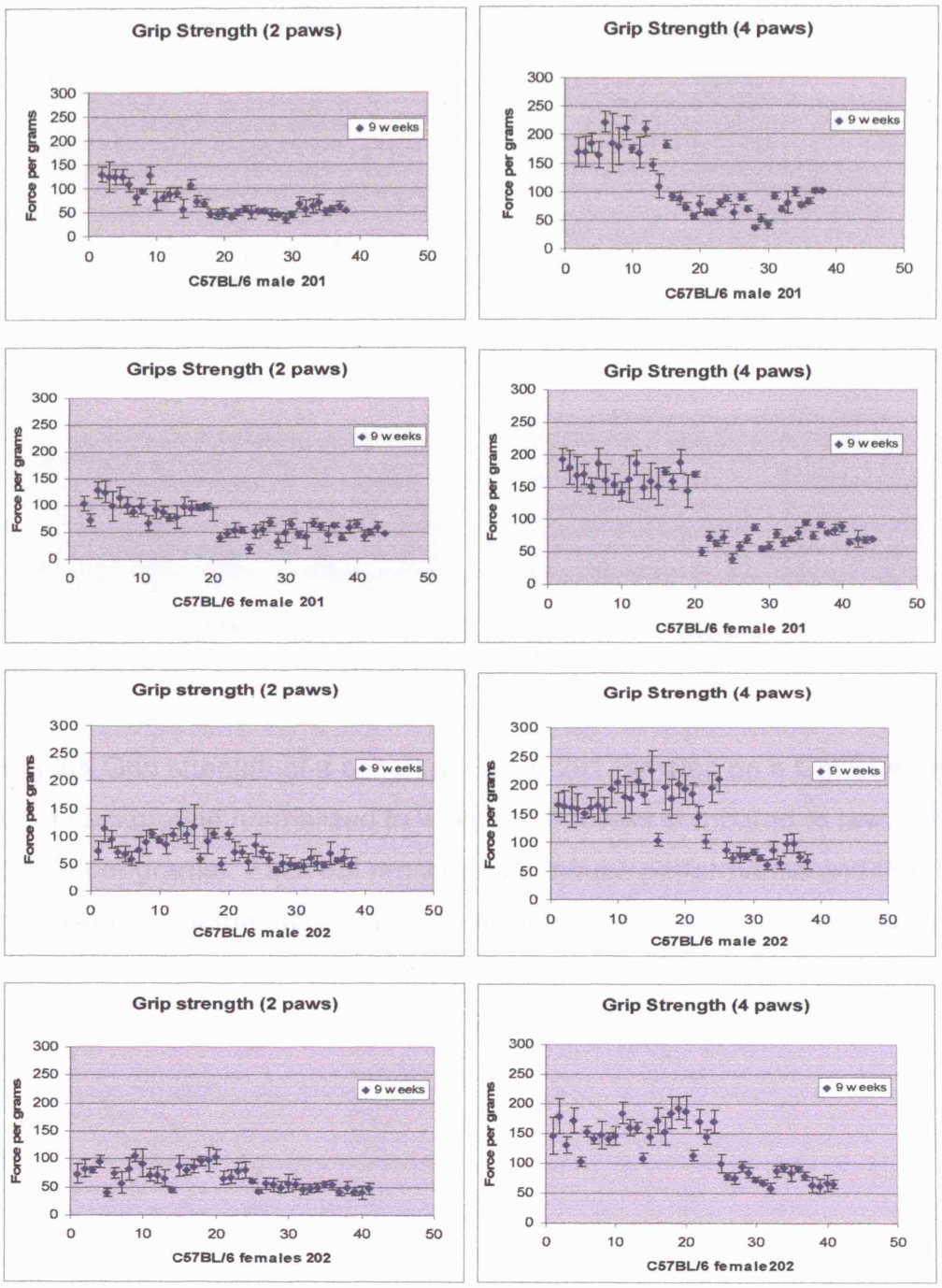

Fig 3.3 Grip strength performance of male and female GENA 201 and 79 GENA 202 N2 mice on a C57BL/6 background at 9 weeks of age. Each dot represents a mouse performance. Mice are in the same order on the "2 paws" and the "4 paws" graphs.

The animals underwent 2 paws and 4 paws trials. (n. male 201=37, n. female 201=43,n. male 202=38, n. female 202=41).

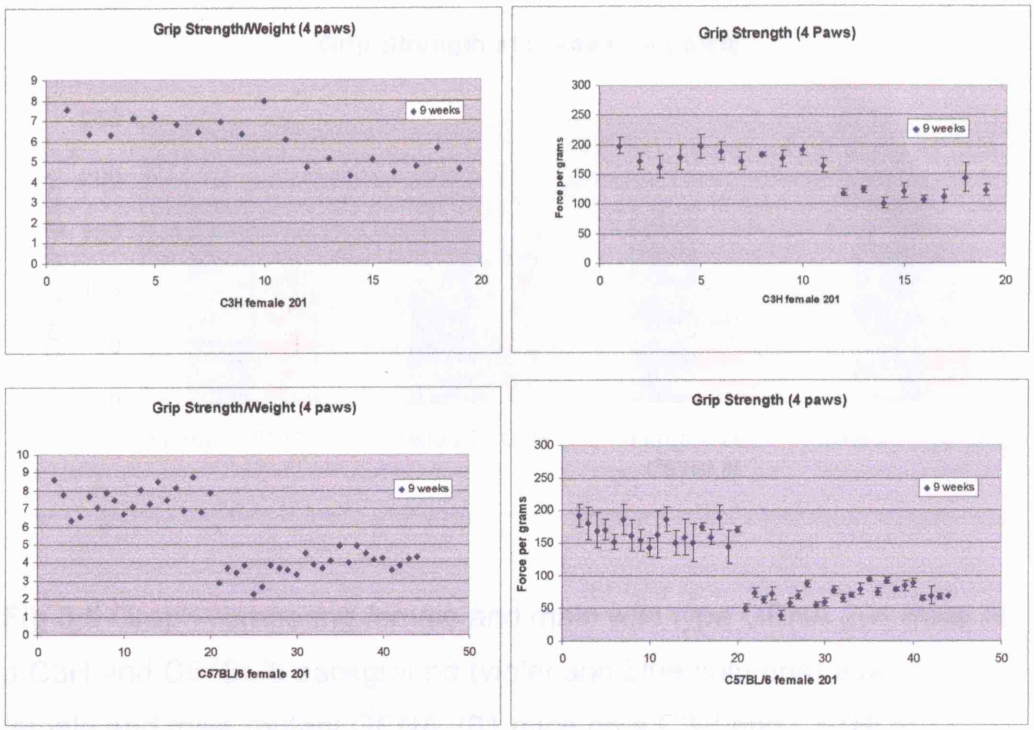

Fig 3.4 Grip strength of a cohort of GENA 201 females on a C57BL/6 and C3H background normalized to weight at 9 weeks compared to raw data (force per grams). Each dot represents a mouse performance and they represent the same order of mice in the normalized and raw data graphs.

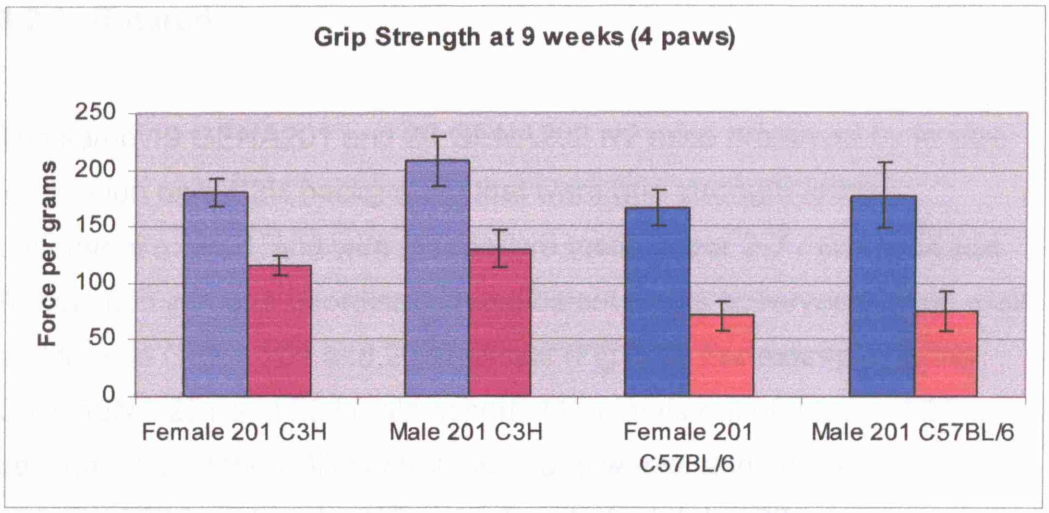

Fig 3.5 Graph comparing female and male wild type GENA 201 mice on a C3H and C57BL/6 background (violet and blue columns) against female and male mutant GENA 201 mice on a C3H and C57BL/6 background (bordeaux and pink columns). Significant difference was observed comparing C3H female mutants grip strength results to C57BL/6 female mutants (P=2.29E-07) and C3H mutant male grip strength results to C57BL/6 male mutants (P=0.004025). N. of C3H female 201 wild types=11, n. of C3H male 201 wild types=10, n. of C3H female 201 mutants=9, n. of C3H male 201 mutants=8, n. of C57BL/6 female 201 wild types=19, n. of C57BL/6 male 201 wild types=14, n. of C57BL/6 female 201 mutants=24, n. of C57BL/6 male 201 mutants=19.

3.2.2 Rotarod

The same 19 GENA201 and 26 GENA202 N2 mice produced by in vitro fertilization on a C3H background that were grip strength tested underwent rotarod and wire manoeuvre testing over 2-7 months of age. A reduction in motor coordination and balance was observed in both male and female GENA 201 and 202 animals (Fig 3.6). For example, in the C3H GENA 201 and 202 male cohort, 11 animals out of a total of 21 were beyond 3 SD of the C3H control mean at 9 weeks and, in the C3H GENA 201 and 202 female cohort, 8 animals out of a total of 23 mice were beyond 3 SD of the C3H control mean at 9 weeks. Like in the grip strength, GENA201 and 202 cohorts showed no significant differences from each other and thus data were combined into one "mutant" and one 'wild type littermate' control cohort

However, when the GENA 201 and 202 grip strength data were compared to the rotarod data at 9 weeks, not all animals with low grip strength showed a reduction in motor coordination. For example, in the C3H male 201 and 202 cohort, out of the 10 animals with poor grip strength only 6 showed reduced motor coordination, in the C3H female 201 and 202 cohort, out of the 11 animals with poor grip strength only 5 showed reduced motor coordintation (Fig 3.7). The poor correlation was also confirmed by plotting grip strength performance versus rotarod performance (Fig 3.8). The R-squared value of 0.0128, which is a measure of how well the regression equation fits the sample data, suggests that the equation does not fit the data very well and hence does not provide a good prediction of correlation. The closer R-squared is to 100%, the better the fit.

The reduced balance and motor coordination tested by the rotarod might not only be due to a muscle defect but by a mixture of neuromuscular, CNS, and equilibrium deficits. A mouse with poor grip strength showing a good performance on the rotarod test might suggest that the

neuromuscular, CNS and equilibrium properties are not affected and are counterbalancing a muscle deficit.

A cohort of N2 backcrossed GENA 201 mice on a C57BL/6 genetic background were rotarod tested at age 5 and 9 weeks. No difference was observed between the GENA 201 rotarod performance on a C3H background compared to rotarod performance on a C57BL/6 background (Fig 3.9) thus rotarod performance did not show a more severe phenotype on a C57BL/6 compared to C3H genetic background.

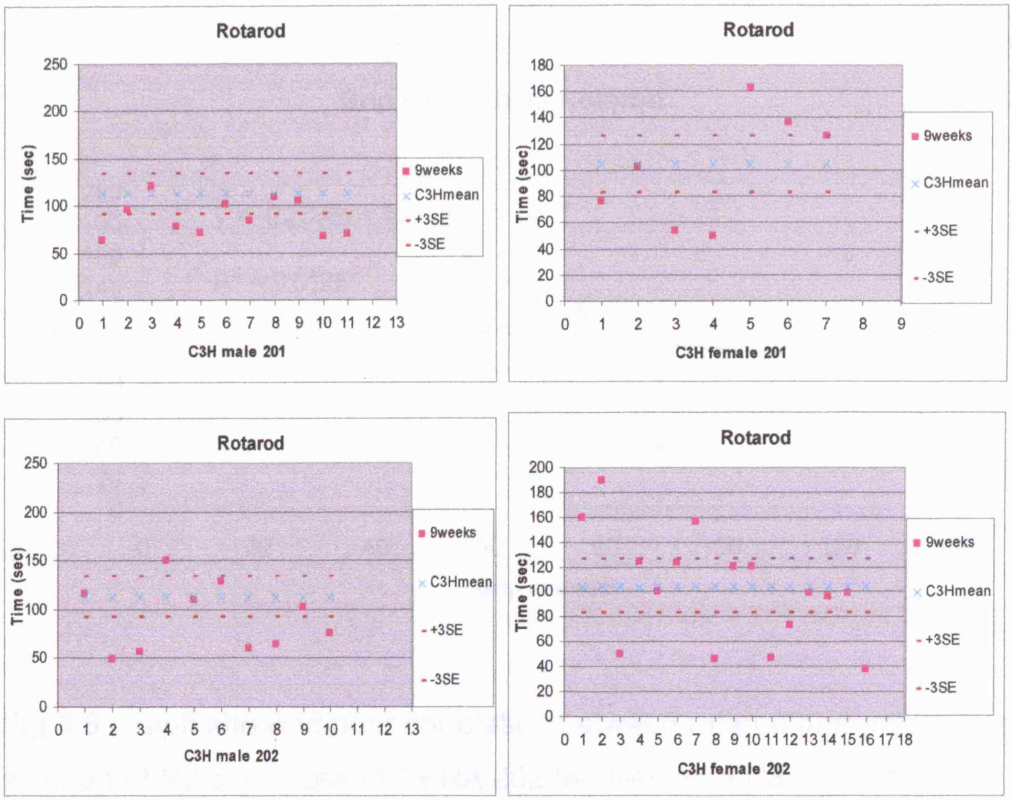

Fig 3.6 Rotarod performance of male and female GENA 201 and GENA 202 N2 individual mice over a period of 2-7 months on a C3H genetic background. The C3H control mean was at 9 weeks of age. N. male 201=11, n. female 201=7,n. male 202=10, n. female 202=16.

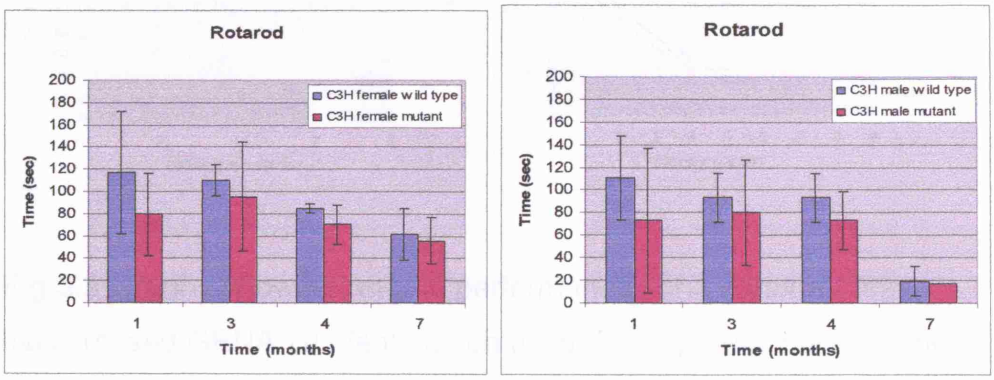

Fig 3.7 Rotarod performances of the poor grip strength male and female GENA 201 and 202 mice cohort on C3H background (mutants) compared to age-and sex-matched wild type littermates. N. of mice sampled varied with the time point: wild type n=3-12; mutant n=1-11.

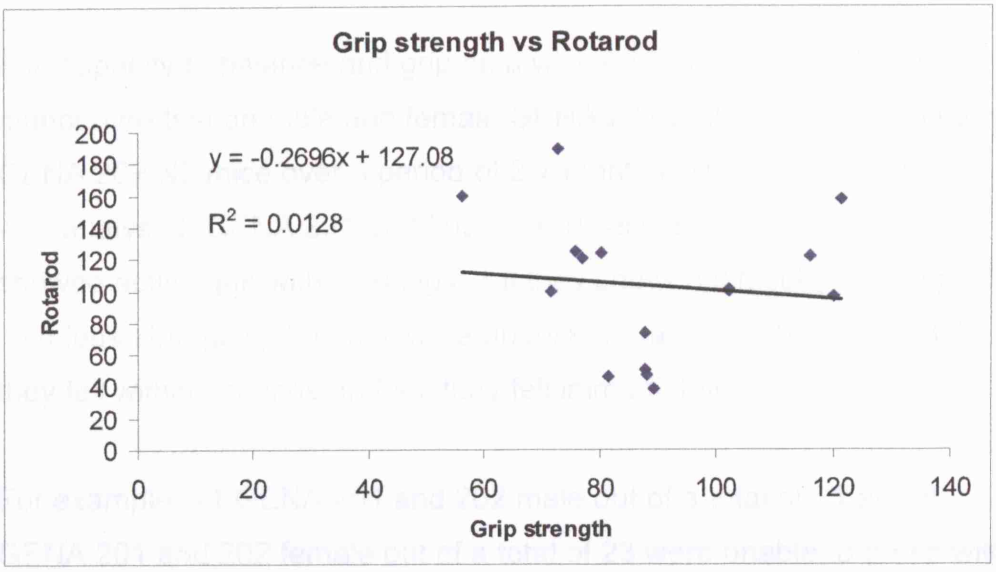

Fig 3.8 Graph showing poor correlation between rotarod performances of a cohort of N2 backcrossed GENA 202 females on a C3H genetic background and grip strength results on the same cohort of mice. Each dot represents a mouse performance. N. C3H female 201=7.

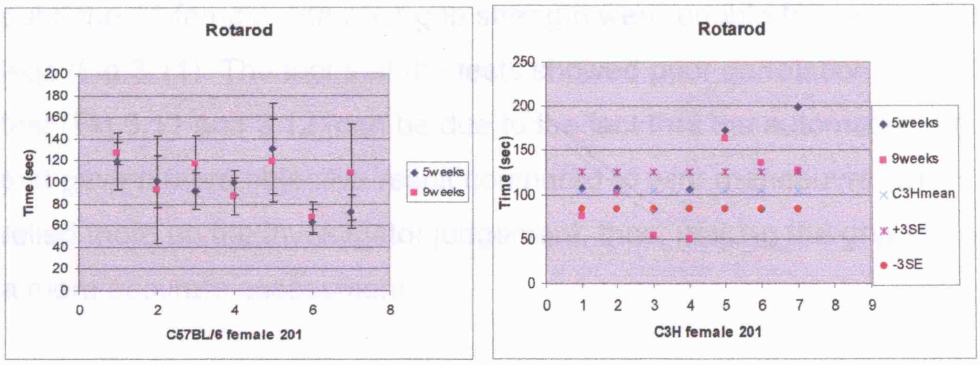

Fig 3.9 Graphs showing rotarod performances of a cohort of N2 backcrossed GENA 201 females on a C57BL/6 genetic background compared to rotarod performance of a N2 cohort of GENA 201 females on a C3H background. N.C57BL/6 female 201=7, n.C3H female 201=7.

3.2.3 Wire manoeuvre

The capacity to balance and grip on a wire was evaluated in the wire manoeuvre test on male and female GENA 201 and male and female GENA 202 N2 mice over a period of 2-7 months. The mean of 3 trials was analysed. GENA 201 and 202 mice received a score of 0 if they showed active grip with hind legs, 1 if they showed difficulty to grasp with hind legs struggling, 2 if they were unable to grasp with hind legs, 3 if they fell within seconds and 4 if they fell immediately.

For example, 11 GENA 201 and 202 male out of a total of 21 and 8 GENA 201 and 202 female out of a total of 23 were unable to grasp with hind legs. As no difference from male and female GENA 201 and 202 was observed, data were combined into one "mutant" and one 'wild type littermate' control cohort (Fig 3.10).

6 GENA 201 and 202 males out of the 10 males with poor grip strength were unable to grasp with hind limbs and 5 GENA 201 and 202 female out if the 11 female with poor grip strength were unable to grasp with hind legs (Fig 3.11). The fact that the tests showed poor correlation with grip test (Fig 3.11 and 3.12) can be due to the fact that the automated grip test gave a more objective result compared to wire manoeuvre which relied more on the investigator judgement, thus, making the grip strength a more accurate assessment.

A cohort of N2 GENA 201 mice on a C57BL/6 genetic background were tested at age 5 and 9 weeks. No difference in phenotype severity was observed between the GENA 201 wire manoeuvre performance on a C3H background compared to wire manoeuvre performance on a C57BL/6 background (Fig 3.13).

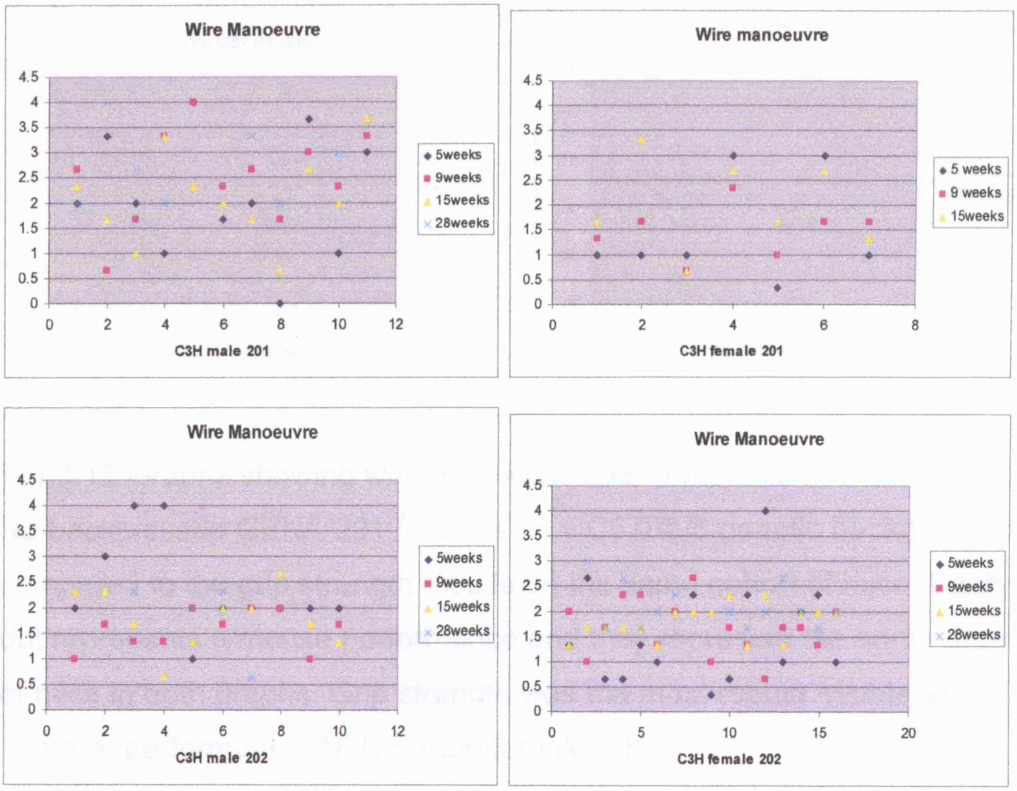

Fig 3.10 Wire manoeuvre performance of 19 GENA 201 and 26 GENA 202 N2 individual mice over a period of 2-7 months on a C3H genetic background. N. male 201=11, n. female 201=7,n. male 202=10, n. female 202=16.

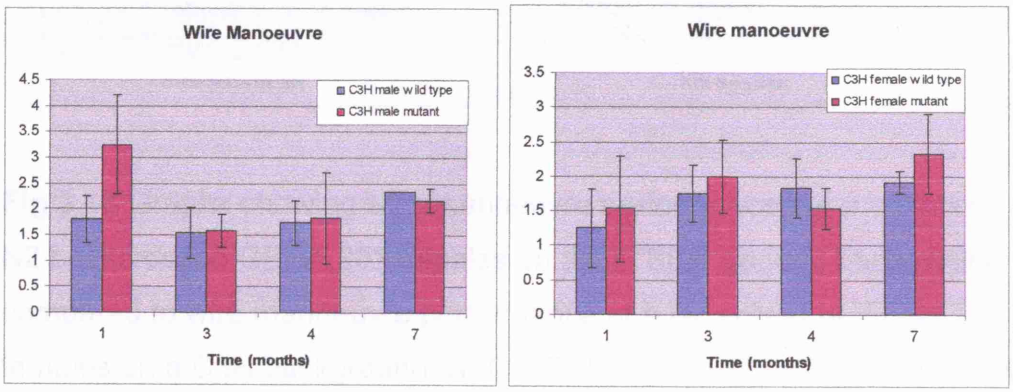

Fig. 3.11 Wire manoeuvre performance of poor grip strength male and female GENA 201 and 202 mice cohorts (mutants) on C3H background compared to age-and sex-matched wild type littermates. N. of mice sampled varied with the time point: wild type n=3-12; mutant n=1-11.

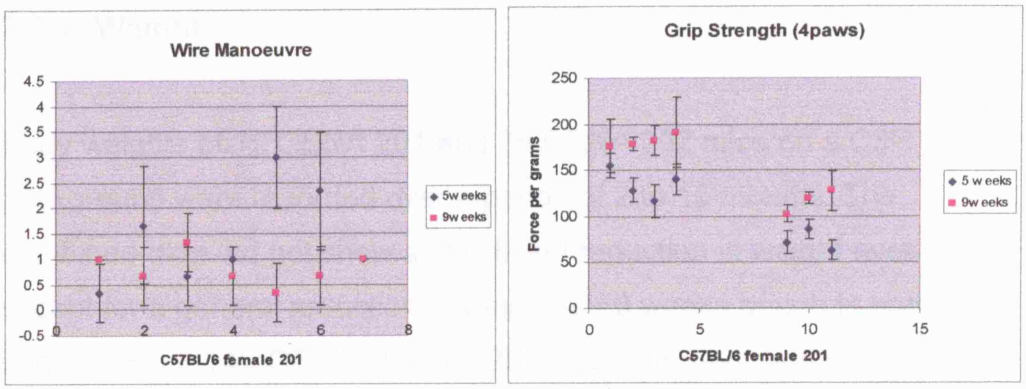

Fig 3.12 Graphs showing wire manoeuvre performances of a cohort of N2 backcrossed GENA 201 females on a C57BL/6 genetic background compared to the grip strength results on the same cohort of mice. Each dot represents a mouse performance and they represent the same order of mice in both graphs. Grip strength was the most robust 'visible' score of motor performance. N. C57BL/6 female 201=7.

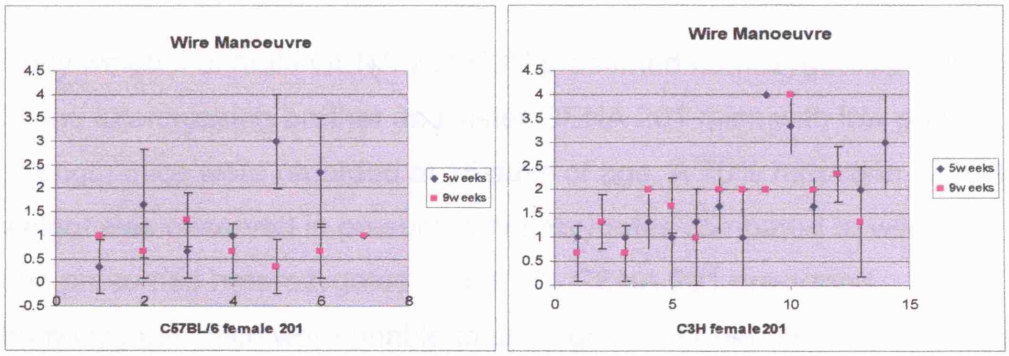

Fig 3.13 Graphs showing wire manoeuvre performances of a cohort of N2 backcrossed GENA 201 females on a C57BL/6 genetic background compared to wire manoeuvre performance of a N2 cohort of GENA 201 females on a C3H background. N. C57BL/6 female 201=7, n.C3H female 201=14.

3.2.4 Weight

Body weights of 19 GENA 201 and 26 GENA 202 mice on a C3H background were recorded over a period of 2 to 15 months. The combined data did not show a significant reduction in weight over time except for a general reduction in weight at 60 weeks of age in both cohorts (Fig 3.14). GENA 201 and 202 mice with poor grip strength did not show a significant reduction in body weight compared to wild type littermates (Fig 3.15), making weight measurements not useful when scoring affected and unaffected mice.

On a C57BL/6 genetic background GENA 201 and GENA 202 mice did not show a significant reduction of body weight compared to wild type littermates when tested at 9 weeks. However, they were slightly lighter compared to a C3H genetic background, although the difference was not significant (Fig 3.16).

Body weights of male GENA 201 C3H presumed homozygotes produced by the intercrossing brother and sister GENA 201 mice with low grip strength mice were recorded at 15 days of age. A 70% reduction in body weight was observed in presumed homozygotes compared to wild type and presumed heterozygotes (Fig 3.17). GENA 201 presumed homozygotes mice were unable to undergo further behavioural screen as the phenotype was more severe compared to litter mates control as explained in more detail in the breeding behaviour section.

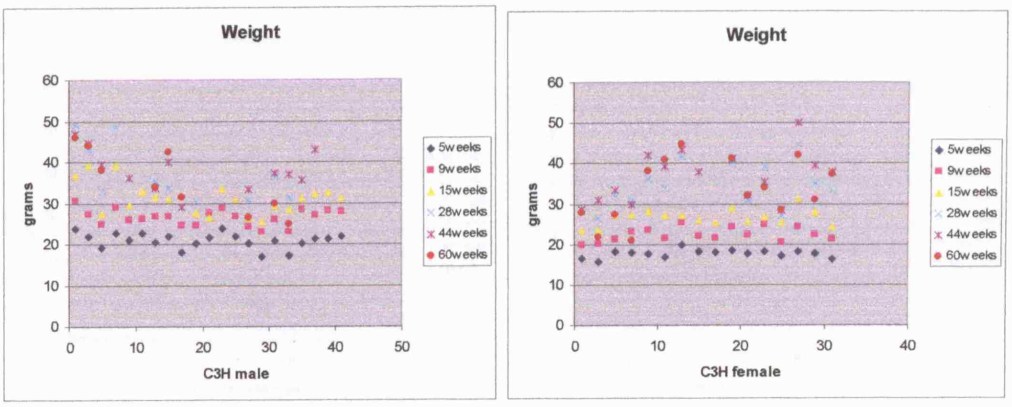

Fig 3.14 Graphs showing recorded weight of 21 GENA 201 and 201 males and 16 GENA 201 and 202 females N2 mice over a period of 2-15 months. Each dot represents a color coded performance of mice at different ages.

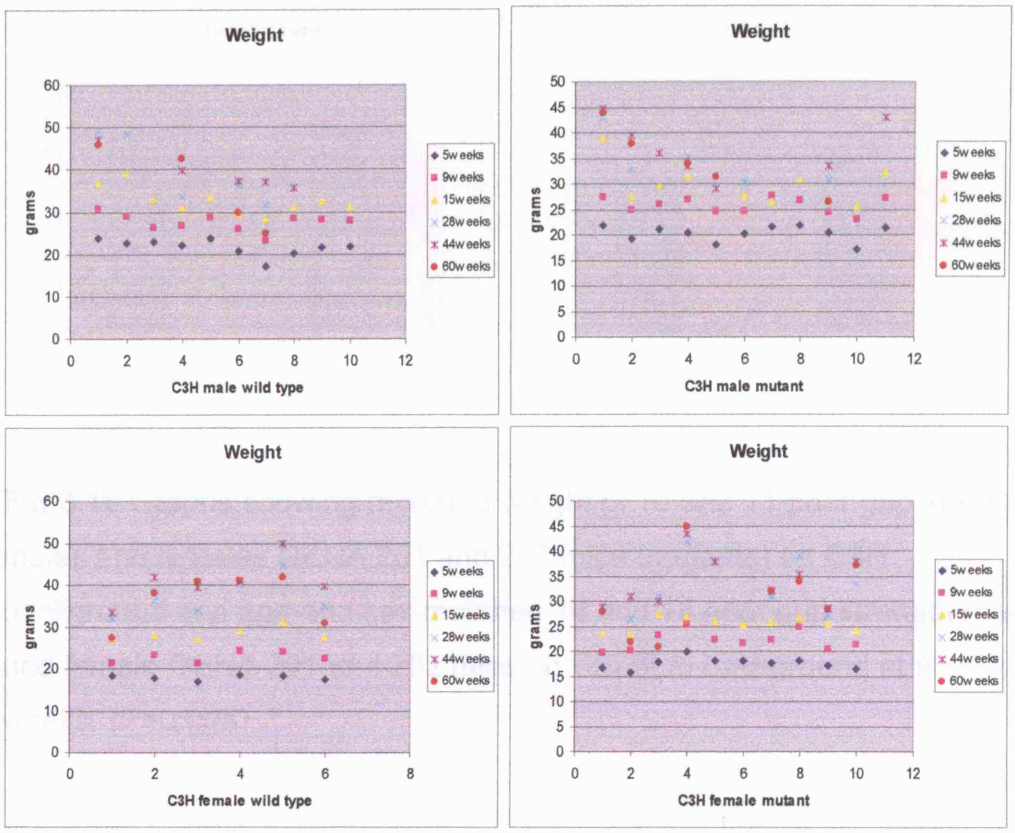

Fig 3.15 Graph showing recorded weight of poor grip strength male and female GENA 201 and 202 mice (mutants) on C3H background compared to age-and sex-matched wild type littermates. Numbers of mice sampled varied with the time point: wild type n=3-7; mutant n=4-11 over a period of 2-15 months.

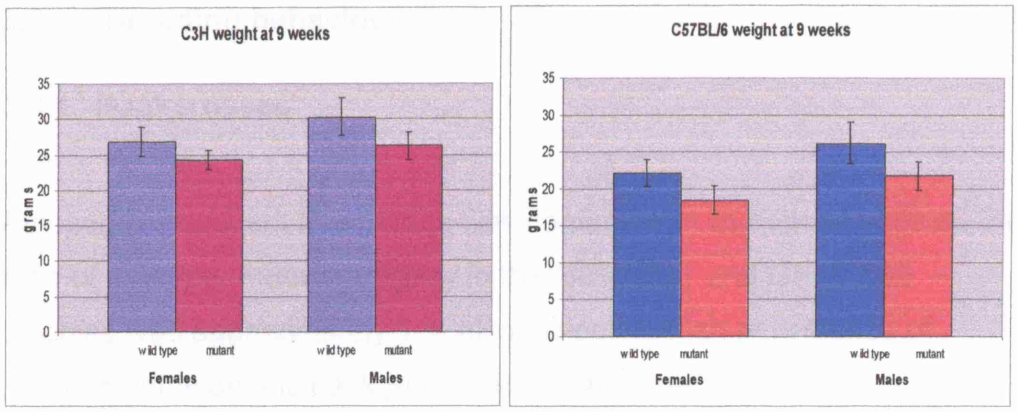

Fig 3.16 Graphs showing recorded weight of 10 and 11 poor grip strength males and females GENA 201 and 202 mice (mutants) on C3H background and age-and sex-matched 16 and 14 poor grip strength male and female GENA 201 and 202 mice on C57BL/6 background at 9 weeks. (P>0.005)

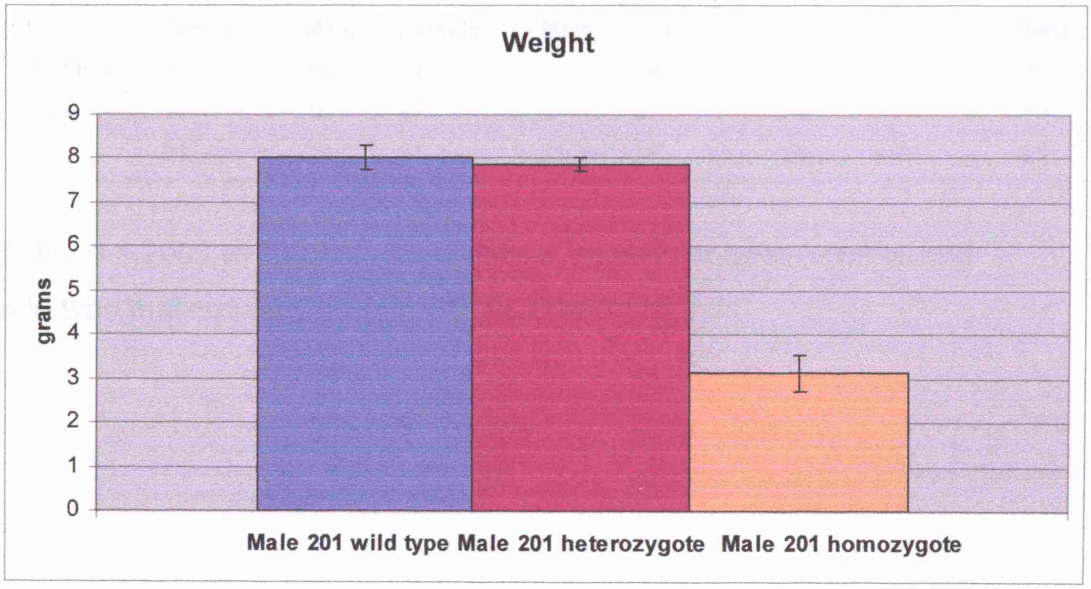

Fig 3.17 Graph showing the weight of 3 15 day old male C3H GENA 201 wild types, 3 15 days old male C3H GENA 201 presumed heterozygotes and 3 15 day old male C3H GENA 201 presumed homozygotes. A significant reduction in weight was observed in presumed homozygotes (P value <0.05).

3.3 Breeding behaviour

3.3.1 Backcrosses

Autosomal dominant inheritance was confirmed from both siblings as the ratio of wildtype: mutant progeny in the GENA201 and GENA202 colonies was approximately 1:1, also indicating high penetrance of heterozygotes on this background at the N2 generation.

Several C3H N2 GENA201 and GENA202 affected mice were crossed to C57BL/6J mates and autosomal dominant inheritance was also confirmed on this background (Table 3.1)

	C3H				C57BL/6				
	GENA201		GENA202		GENA201		GENA201		
	Female	Male	Female	Male	Female	Male	Female	Male	
Wild type	20	14	14	10	24	17	25	25	149
Mutant	11	15	17	11	30	26	16	13	139
Total	31	29	31	21	54	43	41	38	288

Table 3.1 2003 to 2005 breeding data summary for heterozygote and wild type matings on C3H and C57BL/6 backgrounds.

3.3.2 Intercrosses

Intercrosses were set up on both a C57BL/6 and C3H background as it was of interest to establish whether homozygotes mice were viable and to investigate their phenotype relative to that of wild type and heterozygote offspring.

A total of 76 progeny were produced from 7 C57BL/6 intercross matings and a total of 60 progeny were produced from 7 C3H intercross matings (Table 3.2).

Offspring were phenotyped for visible abnormality from birth to weaning. A distinguishable phenotype was observed in 4 offsprings from the total C57/BL6 progeny and in 7 offsprings from the total C3H progeny which was never observed previously. These animals showed reduced body weight and severely impaired limb movement. The phenotype was so severe that the pups had to be culled according to Home Office regulations before weaning (15 days of age) as they could not reach for food.

The presence of intercross offspring with a more severe phenotype than that of heterozygotes mice lent substantial support to the supposition that these animals were homozygotes and that the mutation underlies an impaired motor phenotype.

Intercrosses						
Genetic background	Intercross ID	Date of birth	Wild types	Heterozygotes	Homozygotes	Tot
C57BL/6						
	Mating A	12/11/2005	2	5		7
		19/11/2005		4		4
	Mating B	10/11/2005	4	5		9
		22/12/2005	2	3		5
	Mating C	02/10/2005	4	3		7
		10/11/2005	5	4		9
		19/12/2005	2	5		2
	Mating D	05/03/2007	3	5	1	10
	Mating E	28/02/2007	2	4	1	7
	Mating F	02/03/2007	2	3	1	6
	Mating G	10/03/2007	2	3	1	6
	Total		**28**	**44**	**4**	**76**
C3H						
	Mating A		2	3		5
		11/10/2005		2		2
		01/11/2005	2	1		3
		19/12/2005		3	1	3
		09/01/2006	1	4		5
	Mating B	03/11/2005	1	3		4
		25/11/2005	2	2		4
		31/12/2005		1		1
	Mating C		2	3		5
			2	2	2	4
	Mating D	06/06/2006				
		27/0	3	2		5
		6/20				
		06				
		18/0		3		3
		7/20				
		06				
	Mating E	11/10/2006	1	2	1	3
			1	2	1	3
	Mating F					
		09/11/2006	1	3	2	4
	Mating G	29/11/2006	5	1		6
	Total		**23**	**37**	**7**	**60**

Table 3.2 Breeding summary of intercross matings on C57BL/6 and C3H backgrounds.

3.4 Concluding remarks

The results from the behavioural screen provided valuable data towards the phenotypically characterization of GENA 201 and 202 mice identified during a routine screen in a large ENU mutagenesis project at the MRC Mammalian Genetics Unit, Harwell UK.

Firstly, a significant reduction in grip strength was seen in both male and female GENA 201 and 202 mice compared to sex-matched wildtype littermates from 1 to 15 months of age on both C3H and C57BL/6 backgrounds. However, the phenotype was considerably more pronounced on the C57BL/6 background than the C3H genetic background. This indicates that genetic modifiers segregating between the C3H/HeH and C57BL/6J backgrounds are having a pronounced effect on phenotype.

As there was poor correlation when comparing results of each individual test, grip strength, measured using all 4 paws, was selected as the most robust 'visible' score of motor performance that defined 'affected' and 'unaffected' GENA201 and 202 mice. The affected mice DNA was used in the genetic mapping discussed in the next chapter.

The poor correlation between tests might be due to the fact that each test measures different variables. For example, a mouse with poor grip strength showing a good performance on the rotarod test might suggest that the neuromuscular, CNS and equilibrium properties are not affected and are counterbalancing a muscle deficit. In conclusion, although in some case grip strength and rotarod tests can be correlated successfully, for example in the Huntington mouse model (personal communication by Dr A Acevedo-Arozena), it is not always the case.

As a reduction in grip strength could be observed in mutant GENA 201 and 202 mice as early as 5 week of age, a progressive and late onset phenotype could not be confirmed, suggesting instead a possibility of a developmental defect. To confirm such hypothesis, timed mating were set up in collaboration with Christiana Ruhrberg from the Institute of Ophthalmology, UCL, London, which involved a time controlled pairing of a mutant female GENA 201 and 202 with a C57BL/6 male. This was done to monitor the gestation period of the female in order to extract embryos at specific time points. Although, wholemount neurofilament staining, which reveals defects in the embryo's nervous system, did not show any obvious abnormalities in the peripheral nervous system of 4 heterozygotes embryos at 12.5 dpc (Christiana Ruhrberg, personal communication), more embryonic time points should be studied to definitely rule out the possibility of a developmental defect.

To better understand the reduced grip strength phenotype in the GENA 201 and 202 mice a further behavioural test was done in collaboration with Dr Valter Tucci from MRC Mammalian Genetics Unit, Harwell UK, by measuring performance in an assay for skilled motor function: the Mouse Reaching and Grasping test, MoRaG, (Tucci et al. 2007).

Among other parameters, MoRaG is used to assess forepaw reaching and grasping motor phenotypes and revealed interesting differences between GENA 201 and 202 mice and wildtype littermate controls on the C3H background (Dr Tucci personal communication).

Over a number of sessions mice are trained to reach through a narrow opening using their forepaws to retrieve food pellets. Quantitative analysis revealed a statistically significant increase ($P<0.05$) in the latency to the first reaching (LFR), an indication of decreased motor flexibility (Dr Tucci personal communication).

Furthermore, the percentage of errors in grasping food pellets was approximately 40% higher in the mutants compared to control mice

evident in the first session and sustained (more than 30% higher) during the second session. No significant difference for the accuracy in reaching the target was observed on the first session between the two groups. However, the wildtype group showed a reduction in percentage errors in the second session, an index of motor improvement, whereas mutants mice maintained a low performance in both sessions. Thus the mutant mice have decreased motor flexibility and a diminution in fine motor control (Dr Tucci personal communication).

The intercross produced wild types and heterozygotes as well as a subset of offspring with a more severe motor phenotype. Subsequent genotyping revealed that these mice were homozygous for a T to C transition in the glycyl-tRNA synthetase (*Gars)* gene.

The backcross mating produced roughly equal numbers of wild type and heterozygous mutant offspring (1:1) suggesting an autosomal dominant inheritance while intercross matings produced 4 homozygous mice (5%) out of a total of 76 progeny on a C57BL/6 background and 7 homozygous mice (12%) out of a total of 60 on a C3H background which is significantly reduced from the expected 25% suggesting that the mutation is causing substantial loss of homozygotes.

4. Chapter 4: Genetic mapping

4.1 Introduction

Genetic linkage can be demonstrated in mice through breeding experiments in which one or both parents are detectably heterozygous at each of the loci under investigation. The backcross is the simplest form of linkage analysis as only one parent is heterozygous at each of two or more loci, and the other parent is homozygous at these same loci. As a result, segregation of alternative alleles occurs only in the gametes that derive from one parent, and the genotypes of the offspring provide a direct determination of the allelic constitution of these gametes. This greatly simplifies the interpretation of genetic data because it allows one to jump directly from the genotypes of offspring to the frequencies with which different meiotic products are formed by the heterozygous parent.

The use of inbred mouse strains simplified the linkage analysis of the backcross progeny. The founder animals (F1s) of GENA 201 and 202 were BALB/cAnN x C3H/HeH. All progeny of F1 mice mated to C3H were obligate BALB/c x C3H heterozygotes at the mutation-affected locus. Recombination events and the presence of C3H homozygosity excluded unlinked areas. Once linkage was found, microsatellite markers and more SNPs markers (Appendix 2) that spanned the critical region were genotyped to narrow down the region. Primer sequences and information regarding microsatellite marker polymorphisms between relevant mouse strains was obtained using the Mouse Genome Informatics genes and markers database (http://www.informatics.jax.org/).

4.2 Genome scans

A positional cloning protocol was used to identify the mutation in the GENA201 and GENA202 colonies. It was likely both animals carried the same mutation as they were siblings derived from the same father and had indistinguishable phenotypes on all tests carried out, but nevertheless

the formal possibility remained that they had different mutations that had arisen either on the G0 BALB/c male background or on the female C3H background to which the male had been crossed.

DNA was extracted from 13 N2 GENA 201 and 13 202 mutant tail samples. The mutant DNA, as well as DNA from control F1 mice and BALB/c and C3H background strains was genotyped for 72 polymorphic genome wide SNPs markers (listed in Appendix 1).

Initial genotyping revealed an area of linkage on chromosome (Mmu) 6. All mutants were heterozygous between 22 and 114Mb (GENA201) and 22 and 84Mb (GENA202) (Fig 4.1). Although at the start of the project we were told by the MRC Harwell that GENA 201 and 202 were on a N2 generation, the results from the genome scan indicated that this is not the case and that the progenies are the product of more backcrosses. Although linkage was found, highly backcrossed progenies are not ideal for initial linkage analysis. This is due to the fact that by significantly backcrossing to the C3H background and, thus diluting the BALB/cAnN background, the markers which span the whole genome might exclude the region of heterozygosity between BALB/c x C3H. The whole genome scan results are listed in Appendix 4.

4.3 Fine mapping

To refine the mapping and reduce the critical region, haplotype mapping of 61 (GENA201) and 29 (GENA202) affected mice was carried out

The critical region was narrowed by using a higher density set of polymorphic SNPs and microsatellite markers (D6Mit273 (46Mb), D6Mit183 (53Mb), D6Mit384 (55Mb), D6Mit186 (73Mb), D6Mit188 (75Mb)) to haplotype map 61 affected animals from both the C3H (N3) and C57BL/6 (N2) background for GENA201 and 29 affected mice from the C3H (N3) and C57BL/6 (N2) background for GENA202. Results from this haplotype analysis showed the mutation must lie within the critical

region defined by SNPs at 53Mb and 73Mb for GENA201 and at 53Mb and 58Mb for GENA202 mice (Fig 4.2 and Fig 4.3).

The fact that affected mice bred on C57BL/6 background showed to be heterozygous within the critical region suggested that the mutation arose on a BALB/c background rather than a C3H background (Fig 4.3). In addition, the advantage of breeding GENA 201 and 202 on a different background (C57BL/6) consisted in a wider range of polymorphic markers available. The combined results of both maps identified a small enough critical region to start analysing for candidate genes.

GENA 201		CHROMOSOME 6		
SNP_Mb	22	52	84	114
C3H	A	G	A	G
BALB/c	C	T	G	A
132.2c	1	2	2	1
132.2f	2	2	2	1
201d.3f	2	2	2	1
201d.3g	2	2	2	2
201d.5e	2	2	2	2
201d.5f	2	2	2	1
201d.5g	2	2	2	2
201d.6f	1	2	2	2
201d.5d	1	2	2	2
201d.2d	2	2	1	1
132.2a	2	2	2	1
132.1b	2	2	2	1
132.3a	2	2	2	1

GENA 202		CHROMOSOME 6			
SNP_Mb	22	52	84	114	146
C3H	A	G	A	G	T
BALB/c	C	T	G	A	G
371.3b	1	2	2	1	f
373.2f	1	2	2	1	2
202k.3d	1	2	2	1	2
373.1b	1	2	2	1	2
373.3f	1	2	2	1	1
373.3h	f	2	2	1	1
202k.2b	1	2	2	1	1
373.2b	1	2	2	1	1
373.2c	1	2	2	1	1
373.2c	1	2	1	1	1
373.2d	1	2	2	1	1
373.3b	1	2	2	1	1
373.3c	1	2	1	1	1

Fig 4.1 Initial haplotype obtained following GENA 201 and GENA 202 linkage analysis.

(1=homozygous; 2= heterozygous and f=failed).

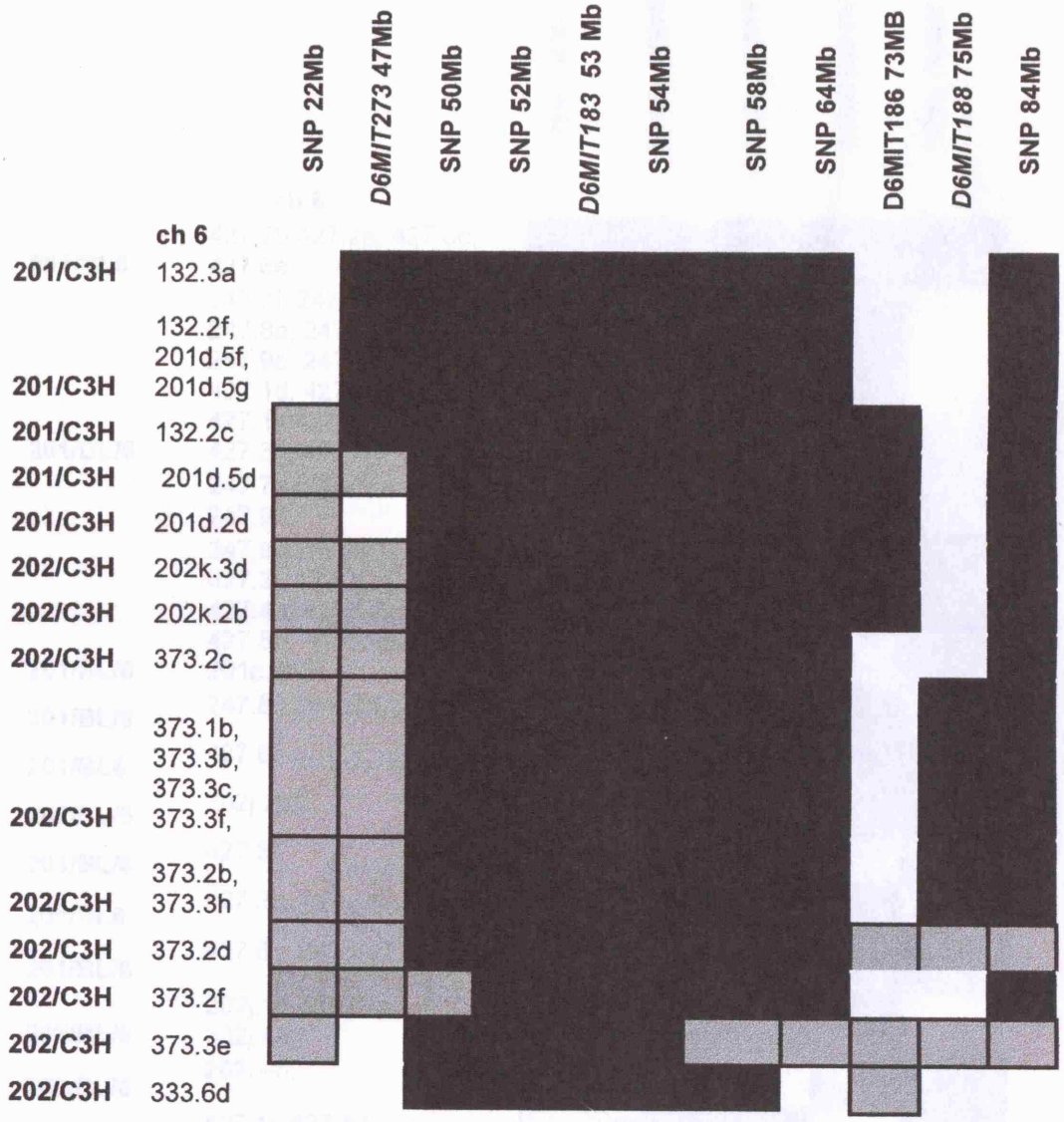

Fig 4.2 Haplotype obtained following GENA 201 and 202 linkage analysis and attempts to narrow down the region of interest on Mmu 6 using affected mice on a C3H background (all map positions according to MGI).

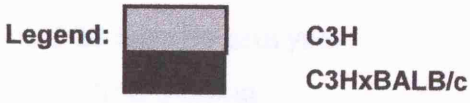

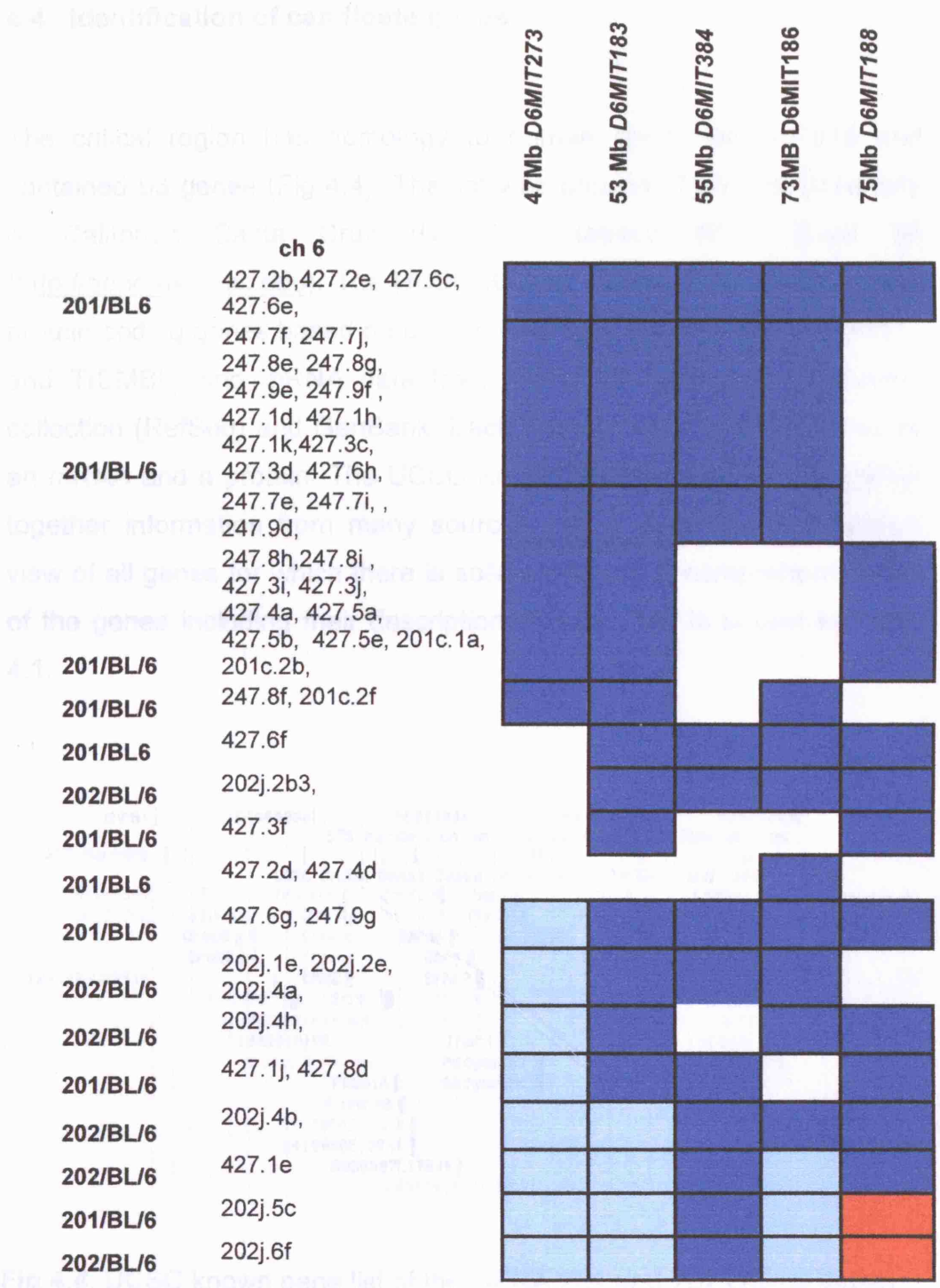

Fig 4.3 Haplotype obtained following GENA 201and 202 linkage analysis and attempts to narrow down the region of interest on Mmu 6 using affected mice on a C57BL/6 background (all map positions according to MGI).

4.4 Identification of candidate genes

The critical region has homology to human chromosome 7p15 and contained 63 genes (Fig 4.4). The list was obtained from the University of California Santa Cruz (UCSC) database NCBI Build 36 (http://genome.ucsc.edu). The UCSC Known Genes track shows known protein-coding genes based on protein data from UniProt (SWISS-PROT and TrEMBL) and mRNA data from the NCBI reference sequences collection (RefSeq) and GenBank. Each known Gene is represented by an mRNA and a protein. The UCSC Known Genes track tries to gather together information from many sources into a non-redundant unified view of all genes for which there is solid evidence. A comprehensive list of the genes including their description and function is shown in Table 4.1.

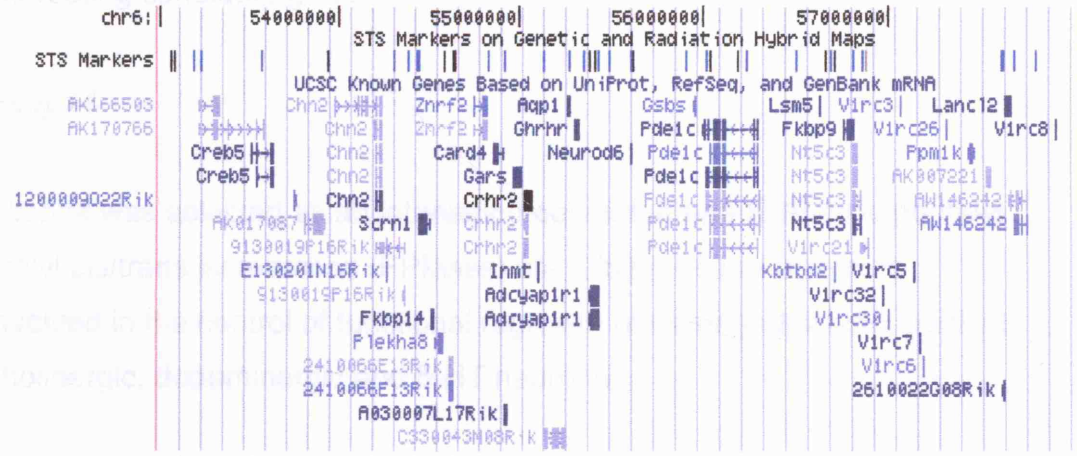

Fig 4.4. UCSC known gene list of the GENA 201 and 202 critical region (http://genome.ucsc.edu).

Although any gene in the minimal interval initially qualified as a candidate, the addition of further genetic, genomic, or biochemical data from the literature relevant to the GENA 201 and 202 low grip strength

phenotype was useful to the prioritization of potential candidate genes for mutation detection analysis

Creb5

A role of *Creb* in neurodegenerative diseases has been shown in mice with disrupted *Creb1*. Mice showed progressive neurodegeneration in the hippocampus and in the dorsolateral striatum (Mantamadiotis et al. 2002).

In addition, in a transgenic mouse model of ALS expressing the G86R mutant superoxide dismutase 1 (mSOD1), CREB-binding protein (CBP) levels were specifically decreased in nuclei of degenerating motor neurons. It was shown that oxidative stress and mSOD1 overexpression can disrupt CBP levels by transcriptional repression, in an motorneuron-derived cell line (Rouaux et al. 2007). This data qualified *Creb 5* as an interesting candidate gene.

Fkbp14

Fkbp14 was selected as an interesting candidate as FKBP-type peptidyl prolyl cis/trans isomerases (PPIases) are folding helper enzymes involved in the control of functional regrowth of damaged sciatic, cortical cholinergic, dopaminergic and 5-HT neurones.

It was shown that the constitutively inactive human FK506-binding protein 38 (FKBP38) was capable of responding directly to intracellular Ca2+ rise through formation of a heterodimeric Ca2+/calmodulin/FKBP38 complex. This complex displayed affinity for Bcl-2 mediated through the PPIase site. Association between Bcl-2 and the active site of Ca2+/calmodulin/FKBP38 regulated Bcl-2 function and thereby participated in the promotion of apoptosis in neuronal tissues (Edlich et al. 2005).

FKBP38 was also shown to be a presenilins 1 and 2 (PS1/2)-interacting protein. PS1/2 is the causative molecules for familial Alzheimer's disease (FAD). PS1/2 and FKBP38 form macromolecular complexes together with anti-apoptotic Bcl-2 and PS1/2 promotes the degradation of FKBP38 and Bcl-2 and sequesters these proteins in the ER/Golgi compartments, thereby inhibiting FKBP38-mediated mitochondrial targeting of Bcl-2 via a gamma-secretase-independent mechanism (Wang et al. 2005).

Alpha2-chimaerin (Chn2)

The morphological and functional differentiation of neuronal dendrites is controlled through transcriptional programs and cell-cell signalling. The signalling pathways that couple neuronal activity and morphological changes in dendrites were not well understood until chimaerin protein function was explored. Alpha1-chimaerin is a neuronal diacylglycerol-binding protein with a Rho GTPase-activating protein domain that inactivates Rac1.

It was observed that stimulation of phospholipase Cbeta-coupled cell surface receptors recruited alpha1-chimaerin to the plasma membrane of cultured hippocampal neurons. Alpha1-chimaerin protein levels were controlled by synaptic activity and that increased Alpha1-chimaerin expression resulted in the pruning of dendritic spines and branches. This pruning activity required both the diacylglycerol-binding and Rac GTPase-activating protein activity of alpha1-chimaerin and suppression of alpha1-chimaerin expression resulted in increased process growth from the dendritic shaft and from spine heads (Hall et al. 1993).

As alpha1—chimaerin was shown to be an activity-regulated Rho GTPase regulator that contributes to pruning of dendritic arbors, alpha2-chimaerin (*Chn2*) was also considered as a potential candidate gene.

Adenylate cyclase activating polypeptide 1 (Adcyap1r1)

Adcyap1r1 is a hormone that was originally isolated from sheep hypothalamus on the basis of its ability to stimulate adenylate cyclase in rat anterior pituitary cell cultures.

Adcyap1r1 represented a good candidate as it is present not only in the central nervous system but also in peripheral tissues and it was shown to function as a neuromodulator/neurotransmitter in the central and peripheral nervous systems (Hosoya et al. 1993).

Neurogenic differentiation 6 (Neurod6)

Neurod6 function in the mammalian nervous system has not been determined. Nevertheless, *Neurod6* was an interesting candidate as Liu et al. (2000) showed that mice homozygous for a deletion of the *NeuroD* gene failed to develop a granule cell layer within the dentate gyrus, one of the principal structures of the hippocampal formation.

Using immunocytochemical markers in the deficient mice, the authors showed that the early cell populations in the dentate gyrus were present and appeared normally organized. The migration of dentate precursor cells in newly born granule cells from the neuroepithelium to the dentate gyrus remained intact. However, there was a dramatic defect in the proliferation of precursor cells once they reached the dentate, and a significant delay in the differentiation of granule cells. This led to malformation of the dentate granule cell layer and excess cell death.

The homozygous-null mice exhibited spontaneous limbic seizures associated with electrophysiologic evidence of seizure activity in the hippocampus and cortex. These findings establish a critical role of NeuroD in the development of a specific class of neurons. Furthermore, failure to express NeuroD leads to a pattern of pathological excitability of the adult central nervous system.

Mouse gene	Description (if known)	Function (if known)
AK166503	Mammary gland RCB-0527 Jyg-MC(B) cDNA, RIKEN full-length enriched library, clone:G930038G11 product:similar to Hypothetical 2Fe-2S ferredoxin/zinc finger.	
AK170766	NOD-derived CD11c +ve dendritic cells cDNA, RIKEN full-length enriched library, clone:F630118P09 product:hypothetical Zn-finger, C2H2 type/Zinc finger C2H2 type domain profile containing protein, full insert sequence.	
Creb5	cAMP responsive element binding protein 5	Binds to the cAMP response element and activates transcription
1200009O22Rik	hypothetical protein LOC66873	
AK017087	Adult male testis cDNA, RIKEN full-length enriched library, clone:4933436L16 product:similar to CARBOXYPEPTIDASE, VITELLOGENIC- LIKE.	
9130019P16Rik	hypothetical protein LOC378878	
E130201N16Rik	RIKEN cDNA E130201N16	
9130019P16Rik	Adult male cecum cDNA, RIKEN full-length enriched library, clone:9130019P16 product:hypothetical protein, full insert sequence.	
Fkbp14	FK506 binding protein 14	PPIases accelerate the folding of proteins during protein synthesis
Plekha8	pleckstrin homology domain containing, family A	
2410066E13Rik	2410066E13Rik protein	
A030007L17Rik	hypothetical protein LOC68252	
C330043M08Rik	13 days embryo lung cDNA, RIKEN full-length enriched library, clone:D430031F07 product:hypothetical protein, full insert sequence.	
Znrf2	zinc finger/RING finger 2	Ubiquitin conjugation; third step
Chn2	chimerin	GTPase-activating protein for p21-rac
Scrn1	secernin 1	Regulates exocytosis in mast cells. Increases both the extent of secretion and the sensitivity of mast cells to stimulation with calcium
Card4	Caspase recruitment domain-containing protein 4.	Enhances caspase-9-mediated apoptosis. Induces NF-kappa- B activity via RICK (CARDIAK, RIP2) and IKK-gamma. Confers responsiveness to intracellular bacterial lipopolysaccharides (LPS)
Gars	glycyl-tRNA synthetase	ATP + glycine + tRNA(Gly) = AMP + diphosphate + glycyl-tRNA(Gly).
Crhr2	corticotropin releasing hormone receptor 2	This is a receptor for corticotropin releasing factor. Shows high-affinity CRF binding. Also binds to urocortin I, II and III. The activity of this receptor is mediated by G proteins which activate adenylyl cyclase

Inmt	indolethylamine N-methyltransferase	Catalyzes the N-methylation of tryptamine and structurally related compounds
Adcyap1r1	adenylate cyclase activating polypeptide 1	This is a receptor for PACAP-27 and PACAP-38. The activity of this receptor is mediated by G proteins which activate adenylyl cyclase. May regulate the release of adrenocorticotropin, luteinizing hormone, growth hormone, prolactin, epinephrine, and catecholamine. May play a role in spermatogenesis and sperm motility. Causes smooth muscle relaxation and secretion in the gastrointestinal tract
Aqp1	aquaporin 1	Forms a water-specific channel that provides the plasma membranes of red cells and kidney proximal tubules with high permeability to water, thereby permitting water to move in the direction of an osmotic gradient
Ghrhr	growth hormone releasing hormone receptor	Receptor for GRF, coupled to G proteins which activate adenylyl cyclase. Stimulates somatotroph cell growth, growth hormone gene transcription and growth hormone secretion
Neurod6	neurogenic differentiation 6	Neurogenic differentiation factor 6 (NeuroD6) (Protein atonal homolog 2) (Helix-loop-helix protein mATH-2) (MATH2) (NEX-1 protein)
Pde1c	Calcium/calmodulin-dependent 3',5'-cyclic nucleotide phosphodiesterase 1C	High affinity cAMP and cGMP calmodulin-dependent phosphodiesterase
Lsm5	LSM5 homolog, U6 small nuclear RNA associated	Plays a role in U6 snRNP assembly and function. Binds to the 3' end of U6 snRNA, thereby facilitating U4/U6 duplex formation in vitro
Fkbp9	FK506 binding protein 9	PPIases accelerate the folding of proteins during protein synthesis
Nt5c3	5'-nucleotidase, cytosolic III	A 5'-ribonucleotide + H(2)O = a ribonucleoside + phosphate
Kbtbd2	kelch repeat and BTB (POZ) domain containing 2	
V1rc5	vomeronasal 1 receptor, C5	Receptor for CCL2, CCL5, CCL7 and CCL8 (By similarity)
V1rc32	vomeronasal 1 receptor, C32	Receptor for CCL2, CCL5, CCL7 and CCL8
V1rc30	vomeronasal 1 receptor, C30	Vomeronasal receptor V1RC1
V1rc7	vomeronasal 1 receptor, C7	Receptor for CCL2, CCL5, CCL7 and CCL8
V1rc6	vomeronasal 1 receptor, C6	Vomeronasal receptor V1RC6

2610022G08Rik	hypothetical protein LOC66459	This gene encodes a small protein with a conserved DUF343 domain. The human ortholog of this gene expresses two distinct proteins from upstream and downstream coding regions. The upstream CDS encoding a DUF343 domain-containing protein has been conserved at this mouse locus, but the downstream CDS encoding a subunit of an enzyme involved in glycosylphosphatidylinositol biosynthesis has not been conserved. Instead, a separate locus on mouse chromosome 9 encodes the mouse homolog of the human phosphatidylinositol glycan anchor biosynthesis, class Y protein
V1rc26	vomeronasal 1 receptor, C26	Receptor for CCL2, CCL5, CCL7 and CCL8
Ppm1k	protein phosphatase 1K (PP2C domain containing)	
AK007221	Adult male testis cDNA, RIKEN full-length enriched library, clone:1700121D12 product:EST AI451296, full insert sequence.	
AW146242	Adult inner ear cDNA, RIKEN full-length enriched library, clone:F930020F11 product:Weakly similar to glioblastoma amplified secreted protein homolog.	
Lancl2	LanC (bacterial lantibiotic synthetase component	Belongs to the LanC-like protein family
V1rc8	vomeronasal 1 receptor, C8	Receptor for CCL2, CCL5, CCL7 and CCL8

Table 4.1 Comprehensive list of genes in the critical region obtained from the UCSC database (http://genome.ucsc.edu).

Phosphodiesterase 1C (Pde1c)

Pde1c function in the mammalian nervous system has not been established. However, its expression in sensory neuron subpopulations in the spinal cord and in the dorsal root ganglia made it another interesting candidate gene for mutation detection.

Lsm5

As reduced U snRNP assembly causes motor axon degeneration in an animal model of spinal muscular atrophy, *Lmn5* was considered a good candidate gene due to its role in U6 snRNP assembly and function. It binds to the 3' end of U6 snRNA, thereby facilitating U4/U6 duplex formation in vitro (Winkler et al. 2005).

Glycyl tRNA synthetase (Gars)

Gars encodes glycyl tRNA synthetase, an enzyme that covalently links glycine onto its cognate tRNAs.

GARS was found to be the causative mutation in families segregating CMT2D and dSMA-V (Antonellis et al. 2003). *GARS* mutations are characterized by autosomal dominant inheritance and adolescent onset of disease with unique motor and sensory deficits.

Patients with the dSMA-V form of the disease show predominant thenar and first dorsal interosseus muscle atrophy and sparing of the hypothenar eminence until later in the illness. In about one-half of the patients, there is lower limb involvement, and in one-third a mild vibration sense loss observed in advanced disease.

In contrast, patients with the CMT2D-like variant show consistent presence of weakness and atrophy in the feet and distal leg muscle, pes cavus and moderate sensory abnormalities. These patients develop peroneal weakness and sensory deficits relatively early in the disease.

Electrophysiological data showed denervation on EMG in the distal muscle groups at normal distal latencies and conduction velocities and histopathological examination revealed sensory axonal loss by examination of sensory nerve (Sivakumar et al. 2005)

Since GENA 201 and 202 mutants have abnormal grip strength and mutations in the *GARS* gene cause a slow progressive neuropathy in humans that affects primarily the distal extremities (Antonellis et al. 2003), *Gars* was considered to be the best candidate gene for mutation detection analysis and thus was prioritized over the rest of the genes (Fig 4.5).

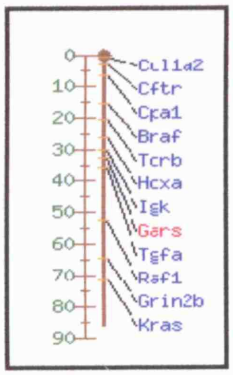

Fig 4.5 Linkage map of mouse chromosome 6, indicating the location of *Gars* at 55Mb (www.informatics.jax.org).

4.5 PCR cloning: *Gars*

The published genomic sequence (AC079183.5, *Mus musculus* clone RP23-258N2) and available information about intron-exon boundaries of *Gars* (http://www.ensembl.org/Mus_musculus/exonview?db=core;transcript=ENSMUST00000003572) were used to design oligonucleotides for the differential amplification of exon 1 to 18 (Appendix 4). The genomic organization of *Gars* is shown in Fig 4.6. The oligonucleotide sequences and specific annealing temperatures used for the PCR amplification of

Gars are listed in table 4.2. All PCRs were optimised using control (BALB/c X C3H) F1 DNA.

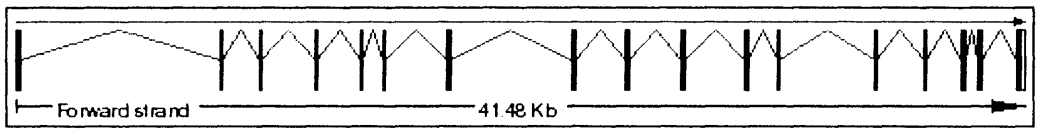

Fig 4.6 Diagram representing the genomic organisation of *Gars*. The gene contains 18 exons and is spread over 41.48Kb (www.ensembl.org).

Gars Exon	Oligonucleotide sequences	Expected product size (bp)	Annealing temperature for PCR (°C)	Notes
1 including 5' upstream sequence	Fw AAGTTGGTGCCCTTCCGGGTT Rv AGAAGCGCGCAGCATCAGCTT	550	60	1µl of 5% DMSO was added to master mix
2	Fw TCACCGTGTGAACCCACTTA Rv GGAGGAAAAGGCACAATGAA	530	60	
3	Fw CTGCTGCTCAAAGTGTTTGTG Rv GTGGTACTACTAAGAGGTGTG	427	60	
4	Fw CATTGCAGTCTGCCTTTTCA RV TTGCCAGCAAACACTTTGAC	399	60	
5	Fw CACGTGCTTGCTCTAGCAAGA Rv GTCTACCACTGAACACAGTCC	422	60	
6	Fw TACCTGCTGAGCCATCTCTC Rv AGAAAACGTGAGGTATGCTCC	339	60	
7	Fw AGGCAGACCTCGTCCTTGTTA Rv CCACCTGCCTATCCTGTGAA	477	60	
8	Fw GTGGGTCTGTGGGAGTGTTT Rv GCCACCTTCACCAGAGGTTA	491	60	
9	Fw GAGCAGCCAGAAATGGGAACC Rv GTTTGCTCATCAGTACCACAA	425	60	
10	Fw CAGTAGACTGACGTAGCTAGG Rv CTATCTCAGCTCCACTGAGGA	494	60	
11 and 12	Fw TGACATTGTAAGCCAGTCTGG Rv AGGGACACCAGCCAACAAGTT	471	60	
13	Fw TGATTGCTGAGCATTTGACC Rv ACAACCCATCTTGTCCCTTG	476	60	
14	Fw CAGTTTGGTGCCAATGTATGG Rv ACACACACACACACGCATCTT	431	60	
15	Fw GGAGTTGGAGTGCCAAGGATT Rv AAGGCTCACAAGGTTGAGGAG	367	60	
16	Fw GGCCATTTACTCCCTGTATGC Rv GACATCTGAGCAAGTCTGCTC	405	60	
17	Fw GACTTGCTGCTCTCATCTCAG Rv TGGGAATCTGGGCTTTGTCTG	448	60	
18 including 3'downstream sequence	Fw CACAGATAGACGGTTTGCTCTG RV GTGTTAAACACAAGCACATC	479	60	

Table 4.2 Oligonucleotides used to clone fragments of *Gars* from genomic DNA with expected product size and annealing temperature used for PCR.

4.6 Sequencing *Gars*

In order to locate the mutation, the oligonucleotides designed for the cloning of *Gars* were used to sequence the entire coding sequence of the gene including the splice sites. Forward and reverse reactions were set up using all the *Gars* exons and purified PCR products from C3H, BALB/c, C57BL/6 controls, 1 mutant and 1 wild type littermate mice. All exons were sequenced in both directions. Mutant, wild type and control sequence was compared to each other to double-check for the presence of mutations in the gene.

4.7 Identification of mutation in GENA 201 and 202

Both GENA201 and 202 mutant individuals were heterozygous for a single base position in exon 5. Heterozygosity was due to a 456T to C transition in the mutant copy of *Gars* (Fig 4.7 and Fig 4.8). All wild types and controls were homozygous T at this base position. This mutation causes a cysteine to argenine substitution at residue 201, and lies with the catalytic domain. The fact that both GENA 201 and 202 share the same mutation suggest that as they are siblings they were almost certainly derived from the same mutant spermatogonial cell on a BALB/c background.

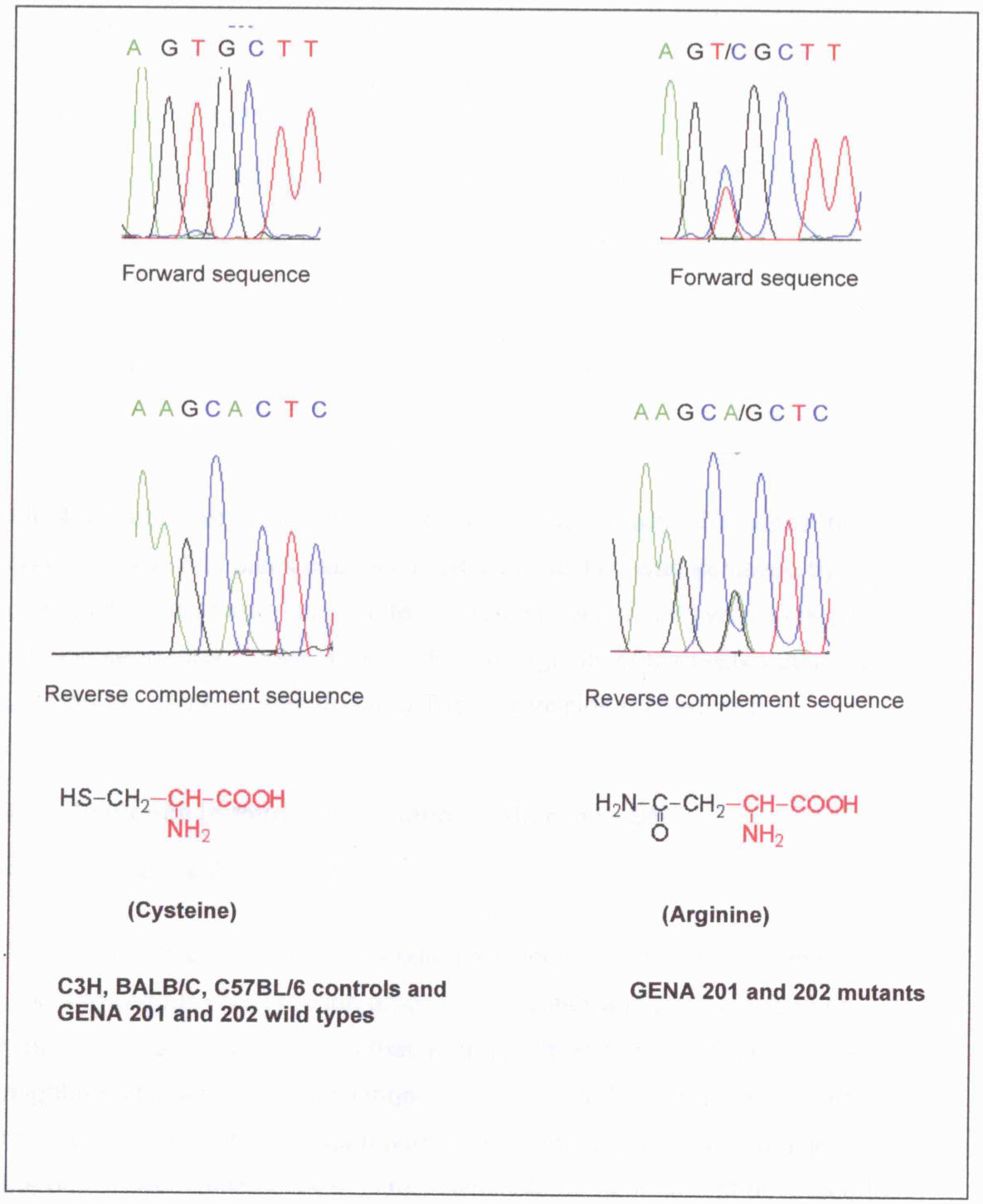

Fig 4.7 Forward and reverse complement electrophoretogram obtained by sequencing C3H, BALB/c, C57BL/6 controls, GENA 201 and 202 wild type and mutant DNA fragments for exon 5 *(Gars)*.

***Gars*, exon 5** (Wild type, Dir 5'-3')

cacgtgcttgctctagcaagacatcctttcacttgtgtgtcccagcagaacatcatttgaagtaactaga
agtgtgtgttcacttgttggttgcttgttcacttag

GACCTCTGGCCACGTAGACAAATTTGCTGACTTCATGGTGAAGGAC

GTGAAGAACGGAGA GTG CTTCCGAGCAGACCACCTGTTGAAAG

gtatgcgtctgcatctttcttgtacttcatcaaaacaaggttggacttatttctcaagtttttctgttttttaaaa
attggcttgttttaacatattcagactaaacatacgtttcaagcttatgttacagagtcacctacagattag
ttatattcaggtagtaatttttctaatcagcaagtgatcaagacattattatgggccgggactgtgttcagt
ggtagac

Fig 4.8 Partial genomic DNA sequence of *Gars* showing the bases that code for exon 5 in black capitals. PCR amplification was achieved by oligonucleotides that recognise templates (shown in pink) with flanking intronic sequence (shown in blue). Heterozygosity of the GENA 201 and 202 mutant samples was due to a T to C transition (boxed text).

4.8 Evidence in favour of mutation rather than SNP

4.8.1 Sequence Conservation

The stretch of amino acid surrounding and including the variant amino acid showed full conservation among eukaryotes with the exception of yeast (Fig 4.9). This suggests that an amino acid change within this area might result in a functional change. To investigate further the impact of the mutation, an attempt was made to model the affected amino acid on the only three-dimensional structure available at the time that belonged to the *Thermus thermophilus* Gars protein. However, by aligning the two sequences together using the alignment programme from NCBI (http://www.ncbi.nlm.nih.gov/blast/bl2seq/wblast2.cgi) the identity between the mouse and the *T.thermophilus* Gars was only 30%. As a minimum 40% sequence identity is required for results to be biologically meaningful (Antonellis et al. 2003), the effects of the mutation on the stability of Gars could not be applied.

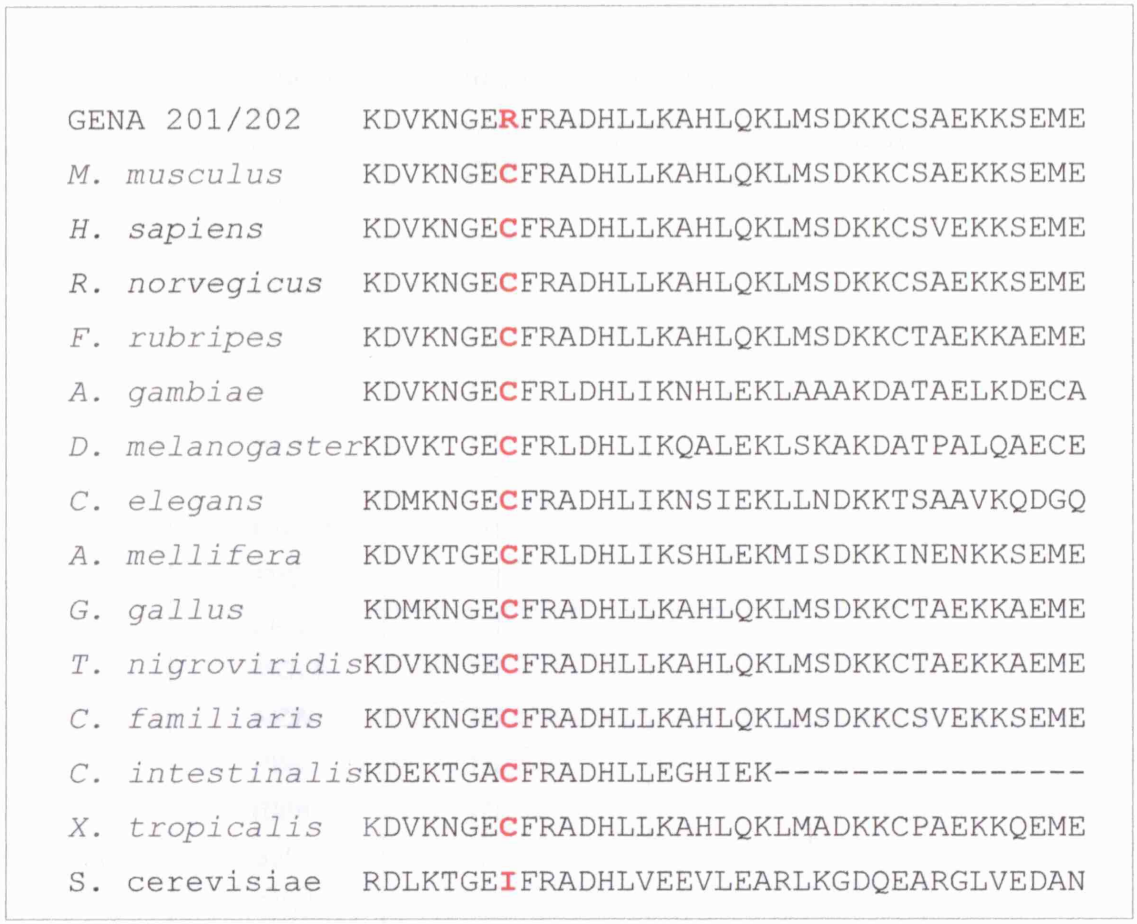

Fig 4.9 Conservation of Gars amino acid sequence in the region flanking the amino acid change observed in GENA 201 and GENA 202 among different organisms.

4.8.2 Sequencing panel of inbred strains

To further rule out the possibility that the above sequence variant represented a rare polymorphism, a wide panel of inbred strains was screened as controls by PCR amplification and DNA sequencing (Table 4.3). None of these strains were heterozygous for the single base position adding more evidence to support the supposition that the variation was not a rare polymorphism.

Inbred strain DNA	Exon 5 GENA 201 and 202 haplotype at 456 base position	
	Homozygous (T/T)	Heterozygous (T/C)
C3H	T/T	
BALB/c	T/T	
C57BL/6,	T/T	
129/J	T/T	
A/J	T/T	
AKR/J	T/T	
CD1	T/T	
DBA/2J	T/T	
FVB/J	T/T	
LP/J	T/T	
MOLF	T/T	
NZW	T/T	
PWK	T/T	
RIIIS	T/T	
SJL	T/T	
SM/J	T/T	
SWR	T/T	
VM	T/T	

Table 4.3 A panel of 18 inbred strains were used as control (DNA from the Jackson Laboratories, http://jaxmice.jax.org/index.html).

4.8.3 Restriction enzyme digestion

This mutation changes a restriction site for the enzymes HaeII and HhaI which further suggested that the variant observed in GENA 201 and 202 was not a sequencing artifact and allowed the designing of a protocol for routine genotyping by PCR followed by RFLP analysis.

PCR primers (forward: GTTTGCTTGTTCACTTAGGAC; reverse: GTCTACCACTGAACACAGTCC) that lie within intron 4 and intron 5 respectively, and thus span exon 5 of *Gars* were used to amplify a 422 bp

product obtained from DNA extracted from wild type and heterozygous, and presumed homozygous offspring.

When digested with HhaI, DNA from the wild type offspring gave the expected fragment of 422 bp (no restriction site) while DNA from heterozygous offspring showed, in addition to the 422 bp band, two bands of 253 bp and 169 bp (restriction site at the site of the *Gars*^{201R} mutant gene) and DNA from the presumed homozygous offspring gave only the expected 253 bp and 169 bp fragments (Fig 4.10).

This showed that the offspring with the more severe phenotype were indeed homozygous (*Gars*$^{201R/201R}$) offspring and that the mutation underlies an impaired motor phenotype.

Fig 4.10 2% Agarose gel showing PCR products from amplification of exon 5 using genomic DNA from C3H control, GENA 201 wild type, heterozygote and homozygote. Following digestion with HhaI, the control and wild type DNA produced a band of the expected size (422bp). The heterozygote sample produced additional bands of 253 bp and 169 bp and the homozygote produced only the expected 253 bp and 169 bp size bands.

4.9 Concluding remarks

The genetic data collected so far suggests that the *Gars*^{C201R} mutation is responsible for the GENA 201 and 202 phenotype. It remains a formal possibility that this mutation is a SNP, and the only way to rule out this possibility is to either sequence all the genes in the critical region or to cross the mice to another Gars mutant mouse and look for non-complementation.

Before sequencing of all the genes, it would advisable to further narrow down the 5 Mb interval to a smaller critical region in which the gene responsible of the mutant phenotype has to be located. This can be achieved by increasing the number of backcross progeny as the resolution of a linkage map increases linearly with the number of offspring typed in a genetic cross. Ideally, a 1 cM region is recommended (E. Fisher personal communication). For example, with ~50 backcross mice, it is possible to map a mutation to a specific chromosome and locate the affected gene to an interval of 10cM to 20cM (Silver 1995). Thus, by increasing the number to 500-1000 backcross mice, the critical region can be narrowed to 1 cM interval. With about 2000 kb in 1 cM and 1 gene every 50 to 100kb, this may reduce the number of candidate genes to less than 100.

As the GENA 201 and 202 progeny used in the mapping was not an N2 as originally thought and as with ~100 backcross mice it was possible to map the mutation to an interval of ~3cM (5 Mb), then by adding less than 40 backcross mice, the critical region could be narrowed to ~1 cM interval.

In vitro fertilization should be considered in order to speed up the production of backcross mice alleviating the pressure of time and animal space. Sperm from the epididymides of mice is obtained and then used as either frozen or fresh to produce 50 offsprings in a single *in vitro* experiment (Glenister & Thornton 2000; Marschall et al. 1999).

We are currently setting up a collaboration to cross the *Gars*^{C201R} mouse to a Gars mutant mouse (*Gars*^{Nmf249}) held by the Jackson Laboratory to look for non-complementation and confirm *Gars*^{C201R} is the causative mutation.

The cross should produce four genetically distinct groups of littermates: wild types, *Gars*^{C201R} heterozygotes, *Gars*^{Nmf249} heterozygotes and *Gars*^{C201R} /*Gars*^{Nmf249} double heterozygotes. Following genotyping, we would examine the phenotype of *Gars*^{C201R} /*Gars*^{Nmf249} double heterozygotes and compare it with the phenotype of the *Gars*^{C201R} mice.

If we don't assess any change in phenotype, we would add evidence towards the *Gars*^{C201R} mutation being a SNP as it is not affecting the severity of the phenotype. However, if we do notice an increase in the severity of the phenotype in the *Gars*^{C201R} /*Gars*^{Nmf249} double heterozygotes, we would be able to add evidence towards the *Gars*^{C201R} mutation being responsible of the mutant phenotype.

However, both the sequencing and the non-complementation strategies, have limitations. For example, to effectively sequence all the genes in the critical interval, one would need to sequence both coding and noncoding regions of all genes to rule out the possibility that the mutation lies in an intron. As this approach is expensive and not practical, usually, in positional cloning studies, coding regions are prioritized.

In addition, if we happen to notice an increase in the severity of the phenotype in the *Gars*^{C201R} /*Gars*^{Nmf249} double heterozygotes, we would not be able to effectively conclude that the *Gars*^{C201R} mutation is responsible of the mutant phenotype as other mutations in the GENA 201 and 202 mice could be also responsible.

Despite the possibility that this mutation is a SNP, as mutations in the *GARS* gene cause a slow progressive neuropathy in humans that affects primarily the distal extremities (Antonellis et al. 2003) and as another

Gars mutant mouse (*Gars*^{Nmf249}) held by the Jackson Laboratory was established to be a valid animal model of progressive neuropathy, *Gars* was still considered to be the best candidate gene for mutation detection analysis and *in vivo* functional studies were carried out, as discussed in the next chapter, to understand the effects of the *Gars*^{C201R} mutation in the mouse.

5. Chapter 5: GARS functional assay

5.1 Introduction

To investigate possible molecular mechanisms of pathology, GARS aminoacylation activity was assayed directly from dissected brain homogenate of (1) 6 wild type and 6 *Gars*$^{C201R/+}$ mice on both C3H and C56BL/6 backgrounds at 3 months of age, and (2) 3 wild type, 3 *Gars*$^{C201R/+}$ and 3 *Gars*$^{C201R/C201R}$ mice on the C3H background at 15 days of age (Table 5.1).

The assay is based on the incorporation of a labelled amino group into tRNA which is insoluble in acid. By radiolabelling with tritated glycine, the assay attempted to quantify how much labelled glycine and tryptophan was incorporated into tRNA in mouse brain homogenates.

Amino acid (i.e. glycine or tryptophan) + ATP+ tRNA↔ aminoacyltRNA + AMP + PPi

The coupling reaction that creates an aminoacyl-tRNA molecule is catalyzed in two steps (Fig 5.1). The energy of ATP hydrolysis is used to attach each amino acid to its tRNA molecule in a high-energy linkage. The amino acid is first activated through the linkage of its carboxyl group directly to an AMP, forming an adenylate amino acid; the linkage of the AMP is driven by the hydrolysis of the ATP molecule that donates the AMP. Without leaving the synthetase enzyme, the AMP-linked carboxyl group on the amino acid is then transferred to a hydroxyl group on the sugar at the 3' end of the tRNA molecule. This transfer joins the amino acid by an activated ester linkage to the tRNA and forms the final aminoacyl-tRNA molecule (Alberts 1994).

An attempt was made to dissect the motor cortex and the sensory cortex as GENA 201 and 202 mice showed an abnormal motor phenotype (Fig 5.2). 10mg of brain samples per ml of buffer were homogenized using

plastic mortar and then centrifuged. Supernatant was aliquoted and stored at -80°C until used. Protein concentrations of homogenates, determined by using BCA assay, are listed in Table 5.1. Assays were carried out blind to genotype, which was decoded afterwards. The activity of tryptophan-tRNA synthetase was used as positive control for each sample and the activity of the glycyl-tRNA synthetase (BIOS&T) with no brain homogenate was used as an internal control for each sample.The negative samples did not include tRNA. All the raw data is listed in Appendix 5.1.

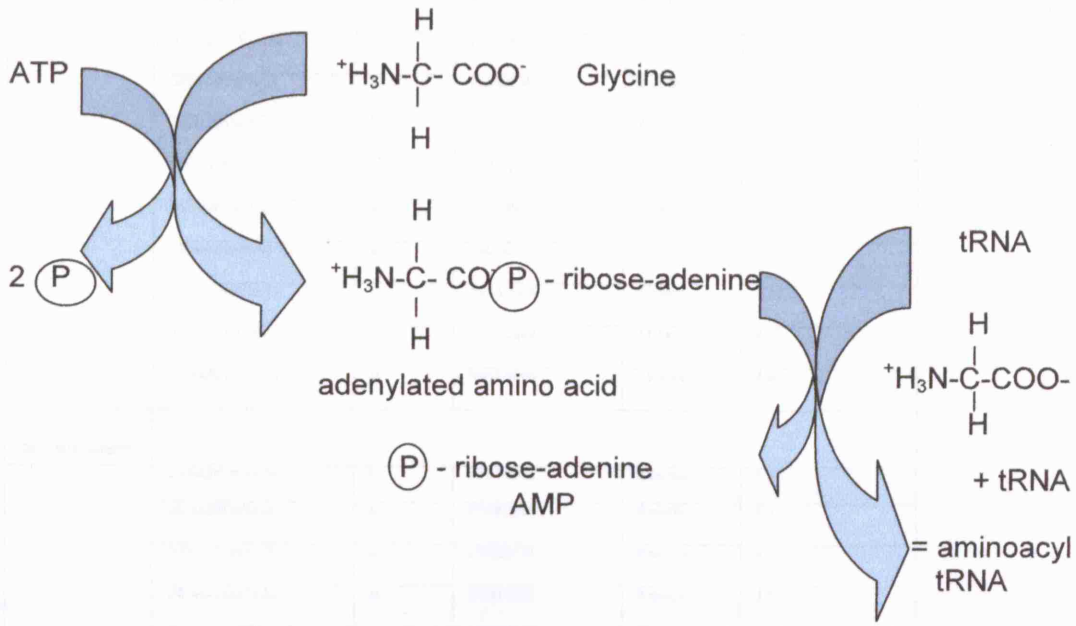

Fig 5.1 A two step process in which an amino acid (glycine, as shown here) is activated for protein synthesis by an aminoacyl-tRNA synthetase enzyme.

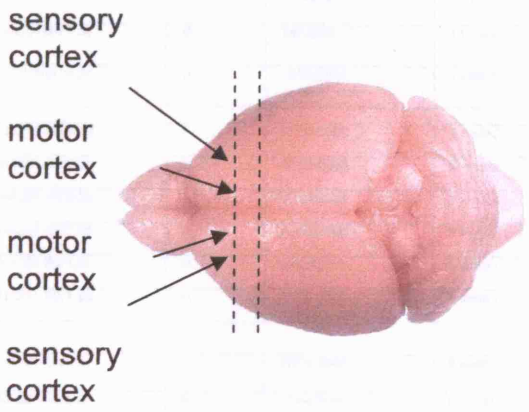

Fig 5.2 Section of mouse brain dissected for aminoacylation assay which includes motor and sensory cortex (mouse atlas http://www.mbl.org/).

	Mouse ID	Sex	Date of Birth	Age when tested	Protein concentration(mg/ml)
C3H wild type					
	GENA201M/14.2a	F	27/06/2006	9 weeks	4.05
	GENA201M/14.2c	F	27/06/2006	9 weeks	3.8
	GENA201M/14.2d	F	27/06/2006	9 weeks	5.5
	GENA201M/14.2f	F	27/06/2006	9 weeks	4.7
	GENA201M/6.2d	M	11/10/05	9 weeks	3.3
	GENA201M/6.2f	M	11/10/05	9 weeks	4.2
	GENA201M/6.6c	M	23/02/06	9 weeks	4.2
	GENA201M/6.6d	M	23/02/06	9 weeks	6.3
	GENA201M/19.1c	F	26/10/2006	15 days	5.54
	GENA201M/19.1e	F	26/10/2006	15 days	6.07
	GENA201M/19.1g	M	26/10/2006	15 days	5.91
C3H heterozygote					
	GENA201M/14.2b	F	27/06/2006	9 weeks	3.3
	GENA201M/14.2e	M	27/06/2006	9 weeks	3.4
	GENA201M/14.2f	M	27/06/2006	9 weeks	4.7
	GENA201M/14.2g	M	27/06/2006	9 weeks	3.7
	GENA201M/6.2e	M	11/10/05	9 weeks	6.4
	GENA201M/6.2g	M	11/10/05	9 weeks	4.6
	GENA201M/6.6a	F	23/02/06	9 weeks	4.4
	GENA201M/6.6b	F	23/02/06	9 weeks	7.2
	GENA201M/19.1a	F	26/10/2006	15 days	5.34
	GENA201M/19.1b	F	26/10/2006	15 days	6.65
	GENA201M/19.1d	M	26/10/2006	15 days	7.77
C3H homozygote					
	GENA201M/11.4d	F	7/01/2006	15 days	9.4
	GENA201M/11.4e	M	7/01/2006	15 days	7.51
	GENA201M/15.2e	M	15/06/2006	15 days	5.75
C57BL/6 wild type					
	GENA201-B6/3.2d	F	07/04/2006	9 weeks	4.7
	GENA201-B6/3.2g	M	07/04/2006	9 weeks	4.32
	GENA201-B6/3.2h	M	07/04/2006	9 weeks	5.07
	GENA201-B6/1.8b	F	02/05/2006	9 weeks	9.4
	GENA201-B6/1.8f	M	02/05/2006	9 weeks	5.1
	GENA201-B6/1.9e	M	26/05/2006	9 weeks	7.48
C57BL/6 heterozygote					
	GENA201-B6/3.2e	F	07/04/2006	9 weeks	6.3
	GENA201-B6/3.2f	M	07/04/2006	9 weeks	5.14
	GENA201-B6/3.2i	M	07/04/2006	9 weeks	4.6
	GENA201-B6/1.8a	F	02/05/2006	9 weeks	5.5
	GENA201-B6/1.8d	M	02/05/2006	9 weeks	8.08
	GENA201-B6/1.9f	M	26/05/2006	9 weeks	7.8

Table 5.1 A list of total number of animals including their sex, date of birth, age tested and protein concentration used in the aminoacylation assay.

5.2 $Gars^{C201R/+}$ aminoacylation activity: wild types compared to heterozygotes on a C3H and C57BL/6 background

Initial tests were done to establish whether the GARS activity could be assessed in brain motor and sensory cortex homogenates using a scintiallation counter by comparing GARS activity with the activity of the positive control. Each brain homogenate was split into 3 aliquots of 20µl each and each 20µl was assayed for GARS activity 3 times, making a total of nine readings for each brain sample. Initial reactions were incubated at 37°C for 20 min with 80uM tRNA-bovine-liver. The reaction mix was spotted on 3MM Whatman filter paper and washed in TCA and ethanol. The filter was then air dried and then counted in a scintillator counter. The scintillator counter reported the number of photons that it detected as counts per minute (cpm) (Fig 5.3).

Having established that counts per minutes were detected by the scintiallator counter, data was then quantified to obtain picomoles per mg of protein per minute of time. As the difference between cpm and disintegration per minute (dpm) is the efficiency (eff) of the counter in detecting the release of beta particles, to obtain dpm the mean of each sample count was divided by the efficiency of the assay. Dpms were converted to disintegration per second and then divided by the specific activity of the radioactive glycine and tryptophan to obtain pmoles.The result was normalized using the protein concentration to obtain picomoles per mg of protein per minute of time (Fig 5.3).

As the coupling reaction that creates an aminoacyl-tRNA molecule is catalyzed in two steps, the reaction was preincubated at 37°C for 20 min to rule out the possibility that the activation of the amino acid by ATP was limiting the reaction. 80uM tRNA-bovine-liver was then added and the reaction was incubated for a further 5 min at 37°C. No significant difference between "preincubation" and "no preincubation" was observed

suggesting that the activation of the amino acid by ATP was not limiting the reaction (Fig 5.4).

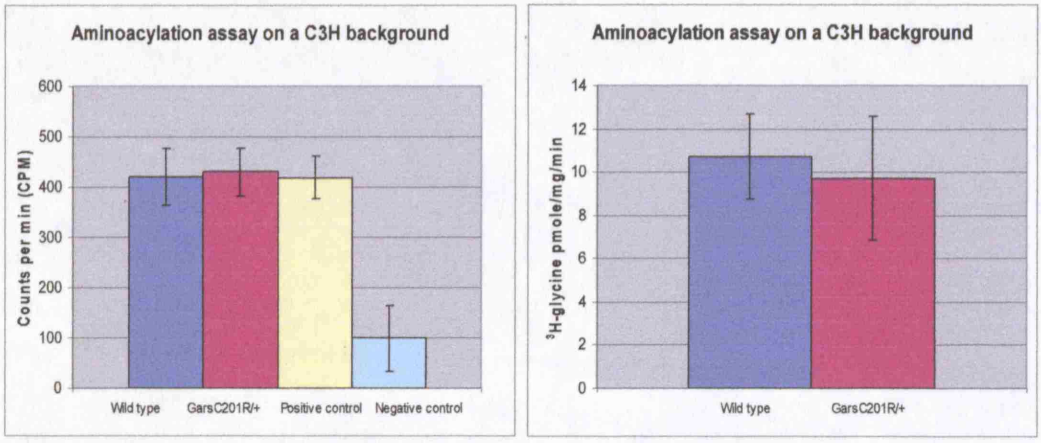

Fig 5.3 The first graph shows 3 month old wild type and *Gars*$^{C201R/+}$ brain homogenate counts per minutes compared to positive and negative controls with no preincubation. The second graph represents data converted into ^{3}H-glycine pmoles/mg/min from the first graph. Each sample was split into 3 aliquots of 20µl each and each 20µl was assayed for GARS activity 3 times, making a total of nine readings for each brain sample. N. of wild type=3, n. of *Gars*$^{C201R/+}$ =3.

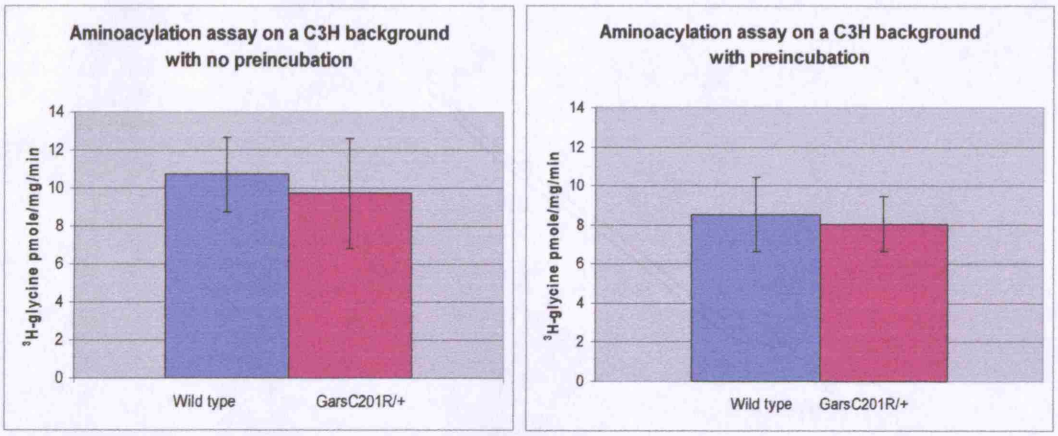

Fig 5.4 Glycyl-tRNA synthetase activity in brain homogenate. In 3 month old mice activity is not significantly different between *Gars*$^{C201R/+}$ and wild type littermates with both no preincubation and preincubation assays on a C3H background. In addition, activity is not significantly different between no preincubation and preincubation assays on a C3H background. Each sample was split into 3 aliquots of 20µl each and each 20µl was assayed for GARS activity 3 times, making a total of nine readings for each brain sample. (N. of wild type=3, n. of *Gars*$^{C201R/+}$ =3 for no preincubation and n=6 for all cohorts assayed with preincubation).

The activity of wild type brain homogenate compared to *Gars*$^{C201R/+}$ on a C3H and C57BL/6 background was then measured and compared between the two genetic backgrounds. GARS aminoacylation activity was assayed from brain homogenate of 6 wild type and 6 *Gars*$^{C201R/+}$ mice on both C3H and C56BL/6 backgrounds at 3 months of age. Each sample was split into 3 aliquots of 20µl each and each 20µl was assayed for GARS activity 3 times, making a total of nine readings for each brain sample. As no significance difference between preincubation and no preincubation was observed, preincubation at 37°C for 20 min was carried out routinely in all the experimetents. 80uM tRNA-bovine liver was then added and the reaction was incubated for a further 5 min at 37°C.

Aminoacylation activity was not significantly different between wild type and *Gars*$^{C201R/+}$ on both C3H and C57BL/6 backgrounds, at both ages (Figure 5.5); for example, mean GARS activity in brain from 3-month old *Gars*$^{C201R/+}$ mice on a C3H background was 8.05±0.93 pmole/mg/min (n=6) compared to 8.5±1.006 pmole/mg/min (n=6) in littermate controls.

The mean activity in 3-month old *Gars*$^{C201R/+}$ mice on a C57BL/6 background was 6.01±0.54 pmole/mg/min (n=6) compared to 6.22±0.62 pmole/mg/min (n=6) in littermate controls (n=6), showing the activity was significantly different between the C3H and C57BL/6 backgrounds for both heterozygote and wild type controls (p= 0.02) (Figure 5.5).

However, this lower enzyme activity does not correlates with the more pronounced phenotype observed for *Gars*$^{C201R/+}$ mice with the C57BL/6 background as also the tryptophan-tRNA synthetase activity that was used as an internal control was shown to be lower in activity as well (Fig 5.6). The reason for this has not yet been established. Occasionally crude extract will contain other activities that may result into the incorporation of an amino acid into material that is not tRNA but, for example, into proteins (personal comunication by Prof David Dignam, Professor of Biochemistry and Cancer Biology, University of Toledo, USA). This might explain why higher glycine activity on the C3H

background was observed compared to the glycine activity on the C57BL/6 backgound.

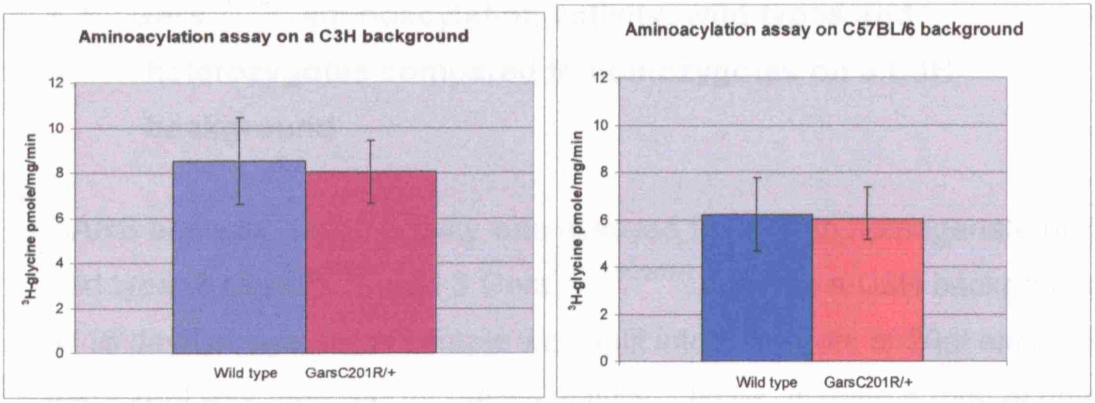

Fig 5.5 Glycyl-tRNA synthetase activity in brain homogenate. In 3 month old mice activity is not significantly different between *Gars*$^{C201R/+}$ and wild type littermates in both C3H and C57BL/6 backgrounds. Each sample was split into 3 aliquots of 20µl each and each 20µl was assayed for GARS activity 3 times, making a total of nine readings for each brain sample. (n=6 for all cohorts assayed).

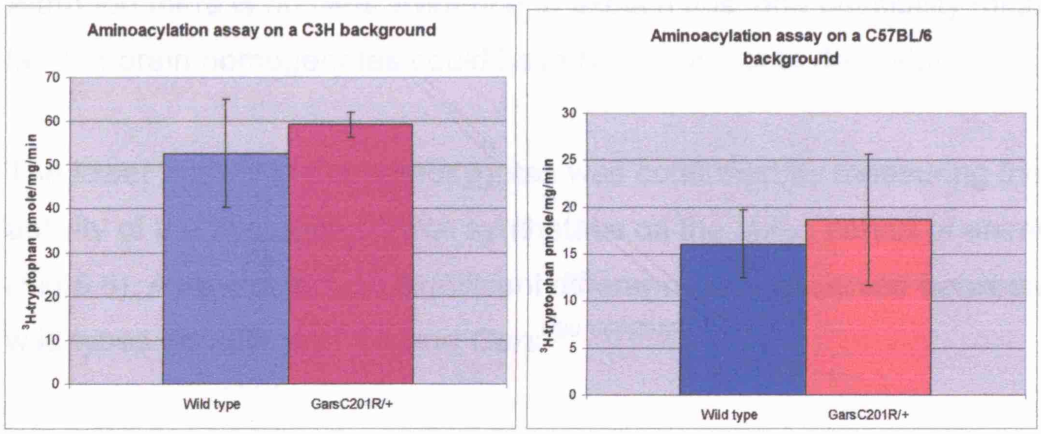

Fig 5.6 Tryptophan-tRNA synthetase activity in brain homogenate. In 3 month old mice, activity is not significantly different between *Gars*$^{C201R/+}$ and wild type littermates in both C3H and C57BL/6 backgrounds. Each sample was split into 3 aliquots of 20µl each and each 20µl was assayed for GARS activity 3 times, making a total of nine readings for each brain sample. (n=5 for all cohorts assayed).

5.3 *Gars*$^{C201R/+}$ aminoacylation activity: wild types and heterozygotes compared to homozygotes on a C3H background

GARS aminoacylation activity was assayed from brain homogenate of 3 wild type, 3 *Gars*$^{C201R/+}$ and 3 *Gars*$^{C201R/C201R}$ mice on a C3H background at 15 days of age. Each sample was split into 3 aliquots of 20µl each and each 20µl was assayed for GARS activity 3 times, making a total of nine readings for each brain sample.

Aminoacylation activity was significantly different between wild types and *Gars*$^{C201R/+}$, and *Gars*$^{C201R/C201R}$ on a C3H background (Fig 5.7). Mean GARS activity in 15 day old *Gars*$^{C201R/C201R}$ mice is 3.38±0.82 pmole/mg/min (n=3) and thus is reduced by 60% in comparison to the mean value of 8.51±0.36 pmole/mg/min (n=3) in wild type littermate controls (P=0.01). *Gars*$^{C201R/+}$ showed high variation within their cohort. Although there is no clear evidence to explain this, one possibility might be that brain homogenates could have been subject to degradation.

The lower activity in the homozygotes was confirmed by measuring the activity of the tryptophan-tRNA synthetase on the same cohort of animals (Fig 5.8). As expected, no significant difference was observed between wild types and *Gars*$^{C201R/+}$, and *Gars*$^{C201R/C201R}$.

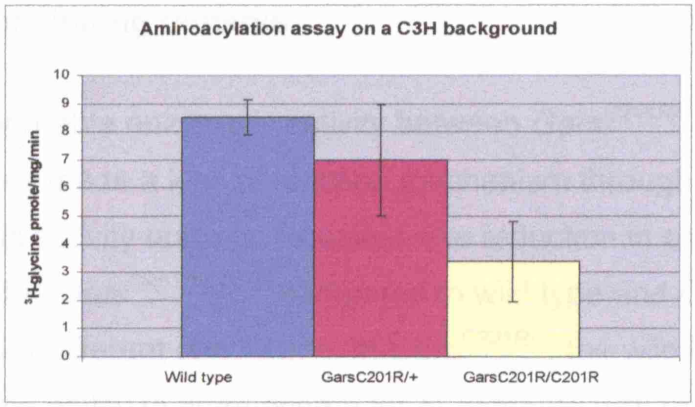

Fig 5.7 In 15 day old mice on a C3H background, glycyl-tRNA synthetase activity in *Gars*$^{C201R/C201R}$ animals was reduced significantly compared to *Gars*$^{C201R/+}$ and wildtype littermates. Each sample was split into 3 aliquots of 20µl each and each 20µl was assayed for GARS activity 3 times, making a total of nine readings for each brain sample. (n=3 for all cohorts assayed).

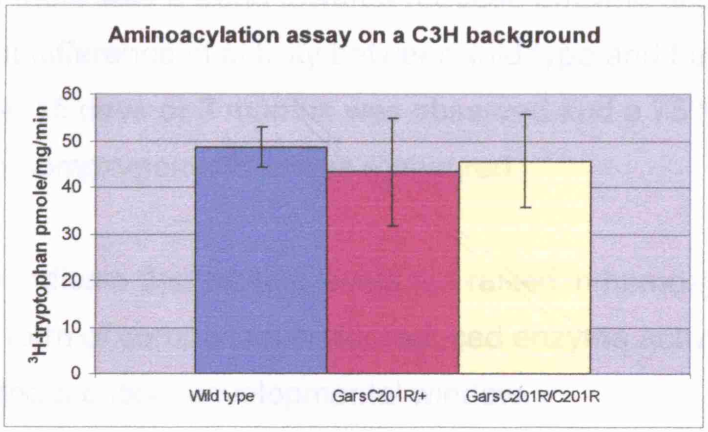

Fig 5.8 In 15 day old mice on a C3H background, tryptophan-tRNA synthetase activity in *Gars*$^{C201R/C201R}$ animals was not reduced significantly compared to *Gars*$^{C201R/+}$ and wild type littermates. Each sample was split into 3 aliquots of 20µl each and each 20µl was assayed for GARS activity 3 times, making a total of nine readings for each brain sample. (n=3 for all cohorts assayed).

5.4 Concluding remarks

The comparable enzymatic activity between *Gars*$^{C201R/+}$ and wild type litter mates made a loss of function mechanism through impaired enzymatic activity unlikely. However, the reduction in enzymatic activity observed in *Gars*$^{C201R/C201R}$ compared to wild type and *Gars*$^{C201R/+}$ indicated a different conclusion. In *Gars*$^{C201R/+}$, the wild type allele could have some ability to compensate for or compete with the mutant protein, while in *Gars*$^{C201R/C201R}$ such ability could be lost, thus, resulting in the observed impaired enzymatic activity.

However, GARS functional holoenzyme exists as a homodimer and to justify the haplo-insufficiency mechanism one should have noticed a 100% enzyme activity in wild types, a 75% activity in heterozygotes and a 50% activity in homozygotes which was not observed.

Although there was a trend towards reduced enzyme activity, no significant difference in activity between wild type and heterozygous animals at 15 days or 3 months was observed and a 75% reduction in activity in homozygous mice was measured.

This may indicate that protein levels are raised in homozygous animals as some form of compensation for reduced enzyme activity, possibly even during a critical developmental window.

Interestingly, in collaboration with Dr Hazel Williams, Institute of Neurology, UCL, protein levels by western hybridisation were analysed and found no differences between heterozygotes and wild type littermates in adults (3-months of age) but significant increase in protein levels in heterozygotes and homozygous mice, compared to wild types, at 15-days of age (Dr Hazel Williams personal communication).

The different enzyme levels between wild type and heterozygotes at 15 days, not at 3 months, may indicate that the function of GARS is more critical during development, rather than in adult mice.

This could imply that at least part of the *Gars*^{C201R} phenotype arises from a loss of enzyme activity, although phenotypic effects from a loss of activity may only be confined to homozygous animals, not necessarily heterozygotes, suggesting different pathological mechanisms may be critical in heterozygotes and homozygotes.

Antonellis and colleagues also found no difference in GARS protein levels in lymophoblastoid cell lines from a human *GARS*^{G240R} heterozygous patient and a wild type individual (Antonellis et al. 2006) similar to the findings for adult *Gars*^{C201R} heterozygote compared to wild type mice.

All GARS mutations so far described in mouse and human are dominant, implying the phenotypes arise from either a dominant gain of function or a loss of function. Data from *Drosophila* and mouse studies suggest both possibilities, depending on the individual mutation (Chihara et al. 2007; Seburn et al. 2006).

From the studies so far either mechanism is possible, suggesting another scenario in which the phenotype could arise from loss of function (such as loss of enzyme activity, as seen in the homozygous *Gars*$^{C201R/C201R}$ mice) and a gain of function, as suggested in the *Gars*^{Nmf249} model (Seburn et al. 2006). In the *Gars*^{C201R} mice it is possible that different pathological mechanisms are critical in heterozygotes and homozygotes.

6. Chapter 6: General histology

6.1 Introduction

This chapter details histological observations made of the GENA 201 and 202 lines which were carried out in parallel with the mapping of the mutation. The data reveal no abnormality in 17th month old GENA 201 and 202 triceps, quadriceps and gastrocnemius muscles which is surprising considering that mutations in the *GARS* gene cause a slow progressive neuropathy in humans that affects primarily the distal extremities (Antonellis et al. 2003). In retrospect, a more detailed muscle study should have been carried out including studies on the neuromuscular junction in order to rule out the possibility of a muscle abnormality.

6.2 General histology of *Gars*$^{C201R/+}$ and *Gars*$^{C201R/C201R}$

Gars$^{C201R/+}$, *Gars*$^{C201R/C201R}$ and wild type littermates on a C3H background were selected for general histological investigations in an attempt to identify any associated changes in tissues.

28 tissues (Table 2.6) were collected from 3 wild types and 6 *Gars*$^{C201R/+}$ mice at 17 months of age. The whole carcass of 2 wild type, 2 *Gars*$^{C201R/+}$and *3 Gars*$^{C201R/C201R}$ mice at 15 days of age was cut in sections to include lumbar, thoracic and cervical spinal cord and brain sections and was processed for general histology. All the animals sacrificed are listed in Table 6.1.

	Mouse ID	Sex	Date of Birth	Age
C3H wild type				
	332.4c	M	22/9/2003	17 months
	333.7a	F	22/9/2003	17 months
	333.7b	F	22/9/2003	17 months
	201m/12.2a	M	20/4/2006	15 days
	201m/12.2c	F	20/4/2006	15 days
C3H *Gars*$^{C201R/+}$				
	332.3f	M	22/9/2003	17 months
	333.5b	F	22/9/2003	17 months
	333.5c	F	22/9/2003	17 months
	333.5d	F	22/9/2003	17 months
	333.6d	M	22/9/2003	17 months
	333.7c	F	22/9/2003	17 months
	201m/12.2b	M	20/4/2006	15 days
	201m/12.2d	F	20/4/2006	15 days
C3H *Gars*$^{C201R/C201R}$				
	201m/12.2e	M	20/4/2006	15 days
	201m/12.2f	F	20/4/2006	15 days
	201m/12.3d	M	20/4/2006	15 days
	201m/19.3a	M	29/6/2006	15 days

Table 6.1 A list of total number of animals including their sex, date of birth and age tested used in the general histology.

2-5 µm haematoxylin and eosin stained sections of all major organs were examined and findings presented in the Table 6.2. The staining method was used to show organ morphology and involved application of the basic dye haematoxylin, which colors basophilic structures with blue-purple hue, and alcohol-based acidic eosin Y, which colors eosinophilic structures bright pink.

Microscopical studies revealed no differences between *Gars*$^{C201R/+}$ mice and littermate wild type controls at 17 months of age in non-neural tissue.

Although the size of all body organs in *Gars*$^{C201R/C201R}$ animals was reduced, in proportion to the reduction in body size, no differences to controls in non-neural tissues of *Gars*$^{C201R/C201R}$ at 15 days of age was observed.

No abnormality was observed in *Gars*^{C201R} mice triceps, quadriceps and gastrocnemius muscles, except for a possible limb girdle dystrophy in 3

adult *Gars*$^{C201R/+}$. Variation in fiber size, central nuclei, fiber splitting, was seen in mutants as well as the wild type animals, suggesting a possible background effect.

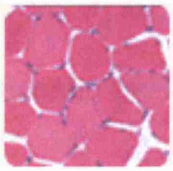

Normal muscle has regular fibres

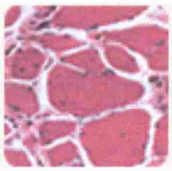

Dystrophic muscle has fibre size variation and split fibres

Fig 6.1 Limb girdle dystrophy was seen in both 17 month old wild type (n=3) and *Gars*$^{C201R/+}$ (n=3) mice.

In addition, there was no evidence of inflammation, degeneration or neoplasm, in any systemic organ examined.

	Wild type (17months)	*Gars*$^{C201R/+}$ (17months)	Wild type (15 days)	*Gars*$^{C201R/+}$ (15 days)	*Gars*$^{C201R/C201R}$ (15 days)
Heart	Normal	Normal	Normal	Normal	Normal
Lungs	Normal	Normal	Normal	Normal	Normal
Liver	Normal	Normal	Normal	Normal	Normal
Kidneys	Normal	Normal	Normal	Normal	Normal
Adrenals	Normal	Normal	Normal	Normal	Normal
Skin	Normal	Normal	Normal	Normal	Normal
Gut	Normal	Normal	Normal	Normal	Normal

Table 6.2 Summary of pathological findings of all major organs of 6 17 month old *Gars*$^{C201R/+}$ mice and 3 aged match wild type controls; and 2 15 days old *Gars*$^{C201R/+}$and 3 *Gars*$^{C201R/C201R}$ mice and 2 aged matched wild type controls.

6.3 Brain, spinal cord and sciatic nerve histology

5-10 μm sections of brain and spinal cord were stained with the following stains and findings presented in the Table 6.3:

- Haematoxylin and eosin were used to show morphological structure.

- Luxol-fast blue – cresyl violet was used to show myelin sheath and Nissl substance. The luxol dyes are insoluble in water and are used as solutions in alcohol or other moderately polar liquids. These dyes stain phospholipids, they probably also enter hydrophobic domains of protein molecules. When a suitable counter stain, e.g. Cresyl Violet or other cationic dye is applied it will bind not only to the nuclei and Nissl substance but will combine with the luxol fast blue anions present in the myelin.

- Glial fibrillary acidic protein immunohistochemistry (GFAP). GFAP is an intermediate filament (IF) protein that is found in glial cells such as astrocytes.It was used as a marker, immunohistochemically, for glial cells.

- Choline acetyltransferase is an enzyme which is synthesized within the body of a neuron. It is then transferred to the nerve terminal via axoplasmic flow. It joins Acetyl CoA to choline, resulting in the formation of the neurotransmitter acetylcholine. It was used as a marker, immunohistochemically, for motor neurons.

Adult brain and spinal cord 15 days old *Gars*$^{C201R/+}$ and 17 month *Gars*$^{C201R/+}$ appeared no different from wild type controls under light microscopy with the methods above.
In 15 days old *Gars*$^{C201R/C201R}$ mice, brain and spinal cord were reduced in size in line with the reduction in size of all other organs. In addition, the following features were observed.

One homozygote animal showed an intracranial cyst. It was rounded thin walled cyst, containing colloid-type material. The cyst compressed adjacent cortex. The cyst was located in the midline of the brain.

	Wild type (17months)	Heterozygote (17months)	Wild type (15 days)	Heterozygote (15 days)	Homozygote (15 days)
BRAIN					
Cortical development	Normal	Normal	Normal	Normal	1/3 included a midline cyst compressing adjacent cortex (see below)
Cerebellar development	Normal	Normal	Normal	Normal	
Cortical Lamination:					
Sensory	Normal	Normal	Normal	Normal	Normal
Motor	Normal	Normal	Normal	Normal	Reduced see Fig 6.2
Auditory	Normal	Normal	Normal	Normal	Normal
Thalamus	Normal	Normal	Normal	Normal	Normal
Red nucleus	Normal	Normal	Normal	Normal	1/3 gliosis others normal
Hippocampus	Normal	Normal	Normal	Normal	Normal
Trigeminal nerve	Normal	Normal	Normal	Normal	Normal
SPINAL CORD					
Dorsal columns	Normal	Normal	Normal	Normal	Marked reduction of dorsal column See Fig 6.3
Dorsal horn	Normal	Normal	Normal	Normal	
Motor tracts	Normal	Normal	Normal	Normal	
Spinocerebellar tracts	Normal	Normal	Normal	Normal	
Anterior horn	Normal	Normal	Normal	Normal	Normal
Ventral roots	Normal	Normal	Normal	Normal	
Dorsal roots	Normal	Normal	Normal	Normal	
GANGLIA					
Dorsal root	Normal	Normal	Normal	Normal	Loss of large diameter fibres see Fig 6.4
Cervical sympathetic	Normal	Normal	Normal	Normal	
Myenteric	Normal	Normal	Normal	Normal	
Trigeminal	Normal	Normal	Normal	Normal	Loss of large diameter fibres see Fig 6.5

Table 6.3 Summary of pathological findings of brain, spinal cord and ganglia of 6 17 month old *Gars*$^{C201R/+}$ mice and 3 aged match wild type controls; and 2 15 days old *Gars*$^{C201R/+}$, 3 *Gars*$^{C201R/C201R}$ and 2 aged matched wild type controls.

Due to the abnormal grip strength assessed in *Gars*^{C201R} mice, the *Gars*^{C201R} motor and sensory pathways were studied to asses whether the grip strength deficit involved a motor or sensory abnormality.

The alpha pathways originate in the brain and descend down the spinal cord to control the ά-motor neurons. The primary motor pathway is also called the corticospinal pathway. This pathway starts in cortex and ends in the spine.

The cortex is the final target of the primary somatosensory pathway where sensation enters the periphery via sensory axons and ends in the cerebral cortex, the final target. Therefore it was crucial to understand whether the cerebral cortex area which included the primary motor and primary sensory pathway of the *Gars*^{C201R} mice was affected.

The motor and sensory cortex area has six varying layers of cells, from the most superficial and cell-free layer I to the deep layer VI (Brumback 1996). Each layer has a slightly different cellular makeup, and the thicknesses of the layers varies with cortical area (Fig 6.2). Neurons form efferents and receive afferent connections characteristic of their layer. They are characterized as follows (Brumback 1996):

I. Molecular layer: the molecular layer I contains few scattered neurons and consists mainly of extensions of apical dendrites.

II. External granular layer: the external granular layer II contains small pyramidal neurons and numerous stellate neurons.

III. External pyramidal layer: the external pyramidal layer III contains small and medium sized pyramidal neurons, as well as non-pyramidal neurons with vertically-oriented intracortical axons. Layer III is the principal source of corticocortical efferents.

IV. Internal granular layer: the internal granular layer IV contains different types of stellate and pyramidal neurons, and is the main target of

thalamocortical afferents as well as intra-hemispheric corticocortical afferents.

V. Internal pyramidal layer: the internal pyramidal layer V contains large pyramidal neurons as well as interneurons, and it is the principal source of efferent for all the motor-related subcortical structures.

VI. Multiform layer: the multiform layer VI contains few large pyramidal neurons and many small spindle-like pyramidal and multiform neurons. The layer VI sends efferent fibers to the thalamus establishing a very precise reciprocal interconnection between the cortex and the thalamus.

For the purpose of the motor study, although all layers were of interest, layer III and V were the most important layers to analyze in the primary motor cortex especially as layer V is where upper motor neuron, which form the motor pathways, originate. For the purpose of the sensory study, layer IV was the most interesting part to analyze in the primary somatosensory cortex as it is the main target of thalamocortical afferents which affect the sensory system.

By analyzing the motor and sensory laminar cortex of 3 17 month old *Gars*$^{C201R/+}$ and 3 aged matched wild type control, and the 15 days old cortex of 2 *Gars*$^{C201R/+}$, 15 days old 3 *Gars*$^{C201R/C201R}$ and 2 aged matched wild type controls no significant difference was observed between all the 6 layers. However, cells in *Gars*$^{C201R/C201R}$ level III of the motor cortex were fewer in numbers than in wild type littermates (Fig 6.3) although it was not significant (p value 0.09).

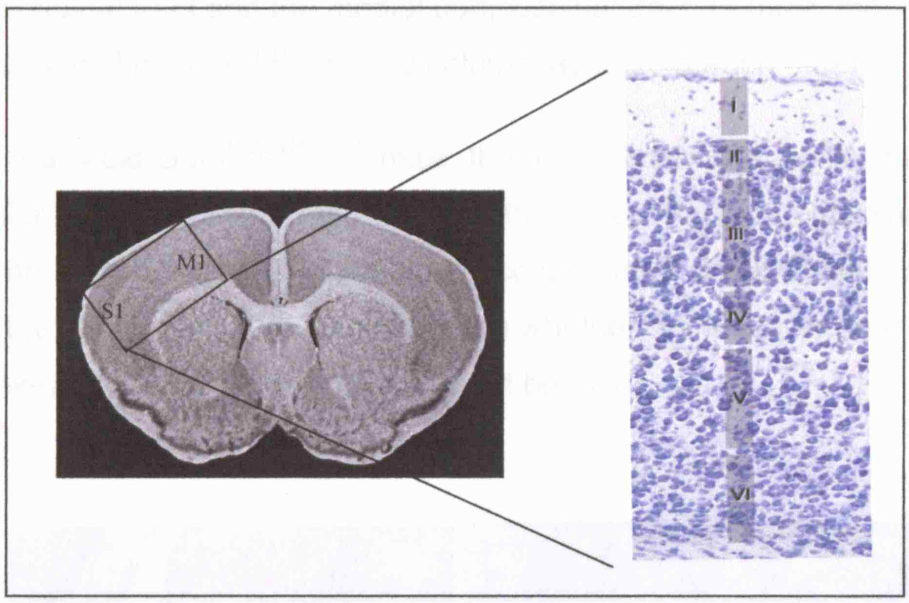

Fig 6.2 I to VI mouse laminar layers of the primary motor cortex (M1) and of the primary somatosensory cortex (S1) (http://www.mbl.org/).

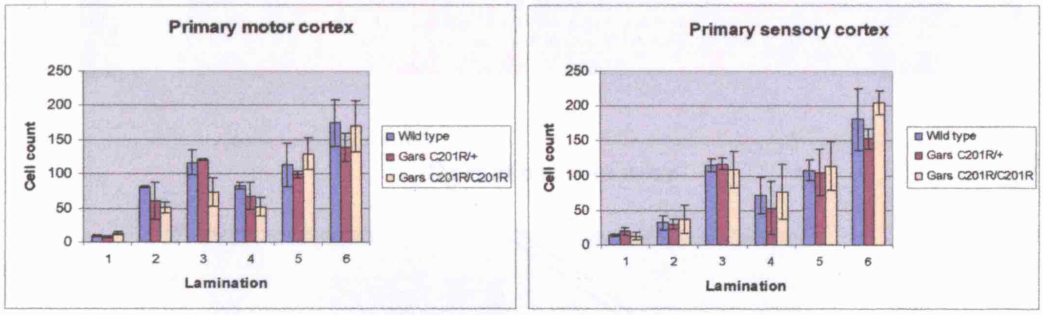

Fig.6 3 Motor and sensory cortical lamination of 15 days old *Gars*$^{C201R/+}$ (n= 2), *Gars*$^{C201R/C201R}$ (n=3) and wild type littermate controls (n=2). Cells in *Gars*$^{C201R/C201R}$ level III of the motor cortex are less than in wild type littermates although not significant (p value 0.09). 250μmX 750μm area analysed (x10 magnification).

The dorsal column-medial lemniscus pathway is the sensory pathway responsible for transmitting fine touch and conscious proprioceptive information from the body to the cerebral cortex (Brumback 1996).

The corticospinal tract mostly contains motor axons. In humans, it actually consists of two separate tracts in the spinal cord: the lateral

corticospinal tract and the medial corticospinal tract. In mice, the corticospinal tract and the dorsal column lay next to each other.

In 15 days old *Gars*$^{C201R/C201R}$ mice, the dorsal column is significantly smaller in size compared to wild type littermates (Fig 6.4). However, as it was not possible to distinguish dorsal column from corticospinal tract with the stains used, an assumption on whether the motor or sensory pathway was affected or both could not be made.

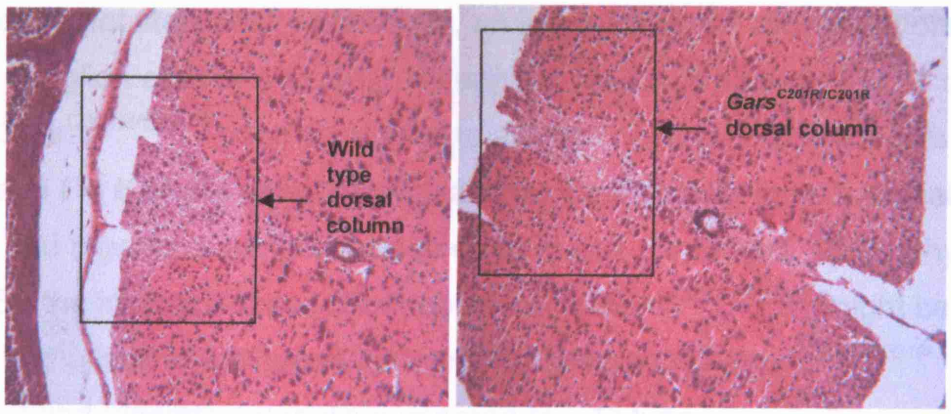

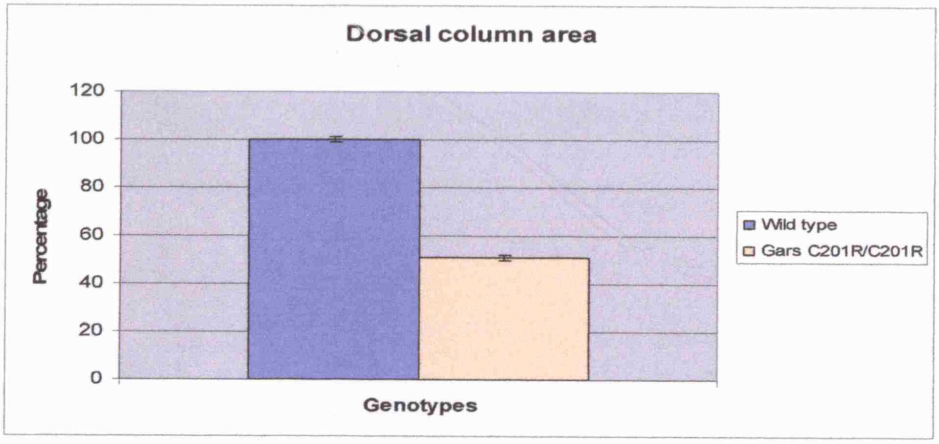

Fig 6.4 5-10 µm haematoxylin and eosin stained sections of thoracic spinal cord of 15 days old *Gars*$^{C201R/C201R}$ mice compared to aged matched wild type littermate controls (x10 magnification). Graph showing area percentage of dorsal column of 15 day old *Gars*$^{C201R/C201R}$ (n=3) compared to littermate control (n=3) (p value 7.37E-05).

Evidence for a sensory deficit arose when the dorsal root ganglion and the trigeminal ganglion were analyzed in the *Gars*$^{C201R/C201R}$ mice.

The dorsal root ganglion is the nodule on a dorsal root that contains cell bodies of neurons in afferent spinal nerves. All of the axons in the dorsal root bring somatosensory information, conveying sensory information into the brain and spinal cord. The trigeminal ganglion is analogous to the dorsal root ganglia as contains the cell bodies of incoming sensory nerve fibers from the rest of the body (Alberts 1994).

Although not statistically significant, an increase in cell counts of dorsal root ganglion cells and trigeminal ganglion cells was observed in 15 days old *Gars*$^{C201R/C201R}$ mice compared to age matched wild type controls (Fig 6.5 and Fig 6.6). As different populations of cells exists in both dorsal root and trigeminal ganglion which differ in size (Brumback 1996; Shy 2005), the increase in cell count observed in *Gars*$^{C201R/C201R}$ might be due to the lack of the large diameter neurons in both *Gars*$^{C201R/C201R}$ dorsal and trigeminal ganglia compared to wild type.

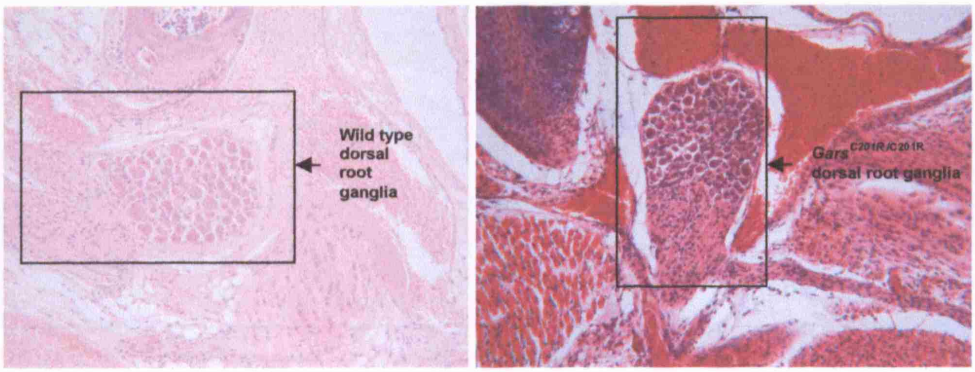

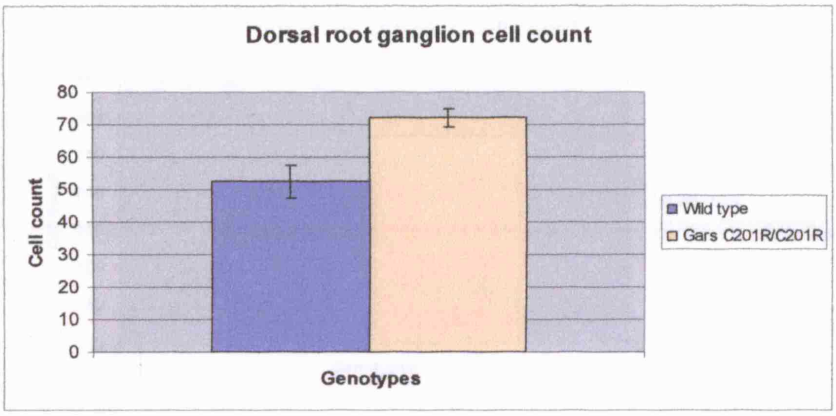

Fig 6.5 2-5 µm haematoxylin and eosin stained sections of dorsal root ganglion of 15day old *Gars*$^{C201R/C201R}$ mice compared to aged matched wild type littermate controls (x10 magnification). Graph showing total cells count of 2 15 day old *Gars*$^{C201R/C201R}$ dorsal root ganglia compared to 2 aged matched wild type littermate controls (p value 0.06) (X10 magnification).

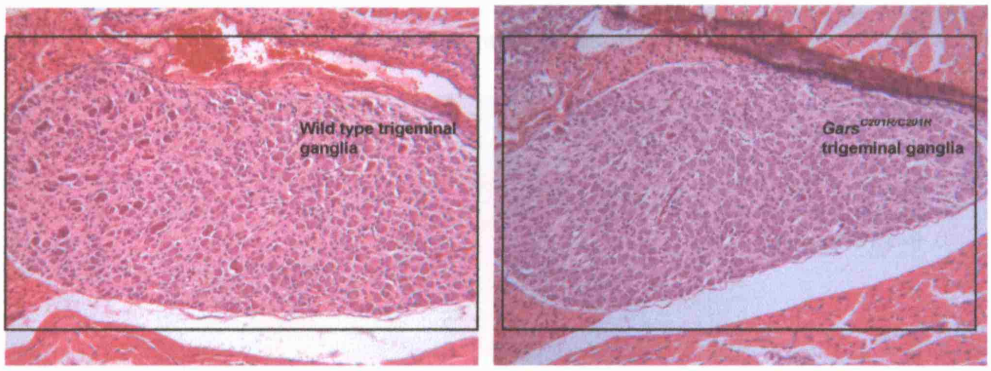

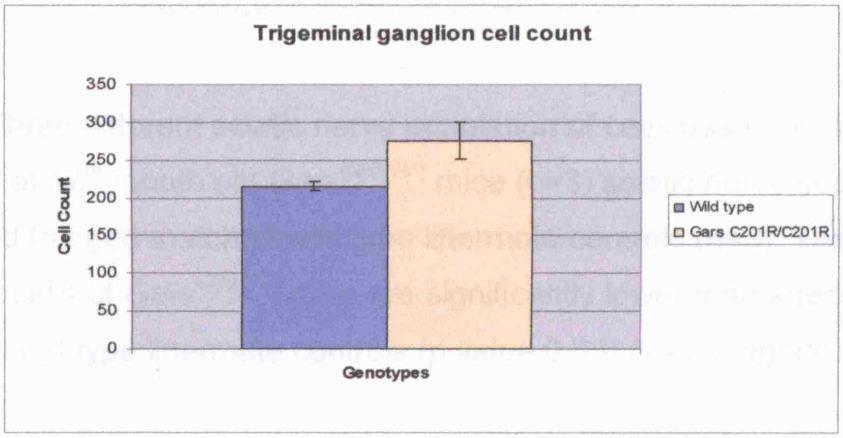

Fig 6.6 2-5 µm haematoxylin and eosin stained sections of trigeminal ganglion of 15 day old *Gars*$^{C201R/C201R}$ mice compared to aged match wild type littermate controls (x10 magnification). Graph showing total cell count of 2 15 day old *Gars*$^{C201R/C201R}$ trigeminal ganglia compared to 2 aged match wild type littermate controls (p value 0.07) (x 10 magnification).

A reduction of large diameter neurons was observed in 17 month old *Gars*$^{C201R+}$mice sciatic nerve compared to wild type littermates. The sciatic nerve is a sensory and motor nerve originating in the sacral plexus and running through the pelvis and upper leg. Therefore it was interesting to observe that large, medium and small diameter fibres of 3 *Gars*$^{C201R+}$ and 3 wild types were measured, counted and the mean number was calculated. A 50% reduction in large diameter fibres was observed in *Gars*$^{C201R+}$ compared to aged match littermate controls (Fig 6.7). Unfortunately, as it is not possible to distinguish in the sciatic nerve which are sensory and motor fibres, an assumption on whether the motor or sensory pathway were affected could not be made.

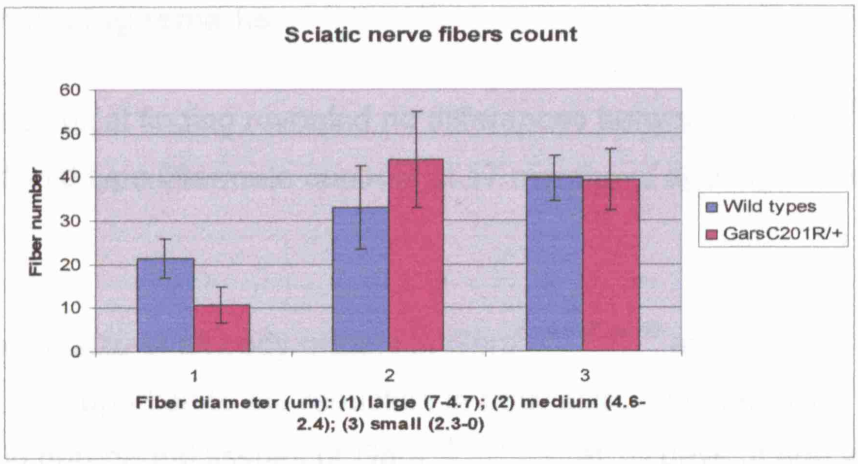

Fig 6.7 Three different sciatic nerve population of cells based on axon diameter of 17th month old *Gars*$^{C201R/+}$ mice (n=3) sciatic nerve sections compared to aged matched wild type littermate controls (n=3). The large diameter cells of *Gars*$^{C201R/+}$ mice are significantly lower than aged matched wild type littermate controls (p value 0.03) (x 40 magnifications).

Deterioration of the sheath in demyelinating diseases is a serious clinical problem (Radtke et al. 2007). Myelin sheath, the lipid-rich sheath surrounding axons in both the central and peripheral nervous systems, is an electrical insulator and allows faster and more energetically efficient conduction of impulses. To asses whether myelin was affected in the *Gars*^{C201R} mice, the g ratio was calculated which represents the thickness of the myelin sheath (the number of wraps around the axon) proportional to the axon's diameter. No significant difference was observed in 17 month old *Gars*$^{C201R/+}$ mice compared to aged match wild type controls in toludine blue stained sciatic nerve sections (data not shown).

6.4 Concluding remarks

Histopathological finding revealed no differences between *Gars*$^{C201R/+}$ mice and wild type littermate controls at 17 months of age in non-neural tissue.

Although the size of all body organs in *Gars*$^{C201R/C201R}$ animals was reduced, in proportion to the reduction in body size, no differences to controls in non-neural tissues of *Gars*$^{C201R/C201R}$ at 15 days of age was observed either.

In addition, there was no evidence of inflammation, degeneration or neoplasm, in any systemic organ examined.

Although sciatic nerve analysis showed no sign of deterioration of the myelin sheath in 17 month old *Gars*$^{C201R/+}$ mice compared to wild type littermate controls, a decrease in sciatic nerve large diameter fibres was observed.

Motor and sensory cortices were also normal in both 17 month old *Gars*$^{C201R/+}$ mice and 15 day old *Gars*$^{C201R/C201R}$ compared to age matched wild type controls. However, spinal cord histology showed a significant reduction in thoracic dorsal column and, although not significant, an increase in neurons numbers in the dorsal root ganglia and trigeminal ganglia of *Gars*$^{C201R/C201R}$ mice at 15 days of age compared to aged matched wild type littermate controls.

Although the histopathological findings suggest that the peripheral nervous system might be involved in the abnormal phenotype observed in the *Gars*^{C201R} animals, from the histological data collected so far, an assumption on whether the motor or sensory pathway is affected or both cannot be made. Thus, more histological investigation should be carried out including studies on the neuromuscular junction to suggest that this

mutation creates a valid model of CMT2D for use in future mechanistic studies.

7. Chapter 7: Characterization of the Moonwalker mouse

This chapter details phenotypic and genetic observations made of the BHV/7 line. BHV/7 mutant mice showed a visible ataxic gait with retropulsion, suggesting that the mice could be of interest as potential models of human ataxia. For in depth phenotyping the same four parameters as GENA 201 and 202 were adopted: grip strength, rotarod, wire manoeuvre and weight. In addition, preliminary histopathology analysis was carried out on the mice. Linkage analysis was carried out which lead to the identification of an area of interest on Mmu3. Due to the peculiar retropulsion phenotype, the BHV/7 mutation was called Moonwalker (Patrick Nolan personal communication).

7.1 Phenotype of Moonwalker

Inheritance

Following backcrossing to C3H and IVF on a C3H background, 61 N2 offspring were produced and the overall sex ration was 1:1 males to females (32 males, 29 females). The small body size and retropulsion phenotypes were detectable in 50% of the resulting progeny suggesting an autosomal dominant inheritance.

Two intercrosses matings were set up in an attempt to breed homozygous offspring. Neither these matings produced any offspring, therefore all the phenotype analysis in this study was done on heterozygotes.

Phenotypic characterization

Although affected and unaffected Moonwalker animals were scored for positional cloning based on small body size and retropulsion phenotypes, further phenotyping was carried out. Four parameters were used to assess the phenotype of the progeny from the founder animal. The parameters measured were (1) grip strength, (2) rotarod performance, (3) wire manoeuvre and (4) weight at 9 weeks of age.

Female and male data were analyzed separately to allow for any size differences in the parameter tested. Male and female means and standard devations were calculated in each test. Mice were classed as mutant or wild type by analysis of the presence or absence of the small body size and ataxic gait with retropulsion phenotype.

Grip strength

N2 12 male Moonwalker animals produced by backcrossing to a C3H background underwent grip strength testing of the combined fore and hind limbs at 9 weeks and additionally at 11 weeks of age. No significant difference was observed between male Moonwalkers and male wild types at both time points (Fig 7.1) suggesting the Moonwalker grip is not compromised by the underlying mutation.

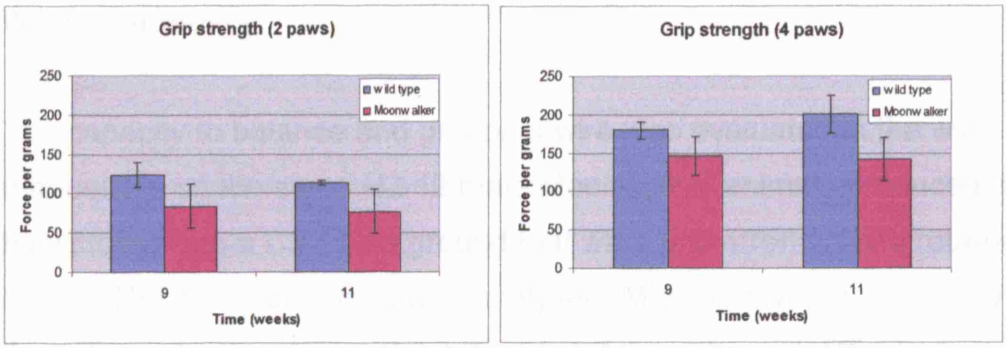

Fig 7.1 Grip strength performances of 5 male Moonwalkers on C3H background compared to age-and sex-matched 7 wild type littermates at 9 and 11 weeks of age. The first graph represent data obtained from 2 paws experiments, whereas the second graph represents data from a 4 paws experiment.

Rotarod

The same N2 12 male Moonwalker animals produced by backcrossing to a C3H background that were grip strength tested underwent rotarod and wire manoeuvre testing at 9 weeks of age. No significant reduction in motor coordination and balance was observed in male Moonwalker and male wild types (Fig 7.2). The high degree of variation in the Moonwalker cohort suggests the rotarod test might not be as effective to further characterize the affected animals.

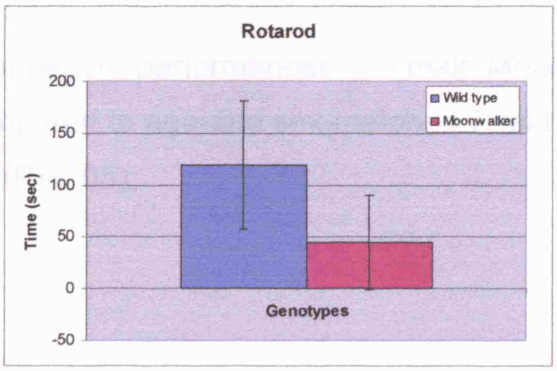

Fig 7.2 Rotarod performances of 5 male Moonwalkers on C3H background compared to age-and sex-matched 7 wild type littermates at 9 weeks of age.

Wire manoeuvre

The capacity to balance and grip on a wire was evaluated in the wire manoeuvre on the same N2 12 male Moonwalker animals produced by backcrossing to a C3H background that were grip strength and rotarod tested. The mean of 3 trials was analysed. Mice received a score of 0 if they showed active grip with hind legs, 1 if they showed difficulty to grasp with hind legs struggling, 2 if they were unable to grasp with hind legs, 3 if they fell within seconds and 4 if they fell immediately.

5 male Moonwalker mice failed to balance and grip on a wire compared to age-and sex-matched 7 wild type littermates at 9 weeks of age. As shown in Fig 7.3 all the Moonwalker mice were unable to grasp with the hind limbs, 3 fell from the wire within seconds and 2 fell immediately.

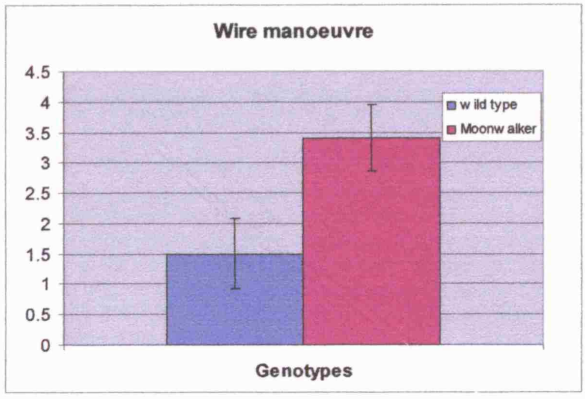

Fig 7.3 Wire manoeuvre performances of 5 male Moonwalkers on C3H background compared to age-and sex-matched 7 wild type littermates at 9 weeks of age ($P<0.05$).

Weight

Body weights of 9 weeks old 5 male and 7 female Moonwalkers on C3H background were taken and compared to age-and sex-matched 7 male and 5 female wild type littermates. The data showed a significant reduction in weight in both male and female cohorts (Fig 7.4).

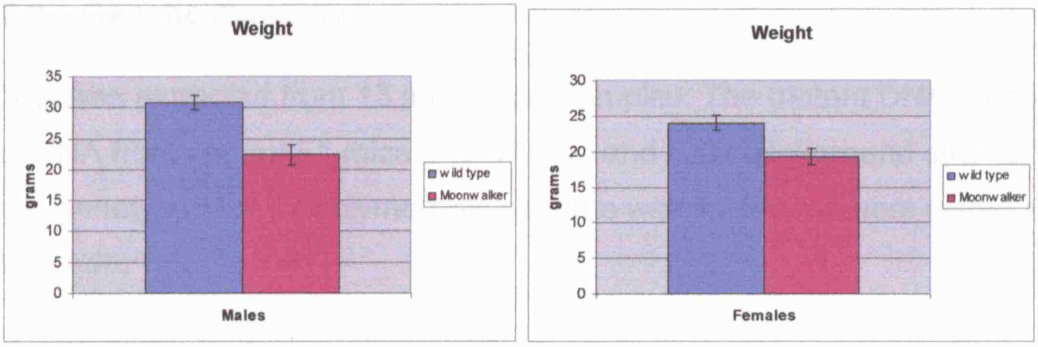

Fig 7.4 Graphs showing recorded weight of 5 male and 7 female Moonwalkers on C3H background compared to age-and sex-matched 7 male and 5 poor females ($P<0.05$).

7.2 Genetic mapping

DNA was extracted from 13 mutant tail samples. The mutant DNA, as well as DNA from control F1 mice and BALB/c and C3H background strains was genotyped for 72 polymorphic genome wide SNPs markers (listed in Appendix 1).

Initial genotyping revealed an area of linkage on chromosome (Mmu) 3. 12 N2 mutants out of 13 N2 were heterozygous between 1 Mb and 88 Mb (Fig 7.5). Sample 12 by showing homozygosity between the 26 Mb and 88 Mb interval proved to be an informative sample. For example, if it showed to be heterozygous by further genotyping the sample with markers positioned before 26 Mb, it could be narrowing down the area of linkage to an interval between 1 Mb and 26 Mb rather than 1 Mb to 88 Mb. However, if it still showed homozygosity then it follows that either sample 12 is not a mutant or that the area of linkage on chromosome (Mmu) 3 is not correct. Unfortunately, no more DNA was available from sample 12 following the genome scan and thus it couldn't be further genotyped with additional markers. The whole genome scan results are listed in Appendix 6.

	CHROMOSOME 3			
SNP_MB	26	88	105	132
C3H	G	C	C	A
BALB/c	A	A	T	G
1 BHV7.5B	2	2	2	2
2BHV7.5A	2	2	2	1
3BHV7A.3F	2	2	2	2
4 BHV7351.6A	2	1	1	1
5BHV7351.2B	2	2	1	1
6 BHV7B.2C	2	2	2	2
7 BHV7C.7E	2	1	1	1
8 BHV7C.2	2	1	1	1
9 BHV7E.3	2	f	2	2
10 BHV7E.1	2	1	1	1
11 BHV7E.C	2	1	1	1
12 BHV7H.1A	1	f	1	f
13 BHV7H.1E	2	f	1	1

Fig 7.5 Initial haplotype obtained following Moonwalker linkage analysis. (1=homozygous; 2= heterozygous and f=failed).

7.3 Fine mapping

The critical region was narrowed by adding more mutants in the panel and by using a few more polymorphic SNPs and microsatellite markers (D3Mit90 (12Mb), D3Mit93 (29Mb), D3Mit333 (44Mb)) to haplotype map 32 affected animals from the C3H (N3) background. Results from this haplotype analysis showed the mutation must lie within the critical region narrowed down between 0 and 26 Mb (Fig 7.7). The region of interest will have to be narrowed down by genotyping additional backcrossed progeny in order to identify a small enough critical region to start analysing for candidate genes.

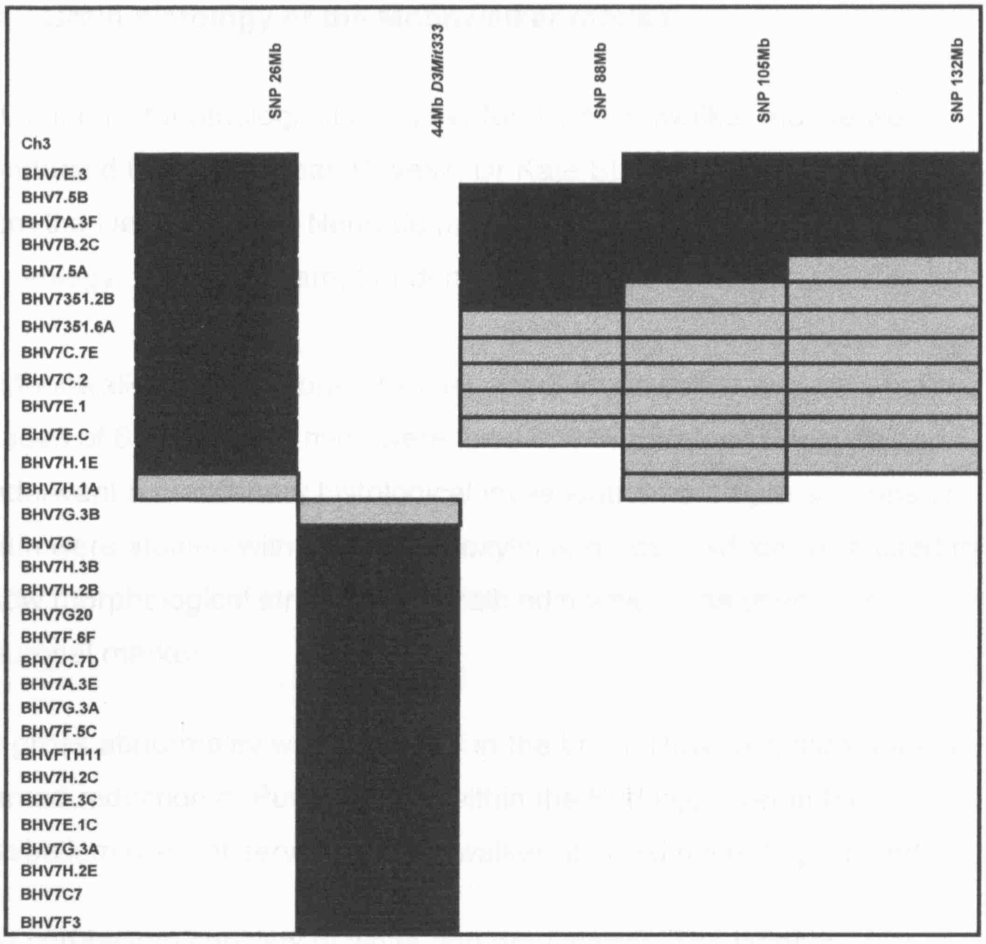

Fig 7.6 Haplotype obtained following Moonwalker linkage analysis and attempts to narrow down the region of interest on Mmu 3 using affected mice on a C3H background (all map positions according to MGI).

7.4 Brain histology of the Moonwalker mouse

All of the histopathological analyses for the Moonwalker mouse were conducted by Prof. Tamas Revesz, Dr Kate Strand and Janice Holton from the Department of Neurodegenerative Disease, Institute of Neurology, Queen Square, London, WC1N 3BG, UK.

3 Moonwalker mutants brain tissues and 3 Moonwalker wild type brain tissues of 6 months old mice were fixed in 4 % paraformaldehyde and underwent a preliminary histological investigation. 5-10 µm sections of brain were stained with the haematoxylin and eosin, which were used to show morphological structure and calbindin which was used as a neuronal marker.

No gross abnormality was observed in the brain. However, gliosis and a marked reduction of Purkinje cells within the Purkinje layer in the cerebellum were observed in Moonwalker affected mice (Fig 7.8 and 7.9).

The cerebellum consists of white and grey matter. The latter is subdivided into molecular, purkinje cell and granular layer. The Purkinje cells can easily be identified due their large size and are found on the border of granular layer facing the molecular layer (Fig 7.8 and 7.9). Purkinje cells send inhibitory projections to the deep cerebellar nuclei, and constitute the sole output of all motor coordination in the cerebellar cortex.

A reduction of these cells might be the cause of the ataxic gait with retropulsion phenotype observed in the Moonwalker mice, as in mammals, a condition where the Purkinje cells begin to atrophy shortly after birth, called cerebellar abiotrophy, can lead to symptoms including ataxia, intention tremors, hyperreactivity, lack of menace reflex, stiff or high-stepping gait, apparent lack of awareness of where the feet are, and a general inability to determine space and distance (Blanco et al. 2006).

In humans, Purkinje cells are affected in a variety of diseases ranging from toxic exposure (alcohol, lithium) (Servais et al. 2007), to autoimmune diseases and to genetic mutations (spinocerebellar ataxias, autism) (Fernandez-Gonzalez et al. 2002; Kutzelnigg et al. 2007) and neurodegenerative diseases that are not thought to have a known genetic basis (cerebellar type of multiple system atrophy, sporadic ataxias)(Sakaguchi et al. 1996).

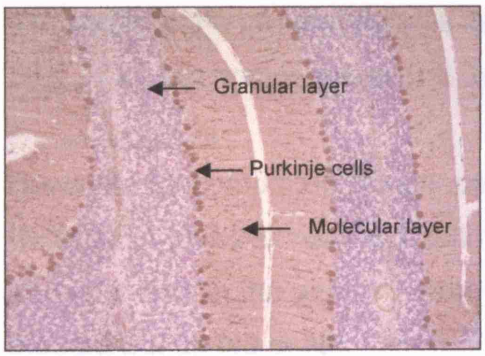

Fig 7.7 6 month wild type cerebellum Calbindin stained tissue.

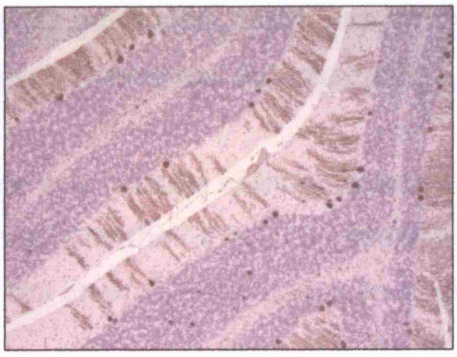

Fig 7.8 6 month Moonwalker cerebellum Calbindin stained tissue.

7.5 Concluding remark

The ataxic gait with retropulsion, small body size and poor wire manoeuvre phenotypes were characteristic of the Moonwalker mouse. In addition, histopathological finding suggested a loss of Purkinje cells in the cerebellum. Although the pathogenic mutation carried by Moonwalker was not uncovered in this study, the available data on the nature of the phenotype as well as the outcome of the preliminary linkage analysis will facilitate future studies of these mice.

The genome scan results of the 13 Moonwalker mutants used clearly showed that the generation was an N2 generation, having approximately 50% of all loci homozygous and the remaining loci heterozygous.

However, by comparing the genome scan results of Moonwalker with the GENA 201 and 202 results, it followed that the GENA 201 and 202 mutants used in the analysis were not on an N2 generation as originally thought but an N8 or N9.

Due to the straightforward concept of the backcross system, the genetic consequences of this breeding protocol can be easily calculated. First, based on the assumption that the BALB/c and C3H strains are completely distinct with different alleles at every locus in the genome, then all F_1 animals will be 100% heterozygous BALB/cxC3H at every locus.

According to Mendel's laws, equal segregation and independent assortment will act to produce gametes from these F_1 animals that carry C3H alleles at a random 50% of their loci and BALB/c alleles at the remaining 50%.

When these gametes combine with gametes produced by the C3H inbred partner (which, by definition, will have only C3H alleles at all loci), they will produce N_2 progeny having genomes in which approximately

50% of all loci will be homozygous C3H/C3H and the remaining loci will be heterozygous BALB/c/C3H.

Thus, in a single generation, the level of heterozygosity is reduced by about 50%. Furthermore, it is easy to see that at every subsequent generation, random segregation from the remaining heterozygous alleles will cause a further ~50% overall reduction in heterozygosity.

At the fifth generation, after only four backcrosses, the developing line will be identical to the inbred partner across ~94% of the genome. By the tenth generation, identity will increase to ~99.8%.

GENA 201 and 202 mutant mice showed to be identical to the inbred line across most of the genome suggesting that they are close to a tenth generation.

8. Chapter 8: Discussion

8.1 Characterization of GENA 201 and 202

The aim of the behavioural screen was to be able to characterize affected and unaffected animals for positional cloning by combining the results of all the tests. However, as there was poor correlation when comparing results of grip strength, rotarod and wire manoeuvre, grip strength, measured using all 4 paws, was selected as the most robust 'visible' score of motor performance that defined 'affected' and 'unaffected' GENA201 and 202 mice.

The poor grip strength phenotype was detectable in 50% of the backcross offspring. This simple pattern of inheritance implies full penetrance of an autosomal dominant mutation. Intercross produced wild types and heterozygotes as well as a subset of offspring with a more severe motor phenotype. Intercross matings produced 4 homozygous mice (5%) out of a total of 76 progeny on a C57BL/6 background and 7 homozygous mice (12%) out of a total of 60 on a C3H background which is significantly reduced from the expected 25% suggesting that the mutation is causing substantial loss of homozygotes.

Linkage analysis revealed an area of interest on Mmu 6. Genotyping for additional polymorphic markers failed to narrow down below 5 Mb. The gene coding for glycyl-tRNA synthetase (*Gars*) is located within the linked area on chromosome 6, and was considered a favourable candidate for mutation detection as *GARS* was recently found to be the causative mutation in families segregating CMT2D and dSMA-V (Antonellis et al. 2003).

This approach was successful since it led to the identification of a point mutation in exon 5 (456T to C transition). Subsequent forward and reverse sequencing of all exons and intron/exon boundaries failed to identify another mutation in the *Gars* gene.

The mutation *Gars*^{C201R} is likely to have arisen from the mutagenic action of ENU. Although ENU preferentially modifies A/T to T/A transversions (~44% of mutations) 38% of ENU mutations involve a A/T to G/C transitions (Justice et al. 1999).

To further rule out the possibility that the above sequence variant represented a rare polymorphisms, a wide panel of inbred strains was screened as controls by PCR amplification and DNA sequencing (Table 4.3). None of these strains were heterozygous for the single base position adding more evidence to support the supposition that the variation was not a rare polymorphism.

In addition, this mutation changes a restriction site for the enzymes HaeII and HhaI which further suggested that the variant observed in GENA 201 and 202 was not a sequencing artifact and allowed the designing of a protocol for routine genotyping by PCR followed by RFLP analysis.

The genetic data collected so far suggests that the *Gars*^{C201R} mutation is responsible for the GENA 201 and 202 phenotype. It remains a formal possibility that this mutation is a SNP, and the only way to rule out this possibility is to either sequence all the genes in the critical region or to cross the mice to another Gars mutant mouse and look for non-complementation.

We are currently setting up collaboration to cross the *Gars*^{C201R} mouse to a Gars mutant mouse held by the Jackson Laboratory to look for non-complementation and confirm *Gars*^{C201R} is the causative mutation.

8.2 Functional investigation into the effect of *Gars*^{C201R} mutation

Aminoacyl-tRNA synthetases (ARSs) catalyze tRNA aminoacylation, a critical step in protein translation. Each ARS conjugates a cognate amino acid onto corresponding tRNA (aminoacylation). In the case of GARS, it recognizes glycine and $tRNA^{gly}$ and synthesizes aminoacylated glycyl-tRNA.

Protein translation is an essential process in all the cells. In neurons, protein translation can occur near the cell body or in distal neuronal processes where proteins are synthesized locally. Local protein synthesis has been implicated in many aspects of neuronal development and function, such as axon guidance, dendritic elaboration, synaptic plasticity and long-term memory formation (Bailey et al. 1996; Martin 2004; Steward & Schuman 2003).

Errors in protein translation can lead to neurodegeneration. For example, a recessive mouse mutation in alanyl-tRNA synthetase (*Aars*) causes cerebellar Purkinje cell loss and ataxia in the mouse sticky mutation. The missense mutation in the editing domain of the alanyl-tRNA synthetase gene compromises the proofreading activity of this enzyme during aminoacylation of tRNAs. The low levels of mischarged transfer RNAs (tRNAs) can lead to an intracellular accumulation of misfolded proteins in neurons. These accumulations are accompanied by upregulation of cytoplasmic protein chaperones and by induction of the unfolded protein response leading to cell death (Lee et al. 2006).

GARS exists as a homodimer and it has two forms, mitochondrial and cytoplasmic that are encoded by the same gene. It contains 3 major domains: (1) a domain that interacts with the acceptor stem of glycyl-tRNA (2) the core catalytic domain; (3) the anticodon recognition domain (Freist et al. 1996).The charging of glycine onto its tRNA is the only known function of the GlyRS enzyme. However, other functions have been demonstrated for other tRNA synthetase which include inhibition of

angiogenesis (Tzima & Schimmel 2006), regulation of the inflammatory response (Wakasugi & Schimmel 1999) and translational silencing (Sampath et al. 2004).

Two forms of Charcot-Marie-Tooth neuropathies (CMTs) are caused by mutations in aminoacyl t-RNA synthetases. Mutation in tyrosyl-tRNA synthetase (TyrRS) cause dominant intermediate CMT type C (Jordanova et al. 2006). These mutations partially lack enzymatic activity, and the mechanism is proposed to be a haplo-insufficiency, in which a defect in protein synthesis affects neurons.

GARS was found to be the causative mutation in families segregating CMT2D and dSMA-V (Antonellis et al. 2003). *GARS* mutations are characterized by autosomal dominant inheritance and adolescent onset of disease with unique motor and sensory deficits. However, haplo-insufficiency or a dominant-negative effect has not yet been clearly demonstrated in the *GARS* gene.

To help our understanding of how aberrant *GARS* sequences result in dominant peripheral neuropathy, several interesting findings followed. Antonellis et al 2006 showed there are not any significant mutation-associated changes in Gars expression and the majority of identified *GARS* mutations modelled in yeast severely impair growth. In addition, GARS localises, immunohistochemically, to peripheral nerve axons in human thoracic spinal cord and sural nerve tissue sections and it is associated with cytoplasmic granules in the axons of the ventral horn, dorsal horn, ventral root, dorsal root and sural nerve (anti-GARS staining was also seen in the nucleus of cells in these structures). However, this localisation is disrupted in the majority of mutant GARS (Antonellis et al. 2006).

In addition, Chihara et al 2007 identified a mutation in *Aats-gly*, the *Drosophila melanogaster* ortholog of the human *GARS* gene. They showed that loss of *gars* in *Drosophila* neurons preferentially affects the

elaboration and stability of terminal arborisation of axons and dendrites and they also provided evidence that human Gars shows equivalent loss of functions observed in *Drosophila* (Chihara et al. 2007).

In this study, the comparable enzymatic activity between $Gars^{C201R/+}$ and wild type litter mates made a loss of function mechanism through impaired enzymatic activity unlikely. However, the reduction in enzymatic activity observed in $Gars^{C201R/C201R}$ compared to wild type and $Gars^{C201R/+}$ indicated a different conclusion. In wild types, GARS is functionally active in the neuronal cells and it is transported to the periphery to support axonal $tRNA^{gly}$ charging. In $Gars^{C201R/+}$, the wild type allele could have some ability to compensate for or compete with the mutant protein, while in $Gars^{C201R/C201R}$ such ability could be lost, thus, resulting in the observed impaired enzymatic activity.

However, GARS functional holoenzyme exists as a homodimer and to justify a haploinsufficiency mechanism one should have noticed a 100% enzyme activity in wild types, a 75% activity in heterozygotes and a 50% activity in homozygotes which was not observed.

Although there was a trend towards reduced enzyme activity, no significant difference in activity between wildtype and heterozygous animals at 15 days or 3 months was observed and a 75% reduction in activity in homozygous mice was measured.

This may indicate that protein levels are raised in homozygous animals as some form of compensation for reduced enzyme activity, possibly even during a critical developmental window.

This could imply that at least part of the $Gars^{C201R}$ phenotype arises from a loss of enzyme activity, although phenotypic effects from a loss of activity may only be confined to homozygous animals, not necessarily heterozygotes, suggesting different pathological mechanisms may be critical in heterozygotes and homozygotes.

From the studies so far either mechanism is possible, suggesting another scenario in which the phenotype could arise from loss of function (such as loss of enzyme activity, as seen in the homozygous *Gars*$^{C201R/C201R}$ mice) and a gain of function, as suggested in the *Gars*^{Nmf249} model (Seburn et al. 2006). In the *Gars*^{C201R} mice it is possible that different pathological mechanisms are critical in heterozygotes and homozygotes.

The association between peripheral neuropathy and mutations in two genes with an important role in protein synthesis indicates that peripheral nerves are susceptible to impaired or altered protein synthesis and that these mutant phenotypes are caused by the disruption of protein translation, rather than by noncanoncal function associated with some ARSs (Lee et al. 2004).

Furthermore, impaired degradation of a protein essential for assembly of the multiple tRNA synthetase complex is associated with neurodegeneration in certain patients with Parkinson's disease (Ko et al. 2005), suggesting that neurons in general may be more susceptible to protein synthesis defects.

8.3 Comparison of *Gars*^{C201R} mutant phenotype with other *Gars* mutant mice

In addition to the *Gars*^{C201R} mutation described here, a second allele of Gars that also causes a dominant neurological dysfunction in mice was reported by Seburn and colleagues (Seburn et al. 2006). *Gars*^{Nmf249} mice have a more severe sensory and motor axonal neuropathy than *Gars*$^{C201R/+}$mice.

A visible phenotype is apparent in *Gars*^{Nmf249} heterozygotes by 3 weeks of age and typically death by 6-8 weeks of age on a C57BL/6J background whereas *Gars*$^{C201R/+}$ mice have no early lethality on either a C3H or C57BL/6J background and the phenotype can be detected by grip strength as the locomotor abnormalities are more subtle.

Gars^{Nmf249} mice have abnormal neuromuscular junctions and impaired transmission, and reduced nerve conduction velocities with loss of large diameter peripheral axons although no defects in myelination. *Gars*$^{C201R/+}$ neuromuscular junctions was not investigated, however, *Gars*$^{C201R/+}$ also have reduced nerve conduction velocities (Prof M Koltzenburg personal communication, data not shown) with loss of large diameter peripheral axons although no defects in myelination.

In *Gars*^{Nmf249} mice, both sensory and motor nerves are clearly affected and muscle showed atrophy and long-term denervation and reinnervation. Sensory and motor nerve involvement remains still ambiguous in the *Gars*$^{C201R/+}$ mice. No muscle abnormality was observed in the *Gars*^{C201R} mice, except for a possible limb girdle dystrophy in adult *Gars*$^{C201R/+}$. Variation in fiber size, central nuclei, fiber splitting, was seen in mutants as well as the wild type animals, suggesting a possible background effect.

Gars^{Nmf249} mice as *Gars*^{C201R} mice are sensitive to genetic background. *Gars*$^{Nmf249/+}$mice in a mixed C57BL/6/BALB/c/CAST background exhibit

better survival than inbred C57BL/6 *Gars*^{Nmf249} mice, although they still show overt neuromuscular dysfunction with a similar age of onset.

Results from both *Gars*^{Nmf249} and *Gars*^{C201R} mice support the influence of genetic background and allelic variability which is consistent with the differences in clinical presentation in CMT2D patients.

As the mutation in the *Gars*^{Nmf249} mouse is dominant and lethal before animals can be effectively bred, the strain is maintained by ovary transplantation. This is not the case for the *Gars*^{C201R} mice that have a normal life span and breed normally, including intercrosses matings which produce live born homozygotes.

No spinal cord pathology was observed in the *Gars*^{Nmf249} mouse. However, in *Gars*$^{C201R/C201R}$ mice spinal cord histology showed a significant reduction in thoracic dorsal column and, although not significant, an increase in fibre numbers in the dorsal root ganglia and trigeminal ganglia of *Gars*$^{C201R/C201R}$ mice at 15 days of age compared to aged matched wild type littermate controls.

Notably, *Gars*^{Nmf249} retained normal aminoacylation activity *in vitro,* and mice heterozygous for a gene trap loss of function *Gars* allele showed no phenotypes, the study concluded that there was a pathogenic role for the mutant GARS in peripheral neurons, whereas here we show that the molecular mechanisms of pathology for the *Gars*^{C201R} mutation might be in fact some loss of function.

The *Gars* gene may be a case where different mutations cause the same disease thorough different mechanisms, with some acting via gain of function mutations (Seburn et al. 2006), and others via haplo-insufficiency due to loss of function mutations.

The mice *gars* mutations represent a useful platform in the analysis of gene fuction and can add to the information already available for targeted mutations (Nolan et al. 2002).

8.4 Comparison *of* $Gars^{C201R}$ mutant phenotype with human disease

GARS was found to be the causative mutation in families segregating CMT2D and dSMA-V. To date 9 CMT2D and dSMA-V associated mutations in the human *GARS* gene (G240R; L129P; E71G; G526R (Antonellis et al. 2003)) (H418R (Sivakumar et al. 2005)) (D500N(Del Bo et al. 2006)), (G598A, S581L, I280F(James et al. 2006)) and 2 in the mouse *gars* gene (P278KY (Seburn et al. 2006)and C201R) have been found and; all of them are dominant missense mutations in conserved aminoacids distributed throughout the GARS protein.

As in the human patients, the $Gars^{C201R}$ mutation is characterized by autosomal dominant inheritance and adolescent onset of disease. In addition, the $Gars^{C201R/+}$ mice show loss of large diameter axons from sciatic nerve causing reduced nerve conduction velocities without contributing defects in myelination.

Sensory and motor nerves involvement is not clear in the $Gars^{C201R}$ mice. In human, sensory involvement is ambiguous as well. CMT2D and dSMA-V are allelic, but the clinical diagnosis of CMT2D depends on the presence of sensory symptoms. In the five pedigrees initially identified, three presented with purely motor dSMA-V, one with CMT2D, and one was ambiguous (Sivakumar et al. 2005).

Modelling human 5 *GARS* mutation in the yeast ortholog (GRS1) revealed that L129P, H418R, and G526R do not complement removal of wild type GRS1 which is consistent with the loss of function mechanism observed in the $Gars^{C201R}$ mutation, whereas others (E71G and G240R) appear to do so (Antonellis et al. 2006).

The different degrees of rescue may reflect the nature of the mutation or the sensitivity of the experimental system used. For example, functional study on *Drosophila* showed that although wild type human GARS rescued *Drosophila gars* mutant defects in dendritic and axonal terminal arborisation, human GARS with E71G mutation rescued the phenotype only partially, and human GARS and L129P did not rescue the phenotype at all. Using the human GARS gene and projection neuron morphology, in the Drosophila study, as a measure, may be sensitive enough to detect the partial-loss of function property of the E71G mutation (Chihara et al. 2007).

Interestingly, L129P, H418R, and G526R are associated with dSMA-V, whereas E71G is associated with CMT2D, and G240R is only associated with CMT2D. Mutations showing a loss of function in yeast are more closely associated with dSMA-V but not CMT2D. As CMT2D and dSMA-V show phenotypic similarities, the mutations associated with dSMA-V might be severe enough to detect a phenotype in yeast but not (or just partially) in *Drosophila*.
As in the $Gars^{C201R}$ mice possible modifiers loci in the genetic background may influence the phenotype, the presence of modifiers of GARS mutations might promote differences in clinical presentation as well i.e. the development of either the CMT2D or dSMA-V phenotype. Thus, the mouse *Gars* mutations will provide important mechanistic and phenotypic insights on how to identify such modifiers which might help our understanding of the molecular basis of the disease.

8.5 GENA 201 and 202: concluding remarks and suggested future work

The identification and characterization of GENA 201 and 202 mutant lines represents a successful example of phenotype driven screens to identify mouse mutants.
GENA 201 and 202 mice are siblings. Heterozygous mice show poor grip strength and have a dominantly inherited phenotype. Homozygotes show compromised hind limb movement resulting in a more severe phenotype.

To identify the mutant gene underlying the GENA201 and 202 phenotypes, mutant backcross progeny were genotyped with a panel of markers spanning the genome. Both GENA 201 and 202 mutations were localised to a 5Mb region on chromosome 6 suggesting they are allelic. A point mutation (T>C transition in exon 5) was identified in the glycyl tRNA synthetase gene in both mouse lines, which charges tRNA with glycine. *Gars*^{C201R} point mutation that leads to partial loss of function in *Gars*$^{C201R/C201R}$ mice, confirms the ability of ENU mutagenesis to induce point mutations ideal for the study of intermediate phenotypes.

Glycyl tRNA synthetase mutations have been identified in two hereditary motor and sensory neuropathies, Charcot Marie Tooth 2D and distal spinal muscular atrophy type V, thus the gene plays a role in neurological diseases.

GENA 201 and 202 mutants are therefore interesting animal models that could provide new insights in the understanding of new biological pathways involved in hereditary motor and sensory neuropathies, demonstrating the ability of phenotype driven screens to identify mouse mutants with phenotypes relevant to the study of human disease condition.

However, it would be interesting to further characterize the *Gars*^{C201R} to be able to consider it a valid model of CMT2D and dSMA-V for future

studies by investigating *Gars* mRNA and protein levels in the affected mice. Loss of function through altered mRNA or protein levels are a common pathological mechanism for genetic disorder although unusual for neurodegenerative disease inherited in an autosomal dominant manner.

In addition, although the aminoacylation assay *in vivo* performed in this project by using brain protein homogenates aimed to recreate the same conditions that would occur in the mice brain, to confirm the *in vivo* aminoacylation assay results, it would appropriate to purify the Gars protein from wild type and mutant animals and perform aminoacylation assay *in vitro* .

Furthermore, since CMT2D causes a distally accentuated loss of motor axons, to investigate motor neuron involvement in the $Gars^{C201R}$ mice it would be useful to examine neuromuscular junctions of the affected mice. On the other hand, to examine sensory involvement in the $Gars^{C201R}$ mice it would be ideal to count axons in the motor and sensory branches of the femoral nerve (Scherer et al. 2005).

Based on the outcome of these biochemical and phenotypic analyses, this mutation will create a valid model of CMT2D and dSMA-V for use in future studies.

8.6 Moonwalker: concluding remarks and suggested future work

The ataxic gait with retropulsion, small body size, poor wire manoeuvre phenotypes and loss of Purkinje cells were characteristic of the moonwalker mouse. As all these phenotypic attributes co-segregate with each other in the moonwalker mouse suggesting that they are direct or indirect consequences of the presumed underlying mutation. Without knowledge of the genetic defect, it would be premature to speculate about how these phenotypes may be associated with each other.

The genome scan revealed an area of linkage on Mmu 3. Additional markers were used to map the mutation to a 26 MB region. As the region is not wide to look for candidate genes, mapping the underlying mutation would therefore require the region of interest to be narrowed down by genotyping additional backcross progeny.

As the loss of Purkinje cells is associated with several neurological disease, it would be highly desiderable to attempt further characterize the moonwalker mouse by investigating whether the loss of Purkinje cells is developmental or progressive. Although the pathogenic mutation carried by this line was not uncovered in this study, the available data on the nature of the phenotype as well as the outcome of the preliminary linkage analysis will facilitate future studies of these mice.

In conclusion, the phenotype driven approach, working from interesting phenotypes to positionally clone the mutation can clearly add to our knowledge of human disease (Gars) and give us new insights from novel mutation (Gars) and new loci (Moonwalker).

Reference List

Airaksinen, M. S., Eilers, J., Garaschuk, O., Thoenen, H., Konnerth, A. & Meyer, M. 1997 Ataxia and altered dendritic calcium signaling in mice carrying a targeted null mutation of the calbindin D28k gene. *Proc Natl Acad Sci U S A* **94**, 1488-93.

Alberts, B., Bray, D., Lewis, J., Raff, M., Roberts, K., Watson, J.D. 1994 Molecular biology of the cell. Garland Publishing. New York.

Antonellis, A., Ellsworth, R. E., Sambuughin, N., Puls, I., Abel, A., Lee-Lin, S. Q., Jordanova, A., Kremensky, I., Christodoulou, K., Middleton, L. T., Sivakumar, K., Ionasescu, V., Funalot, B., Vance, J. M., Goldfarb, L. G., Fischbeck, K. H. & Green, E. D. 2003 Glycyl tRNA synthetase mutations in Charcot-Marie-Tooth disease type 2D and distal spinal muscular atrophy type V. *Am J Hum Genet* **72**, 1293-9.

Antonellis, A., Lee-Lin, S. Q., Wasterlain, A., Leo, P., Quezado, M., Goldfarb, L. G., Myung, K., Burgess, S., Fischbeck, K. H. & Green, E. D. 2006 Functional analyses of glycyl-tRNA synthetase mutations suggest a key role for tRNA-charging enzymes in peripheral axons. *J Neurosci* **26**, 10397-406.

Anzini, P., Neuberg, D. H., Schachner, M., Nelles, E., Willecke, K., Zielasek, J., Toyka, K. V., Suter, U. & Martini, R. 1997 Structural abnormalities and deficient maintenance of peripheral nerve myelin in mice lacking the gap junction protein connexin 32. *J Neurosci* **17**, 4545-51.

Bailey, C. H., Bartsch, D. & Kandel, E. R. 1996 Toward a molecular definition of long-term memory storage. *Proc Natl Acad Sci U S A* **93**, 13445-52.

Balling, R. 2001 ENU mutagenesis: analyzing gene function in mice. *Annu Rev Genomics Hum Genet* **2**, 463-92.

Beck, J. A., Lloyd, S., Hafezparast, M., Lennon-Pierce, M., Eppig, J. T., Festing, M. F. & Fisher, E. M. 2000 Genealogies of mouse inbred strains. *Nat Genet* **24**, 23-5.

Berger, P., Bonneick, S., Willi, S., Wymann, M. & Suter, U. 2002 Loss of phosphatase activity in myotubularin-related protein 2 is associated with Charcot-Marie-Tooth disease type 4B1. *Hum Mol Genet* **11**, 1569-79.

Blanco, A., Moyano, R., Vivo, J., Flores-Acuna, R., Molina, A., Blanco, C. & Monterde, J. G. 2006 Purkinje cell apoptosis in arabian horses with cerebellar abiotrophy. J Vet Med A Physiol Pathol Clin Med **53**, 286-7.

Boerkoel, C. F., Takashima, H., Stankiewicz, P., Garcia, C. A., Leber, S. M., Rhee-Morris, L. & Lupski, J. R. 2001 Periaxin mutations cause recessive Dejerine-Sottas neuropathy. *Am J Hum Genet* **68**, 325-33.

Boguski, M. S. 2002 Comparative genomics: the mouse that roared. *Nature* **420**, 515-6.

Bolino, A., Bolis, A., Previtali, S. C., Dina, G., Bussini, S., Dati, G., Amadio, S., Del Carro, U., Mruk, D. D., Feltri, M. L., Cheng, C. Y., Quattrini, A. & Wrabetz, L. 2004 Disruption of Mtmr2 produces CMT4B1-like neuropathy with myelin outfolding and impaired spermatogenesis. *J Cell Biol* **167**, 711-21.

Bolis, A., Coviello, S., Bussini, S., Dina, G., Pardini, C., Previtali, S. C., Malaguti, M., Morana, P., Del Carro, U., Feltri, M. L., Quattrini, A., Wrabetz, L. & Bolino, A. 2005 Loss of Mtmr2 phosphatase in Schwann cells but not in motor neurons causes Charcot-Marie-Tooth type 4B1 neuropathy with myelin outfoldings. *J Neurosci* **25**, 8567-77.

Brown, S. D. & Hardisty, R. E. 2003 Mutagenesis strategies for identifying novel loci associated with disease phenotypes. *Semin Cell Dev Biol* **14**, 19-24.

Brumback, R. A. 1996 Neurology and clinical neuroscience. New York: Springer.

Capecchi, M. R. 1989 The new mouse genetics: altering the genome by gene targeting. *Trends Genet* **5**, 70-6.

Carter, R. J., Lione, L. A., Humby, T., Mangiarini, L., Mahal, A., Bates, G. P., Dunnett, S. B. & Morton, A. J. 1999 Characterization of progressive motor deficits in mice transgenic for the human Huntington's disease mutation. *J Neurosci* **19**, 3248-57.

Chen, H., Detmer, S. A., Ewald, A. J., Griffin, E. E., Fraser, S. E. & Chan, D. C. 2003 Mitofusins Mfn1 and Mfn2 coordinately regulate mitochondrial fusion and are essential for embryonic development. *J Cell Biol* **160**, 189-200.

Chihara, T., Luginbuhl, D. & Luo, L. 2007 Cytoplasmic and mitochondrial protein translation in axonal and dendritic terminal arborization. *Nat Neurosci* **10**, 828-837.

Coghill, E. L., Hugill, A., Parkinson, N., Davison, C., Glenister, P., Clements, S., Hunter, J., Cox, R. D. & Brown, S. D. 2002 A gene-driven approach to the identification of ENU mutants in the mouse. *Nat Genet* **30**, 255-6.

Cox, R. D. & Brown, S. D. 2003 Rodent models of genetic disease. *Curr Opin Genet Dev* **13**, 278-83.

De Sandre-Giovannoli, A., Chaouch, M., Kozlov, S., Vallat, J. M., Tazir, M., Kassouri, N., Szepetowski, P., Hammadouche, T., Vandenberghe, A., Stewart, C. L., Grid, D. & Levy, N. 2002 Homozygous defects in LMNA, encoding lamin A/C nuclear-envelope proteins, cause autosomal recessive axonal neuropathy in human (Charcot-Marie-Tooth disorder type 2) and mouse. *Am J Hum Genet* **70**, 726-36.

Del Bo, R., Locatelli, F., Corti, S., Scarlato, M., Ghezzi, S., Prelle, A., Fagiolari, G., Moggio, M., Carpo, M., Bresolin, N. & Comi, G. P. 2006 Coexistence of CMT-2D and distal SMA-V phenotypes in an Italian family with a GARS gene mutation. Neurology **66**, 752-4.

Edlich, F., Weiwad, M., Erdmann, F., Fanghanel, J., Jarczowski, F., Rahfeld, J. U. & Fischer, G. 2005 Bcl-2 regulator FKBP38 is activated by Ca2+/calmodulin. Embo J **24**, 2688-99.

Festing, M. F. & Fisher, E. M. 2000 Mighty mice. *Nature* **404**, 815.

Fernandez-Gonzalez, A., La Spada, A. R., Treadaway, J., Higdon, J. C., Harris, B. S., Sidman, R. L., Morgan, J. I. & Zuo, J. 2002 Purkinje cell degeneration (pcd) phenotypes caused by mutations in the axotomy-induced gene, Nna1. Science 295, 1904-6.

Fisher, E. M. 1997 The contribution of the mouse to advances in human genetics
Adv Genet **35**, 155-205.

Fortun, J., Go, J. C., Li, J., Amici, S. A., Dunn, W. A., Jr. & Notterpek, L. 2006 Alterations in degradative pathways and protein aggregation in a neuropathy model based on PMP22 overexpression. *Neurobiol Dis* **22**, 153-64.

Freist, W., Logan, D. T. & Gauss, D. H. 1996 Glycyl-tRNA synthetase. *Biol Chem Hoppe Seyler* **377**, 343-56.

Gillespie, C. S., Sherman, D. L., Fleetwood-Walker, S. M., Cottrell, D. F., Tait, S., Garry, E. M., Wallace, V. C., Ure, J., Griffiths, I. R., Smith, A. & Brophy, P. J. 2000 Peripheral demyelination and neuropathic pain behavior in periaxin-deficient mice. *Neuron* **26**, 523-31.

Glenister, P. H. & Thornton, C. E. 2000 Cryoconservation--archiving for the future. *Mamm Genome* **11**, 565-71.

Godinho, S. I., Maywood, E. S., Shaw, L., Tucci, V., Barnard, A. R., Busino, L., Pagano, M., Kendall, R., Quwailid, M. M., Romero, M. R., O'Neill, J., Chesham, J. E., Brooker, D., Lalanne, Z., Hastings, M. H. & Nolan, P. M. 2007 The after-hours mutant reveals a role for Fbxl3 in determining mammalian circadian period. *Science* **316**, 897-900.

Gregory, S. G., Sekhon, M., Schein, J., Zhao, S., Osoegawa, K., Scott, C. E., Evans, R. S., Burridge, P. W., Cox, T. V., Fox, C. A., Hutton, R. D., Mullenger, I. R., Phillips, K. J., Smith, J., Stalker, J., Threadgold, G. J., Birney, E., Wylie, K., Chinwalla, A., Wallis, J., Hillier, L., Carter, J., Gaige, T., Jaeger, S., Kremitzki, C., Layman, D., Maas, J., McGrane, R., Mead, K., Walker, R., Jones, S., Smith, M., Asano, J., Bosdet, I., Chan, S., Chittaranjan, S., Chiu, R., Fjell, C., Fuhrmann, D., Girn, N., Gray, C., Guin, R., Hsiao, L., Krzywinski, M., Kutsche, R., Lee, S. S., Mathewson, C., McLeavy, C., Messervier, S., Ness, S., Pandoh, P., Prabhu, A. L., Saeedi, P., Smailus, D., Spence, L., Stott, J., Taylor, S., Terpstra, W., Tsai, M., Vardy, J., Wye, N., Yang, G., Shatsman, S., Ayodeji, B., Geer, K., Tsegaye, G., Shvartsbeyn, A., Gebregeorgis, E., Krol, M., Russell, D., Overton, L., Malek, J. A., Holmes, M., Heaney, M., Shetty, J., Feldblyum, T., Nierman, W. C., Catanese, J. J., Hubbard, T., Waterston, R. H., Rogers, J., de Jong, P. J., Fraser, C. M., Marra, M., McPherson, J. D. & Bentley, D. R. 2002 A physical map of the mouse genome. *Nature* **418**, 743-50.

Guilbot, A., Williams, A., Ravise, N., Verny, C., Brice, A., Sherman, D. L., Brophy, P. J., LeGuern, E., Delague, V., Bareil, C., Megarbane, A. & Claustres, M. 2001 A mutation in periaxin is responsible for CMT4F, an autosomal recessive form of Charcot-Marie-Tooth disease. *Hum Mol Genet* **10**, 415-21.

Hafezparast, M., Klocke, R., Ruhrberg, C., Marquardt, A., Ahmad-Annuar, A., Bowen, S., Lalli, G., Witherden, A. S., Hummerich, H., Nicholson, S., Morgan, P. J., Oozageer, R., Priestley, J. V., Averill, S., King, V. R., Ball, S., Peters, J., Toda, T., Yamamoto, A., Hiraoka, Y., Augustin, M., Korthaus, D., Wattler, S., Wabnitz, P., Dickneite, C., Lampel, S., Boehme, F., Peraus, G., Popp, A., Rudelius, M., Schlegel, J., Fuchs, H., Hrabe de Angelis, M., Schiavo, G., Shima, D. T., Russ, A. P., Stumm, G., Martin, J. E. & Fisher, E. M. 2003 Mutations in dynein link motor neuron degeneration to defects in retrograde transport. *Science* **300**, 808-12.

Hall, C., Sin, W. C., Teo, M., Michael, G. J., Smith, P., Dong, J. M., Lim, H. H., Manser, E., Spurr, N. K., Jones, T. A. & et al. 1993 Alpha 2-chimerin, an SH2-containing GTPase-activating protein for the ras-related protein p21rac derived by alternate splicing of the human n-chimerin gene, is selectively expressed in brain regions and testes. Mol Cell Biol **13**, 4986-98.

Herron, B. J., Lu, W., Rao, C., Liu, S., Peters, H., Bronson, R. T., Justice, M. J., McDonald, J. D. & Beier, D. R. 2002 Efficient generation and mapping of recessive developmental mutations using ENU mutagenesis. *Nat Genet* **30**, 185-9.

Hess, D. T., Slater, T. M., Wilson, M. C. & Skene, J. H. 1992 The 25 kDa synaptosomal-associated protein SNAP-25 is the major methionine-rich polypeptide in rapid axonal transport and a major substrate for palmitoylation in adult CNS. *J Neurosci* **12**, 4634-41.

Hitotsumachi, S., Carpenter, D. A. & Russell, W. L. 1985 Dose-repetition increases the mutagenic effectiveness of N-ethyl-N-nitrosourea in mouse spermatogonia. *Proc Natl Acad Sci U S A* **82**, 6619-21.

Hosoya, M., Onda, H., Ogi, K., Masuda, Y., Miyamoto, Y., Ohtaki, T., Okazaki, H., Arimura, A. & Fujino, M. 1993 Molecular cloning and functional expression of rat cDNAs encoding the receptor for pituitary adenylate cyclase activating polypeptide (PACAP). *Biochem Biophys Res Commun* **194**, 133-43.

Hough, T. A., Polewski, M., Johnson, K., Cheeseman, M., Nolan, P. M., Vizor, L., Rastan, S., Boyde, A., Pritzker, K., Hunter, A. J., Fisher, E. M., Terkeltaub, R. & Brown, S. D. 2007 Novel mouse model of autosomal semidominant adult hypophosphatasia has a splice site mutation in the tissue nonspecific alkaline phosphatase gene Akp2. *J Bone Miner Res* **22**, 1397-407.

Houlden, H., King, R. H., Wood, N. W., Thomas, P. K. & Reilly, M. M. 2001 Mutations in the 5' region of the myotubularin-related protein 2 (MTMR2) gene in autosomal recessive hereditary neuropathy with focally folded myelin. *Brain* **124**, 907-15.

Hrabe de Angelis, M. H., Flaswinkel, H., Fuchs, H., Rathkolb, B., Soewarto, D., Marschall, S., Heffner, S., Pargent, W., Wuensch, K., Jung, M., Reis, A., Richter, T., Alessandrini, F., Jakob, T., Fuchs, E., Kolb, H., Kremmer, E., Schaeble, K., Rollinski, B., Roscher, A., Peters, C., Meitinger, T., Strom, T., Steckler, T., Holsboer, F., Klopstock, T., Gekeler, F., Schindewolf, C., Jung, T., Avraham, K., Behrendt, H., Ring, J., Zimmer, A., Schughart, K., Pfeffer, K., Wolf, E. & Balling, R. 2000 Genome-wide, large-scale production of mutant mice by ENU mutagenesis. *Nat Genet* **25**, 444-7.

Huxley, C., Passage, E., Robertson, A. M., Youl, B., Huston, S., Manson, A., Saberan-Djoniedi, D., Figarella-Branger, D., Pellissier, J. F., Thomas, P. K. & Fontes, M. 1998 Correlation between varying levels of PMP22 expression and the degree of demyelination and reduction in nerve conduction velocity in transgenic mice. *Hum Mol Genet* **7**, 449-58.

Irwin, S. 1968 Comprehensive observational assessment: Ia. A systematic, quantitative procedure for assessing the behavioral and physiologic state of the mouse. *Psychopharmacologia* **13**, 222-57.

Isaacs, A. M., Davies, K. E., Hunter, A. J., Nolan, P. M., Vizor, L., Peters, J., Gale, D. G., Kelsell, D. P., Latham, I. D., Chase, J. M., Fisher, E. M., Bouzyk, M. M., Potter, A., Masih, M., Walsh, F. S., Sims, M. A., Doncaster, K. E., Parsons, C. A., Martin, J., Brown, S. D., Rastan, S., Spurr, N. K. & Gray, I. C. 2000 Identification of two new Pmp22 mouse mutants using large-scale mutagenesis and a novel rapid mapping strategy. *Hum Mol Genet* **9**, 1865-71.

Isaacs, A. M., Jeans, A., Oliver, P. L., Vizor, L., Brown, S. D., Hunter, A. J. & Davies, K. E. 2002 Identification of a new Pmp22 mouse mutant and trafficking analysis of a Pmp22 allelic series suggesting that protein aggregates may be protective in Pmp22-associated peripheral neuropathy. *Mol Cell Neurosci* **21**, 114-25.

Isaacs, A. M., Oliver, P. L., Jones, E. L., Jeans, A., Potter, A., Hovik, B. H., Nolan, P. M., Vizor, L., Glenister, P., Simon, A. K., Gray, I. C., Spurr, N. K., Brown, S. D., Hunter, A. J. & Davies, K. E. 2003 A mutation in Af4 is predicted to cause cerebellar ataxia and cataracts in the robotic mouse. *J Neurosci* **23**, 1631-7.

James, P. A., Cader, M. Z., Muntoni, F., Childs, A. M., Crow, Y. J. & Talbot, K. 2006 Severe childhood SMA and axonal CMT due to anticodon binding domain mutations in the GARS gene. *Neurology* **67**, 1710-2.

Jordanova, A., Irobi, J., Thomas, F. P., Van Dijck, P., Meerschaert, K., Dewil, M., Dierick, I., Jacobs, A., De Vriendt, E., Guergueltcheva, V., Rao, C. V., Tournev, I., Gondim, F. A., D'Hooghe, M., Van Gerwen, V., Callaerts, P., Van Den Bosch, L., Timmermans, J. P., Robberecht, W., Gettemans, J., Thevelein, J. M., De Jonghe, P., Kremensky, I. & Timmerman, V. 2006 Disrupted function and axonal distribution of mutant tyrosyl-tRNA synthetase in dominant intermediate Charcot-Marie-Tooth neuropathy. *Nat Genet* **38**, 197-202.

Jones, B. J. & Roberts, D. J. 1968 The effects of intracerebroventricularly administered noradnamine and other sympathomimetic amines upon leptazol convulsions in mice. *Br J Pharmacol* **34**, 27-31.

Justice, M. J., Noveroske, J. K., Weber, J. S., Zheng, B. & Bradley, A. 1999 Mouse ENU mutagenesis. *Hum Mol Genet* **8**, 1955-63.

Kiernan, A. E., Ahituv, N., Fuchs, H., Balling, R., Avraham, K. B., Steel, K. P. & Hrabe de Angelis, M. 2001 The Notch ligand Jagged1 is required for inner ear sensory development. *Proc Natl Acad Sci U S A* **98**, 3873-8.

King, D. P., Vitaterna, M. H., Chang, A. M., Dove, W. F., Pinto, L. H., Turek, F. W. & Takahashi, J. S. 1997 The mouse Clock mutation

behaves as an antimorph and maps within the W19H deletion, distal of Kit. *Genetics* **146**, 1049-60.

Ko, H. S., von Coelln, R., Sriram, S. R., Kim, S. W., Chung, K. K., Pletnikova, O., Troncoso, J., Johnson, B., Saffary, R., Goh, E. L., Song, H., Park, B. J., Kim, M. J., Kim, S., Dawson, V. L. & Dawson, T. M. 2005 Accumulation of the authentic parkin substrate aminoacyl-tRNA synthetase cofactor, p38/JTV-1, leads to catecholaminergic cell death. *J Neurosci* **25**, 7968-78.

Kutzelnigg, A., Faber-Rod, J. C., Bauer, J., Lucchinetti, C. F., Sorensen, P. S., Laursen, H., Stadelmann, C., Bruck, W., Rauschka, H., Schmidbauer, M. & Lassmann, H. 2007 Widespread demyelination in the cerebellar cortex in multiple sclerosis. *Brain Pathol* 17, 38-44.

Lander, E. S., Linton, L. M., Birren, B., Nusbaum, C., Zody, M. C., Baldwin, J., Devon, K., Dewar, K., Doyle, M., FitzHugh, W., Funke, R., Gage, D., Harris, K., Heaford, A., Howland, J., Kann, L., Lehoczky, J., LeVine, R., McEwan, P., McKernan, K., Meldrim, J., Mesirov, J. P., Miranda, C., Morris, W., Naylor, J., Raymond, C., Rosetti, M., Santos, R., Sheridan, A., Sougnez, C., Stange-Thomann, N., Stojanovic, N., Subramanian, A., Wyman, D., Rogers, J., Sulston, J., Ainscough, R., Beck, S., Bentley, D., Burton, J., Clee, C., Carter, N., Coulson, A., Deadman, R., Deloukas, P., Dunham, A., Dunham, I., Durbin, R., French, L., Grafham, D., Gregory, S., Hubbard, T., Humphray, S., Hunt, A., Jones, M., Lloyd, C., McMurray, A., Matthews, L., Mercer, S., Milne, S., Mullikin, J. C., Mungall, A., Plumb, R., Ross, M., Shownkeen, R., Sims, S., Waterston, R. H., Wilson, R. K., Hillier, L. W., McPherson, J. D., Marra, M. A., Mardis, E. R., Fulton, L. A., Chinwalla, A. T., Pepin, K. H., Gish, W. R., Chissoe, S. L., Wendl, M. C., Delehaunty, K. D., Miner, T. L., Delehaunty, A., Kramer, J. B., Cook, L. L., Fulton, R. S., Johnson, D. L., Minx, P. J., Clifton, S. W., Hawkins, T., Branscomb, E., Predki, P., Richardson, P., Wenning, S., Slezak, T., Doggett, N., Cheng, J. F., Olsen, A., Lucas, S., Elkin, C., Uberbacher, E., Frazier, M., et al. 2001 Initial sequencing and analysis of the human genome. *Nature* **409**, 860-921.

Lawson, V. H., Graham, B. V. & Flanigan, K. M. 2005 Clinical and electrophysiologic features of CMT2A with mutations in the mitofusin 2 gene. *Neurology* **65**, 197-204.

Lee, J. W., Beebe, K., Nangle, L. A., Jang, J., Longo-Guess, C. M., Cook, S. A., Davisson, M. T., Sundberg, J. P., Schimmel, P. & Ackerman, S. L. 2006 Editing-defective tRNA synthetase causes protein misfolding and neurodegeneration. *Nature* **443**, 50-5.

Lee, S. W., Cho, B. H., Park, S. G. & Kim, S. 2004 Aminoacyl-tRNA synthetase complexes: beyond translation. *J Cell Sci* **117**, 3725-34.

Lupski, J., Chance, P.F. 2005 Hereditary motor and sensory neuropathies involving
altered dosage or mutation of PMP22: the CMT1A duplication and HNPP deletion. In:Peripheral neuropathy. Elsevier Saunders. Amsterdam.

Mantamadiotis, T., Lemberger, T., Bleckmann, S. C., Kern, H., Kretz, O., Martin Villalba, A., Tronche, F., Kellendonk, C., Gau, D., Kapfhammer, J., Otto, C., Schmid, W. & Schutz, G. 2002 Disruption of CREB function in brain leads to neurodegeneration. *Nat Genet* **31**, 47-54.

Marschall, S., Huffstadt, U., Balling, R. & Hrabe de Angelis, M. 1999 Reliable recovery of inbred mouse lines using cryopreserved spermatozoa. *Mamm Genome* **10**, 773-6.

Martin, K. C. 2004 Local protein synthesis during axon guidance and synaptic plasticity. *Curr Opin Neurobiol* **14**, 305-10.

Martini, R., Zielasek, J., Toyka, K. V., Giese, K. P. & Schachner, M. 1995 Protein zero (P0)-deficient mice show myelin degeneration in peripheral nerves characteristic of inherited human neuropathies. *Nat Genet* **11**, 281-6.

Meisler, M. H. 1996 The role of the laboratory mouse in the human genome project. *Am J Hum Genet* **59**, 764-71.

Michell, R. H., Heath, V. L., Lemmon, M. A. & Dove, S. K. 2006 Phosphatidylinositol 3,5-bisphosphate: metabolism and cellular functions. *Trends Biochem Sci* **31**, 52-63.

Morse, H. C. 1978 Introduction. In Origin of Inbred Mice: Academic Press.New York.

Nadeau, J. H., Balling, R., Barsh, G., Beier, D., Brown, S. D., Bucan, M., Camper, S., Carlson, G., Copeland, N., Eppig, J., Fletcher, C., Frankel, W. N., Ganten, D., Goldowitz, D., Goodnow, C., Guenet, J. L., Hicks, G., Hrabe de Angelis, M., Jackson, I., Jacob, H. J., Jenkins, N., Johnson, D., Justice, M., Kay, S., Kingsley, D., Lehrach, H., Magnuson, T., Meisler, M., Poustka, A., Rinchik, E. M., Rossant, J., Russell, L. B., Schimenti, J., Shiroishi, T., Skarnes, W. C., Soriano, P., Stanford, W., Takahashi, J. S., Wurst, W. & Zimmer, A. 2001 Sequence interpretation. Functional annotation of mouse genome sequences. *Science* **291**, 1251-5.

Nagarajan, R., Le, N., Mahoney, H., Araki, T. & Milbrandt, J. 2002 Deciphering peripheral nerve myelination by using Schwann cell expression profiling. *Proc Natl Acad Sci U S A* **99**, 8998-9003.

Nagarajan, R., Svaren, J., Le, N., Araki, T., Watson, M. & Milbrandt, J. 2001 EGR2 mutations in inherited neuropathies dominant-negatively inhibit myelin gene expression. *Neuron* **30**, 355-68.

Neuspiel, M., Zunino, R., Gangaraju, S., Rippstein, P. & McBride, H. 2005 Activated mitofusin 2 signals mitochondrial fusion, interferes with Bax activation, and reduces susceptibility to radical induced depolarization. *J Biol Chem* **280**, 25060-70.

Nolan, P. M., Hugill, A. & Cox, R. D. 2002 ENU mutagenesis in the mouse: application to human genetic disease. *Brief Funct Genomic Proteomic* **1**, 278-89.

Notterpek, L., Tolwani, R. J., Notterpek, L., Ryan, M. C., Tobler, A. R. & Shooter, E. M. 1999 Experimental models of peripheral neuropathies PMP22 accumulation in aggresomes: implications for CMT1A pathology. *Lab Anim Sci* **49**, 588-99.

Noveroske, J. K., Weber, J. S. & Justice, M. J. 2000 The mutagenic action of N-ethyl-N-nitrosourea in the mouse. *Mamm Genome* **11**, 478-83.

O'Callaghan, J. P. & Holtzman, S. G. 1975 Quantification of the analgesic activity of narcotic antagonists by a modified hot-plate procedure. *J Pharmacol Exp Ther* **192**, 497-505.

Oda, T., Elkahloun, A. G., Pike, B. L., Okajima, K., Krantz, I. D., Genin, A., Piccoli, D. A., Meltzer, P. S., Spinner, N. B., Collins, F. S. & Chandrasekharappa, S. C. 1997 Mutations in the human Jagged1 gene are responsible for Alagille syndrome. *Nat Genet* **16**, 235-42.

Paigen, K. 1995 A miracle enough: the power of mice. *Nat Med* **1**, 215-20.

Pareyson, D., Menichella, D., Botti, S., Sghirlanzoni, A., Fallica, E., Mora, M., Ciano, C., Shy, M. E. & Taroni, F. 1999 Heterozygous null mutation in the P0 gene associated with mild Charcot-Marie-Tooth disease. *Ann N Y Acad Sci* **883**, 477-80.

Parkinson, N. & Brown, S. D. 2002 Focusing on the genetics of hearing: you ain't heard nothin' yet. *Genome Biol* **3**:2006.1-6

Parkinson, N., Hardisty-Hughes, R. E., Tateossian, H., Tsai, H. T., Brooker, D., Morse, S., Lalane, Z., MacKenzie, F., Fray, M., Glenister, P., Woodward, A. M., Polley, S., Barbaric, I., Dear, N., Hough, T. A., Hunter, A. J., Cheeseman, M. T. & Brown, S. D. 2006 Mutation at the Evi1 locus in Junbo mice causes susceptibility to otitis media. *PLoS Genet* **2**, e149.

Perea, J., Robertson, A., Tolmachova, T., Muddle, J., King, R. H., Ponsford, S., Thomas, P. K. & Huxley, C. 2001 Induced myelination and

demyelination in a conditional mouse model of Charcot-Marie-Tooth disease type 1A. *Hum Mol Genet* **10**, 1007-18.

Radtke, C., Spies, M., Sasaki, M., Vogt, P. M. & Kocsis, J. D. 2007 Demyelinating diseases and potential repair strategies. *Int J Dev Neurosci* **25**, 149-53.

Reilly, M. M. 2005 Axonal Charcot-Marie-Tooth disease: the fog is slowly lifting! *Neurology* **65**, 186-7.

Roa, B. B., Dyck, P. J., Marks, H. G., Chance, P. F. & Lupski, J. R. 1993 Dejerine-Sottas syndrome associated with point mutation in the peripheral myelin protein 22 (PMP22) gene. *Nat Genet* **5**, 269-73.

Robertson, A. H., C. 2005 Transgenic models of inherited neuropathy. In:Peripheral neuropathy. Amsterdam: Elsevier Saunders.

Robertson, A. M., Perea, J., McGuigan, A., King, R. H., Muddle, J. R., Gabreels-Festen, A. A., Thomas, P. K. & Huxley, C. 2002 Comparison of a new pmp22 transgenic mouse line with other mouse models and human patients with CMT1A. *J Anat* **200**, 377-90.

Rogers, D. C., Fisher, E. M., Brown, S. D., Peters, J., Hunter, A. J. & Martin, J. E. 1997 Behavioral and functional analysis of mouse phenotype: SHIRPA, a proposed protocol for comprehensive phenotype assessment. *Mamm Genome* **8**, 711-3.

Rouaux, C., Panteleeva, I., Rene, F., Gonzalez de Aguilar, J. L., Echaniz-Laguna, A., Dupuis, L., Menger, Y., Boutillier, A. L. & Loeffler, J. P. 2007 Sodium valproate exerts neuroprotective effects in vivo through CREB-binding protein-dependent mechanisms but does not improve survival in an amyotrophic lateral sclerosis mouse model. *J Neurosci* **27**, 5535-45.

Russell, W. L., Kelly, E. M., Hunsicker, P. R., Bangham, J. W., Maddux, S. C. & Phipps, E. L. 1979 Specific-locus test shows ethylnitrosourea to be the most potent mutagen in the mouse. *Proc Natl Acad Sci U S A* **76**, 5818-9.

Ryan, M. C., Shooter, E. M. & Notterpek, L. 2002 Aggresome formation in neuropathy models based on peripheral myelin protein 22 mutations. *Neurobiol Dis* **10**, 109-18.

Sage, R. D. 1981 Wild Mice. In The mouse in Biomedical Research. Academic Press. New York.

Sakaguchi, S., Katamine, S., Nishida, N., Moriuchi, R., Shigematsu, K., Sugimoto, T., Nakatani, A., Kataoka, Y., Houtani, T., Shirabe, S., Okada, H., Hasegawa, S., Miyamoto, T. & Noda, T. 1996 Loss of cerebellar

Purkinje cells in aged mice homozygous for a disrupted PrP gene. *Nature* **380**, 528-31.

Sampath, P., Mazumder, B., Seshadri, V., Gerber, C. A., Chavatte, L., Kinter, M., Ting, S. M., Dignam, J. D., Kim, S., Driscoll, D. M. & Fox, P. L. 2004 Noncanonical function of glutamyl-prolyl-tRNA synthetase: gene-specific silencing of translation. *Cell* **119**, 195-208.

Scherer, S. S., Bone, L. J., Deschenes, S. M., Abel, A., Balice-Gordon, R. J. & Fischbeck, K. H. 1999 The role of the gap junction protein connexin32 in the pathogenesis of X-linked Charcot-Marie-Tooth disease. *Novartis Found Symp* **219**, 175-85; discussion 185-7.

Scherer, S. S., Xu, Y. T., Messing, A., Willecke, K., Fischbeck, K. H. & Jeng, L. J. 2005 Transgenic expression of human connexin32 in myelinating Schwann cells prevents demyelination in connexin32-null mice. *J Neurosci* **25**, 1550-9.

Scherer, S. S., Xu, Y. T., Messing, A., Willecke, K., Fischbeck, K. H. & Jeng, L. J. 2005 Transgenic expression of human connexin32 in myelinating Schwann cells prevents demyelination in connexin32-null mice. *J Neurosci* **25**, 1550-9.

Schmidt, M. J., Sawyer, B. D., Perry, K. W., Fuller, R. W., Foreman, M. M. & Ghetti, B. 1982 Dopamine deficiency in the weaver mutant mouse. *J Neurosci* **2**, 376-80.

Seburn, K. L., Nangle, L. A., Cox, G. A., Schimmel, P. & Burgess, R. W. 2006 An active dominant mutation of glycyl-tRNA synthetase causes neuropathy in a Charcot-Marie-Tooth 2D mouse model. *Neuron* **51**, 715-26.

Sereda, M. W. & Nave, K. A. 2006 Animal models of Charcot-Marie-Tooth disease type 1A. *Neuromolecular Med* **8**, 205-16.

Servais, L., Hourez, R., Bearzatto, B., Gall, D., Schiffmann, S. N. & Cheron, G. 2007 Purkinje cell dysfunction and alteration of long-term synaptic plasticity in fetal alcohol syndrome. *Proc Natl Acad Sci* U S A 104, 9858-63.

Sherman, D. L., Fabrizi, C., Gillespie, C. S. & Brophy, P. J. 2001 Specific disruption of a schwann cell dystrophin-related protein complex in a demyelinating neuropathy. *Neuron* **30**, 677-87.

Shibuya, T. & Morimoto, K. 1993 A review of the genotoxicity of 1-ethyl-1-nitrosourea. *Mutat Res* **297**, 3-38.

Shy, M., Lupski JR, Chance PF. 2005 Hereditary motor and sensory neuropathies: an overview of clinical, genetic, electrophysiologic, and pathologic

features. In Peripheral neuropathy.. Elsevier Saunders. Amsterdam.

Shy, M. E. 2006 Peripheral neuropathies caused by mutations in the myelin protein zero. *J Neurol Sci* **242**, 55-66.

Silver, L. M. 1995 *Mouse Genetics- Concepts and Application.*: Oxford University Press.Oxford.

Sivakumar, K., Kyriakides, T., Puls, I., Nicholson, G. A., Funalot, B., Antonellis, A., Sambuughin, N., Christodoulou, K., Beggs, J. L., Zamba-Papanicolaou, E., Ionasescu, V., Dalakas, M. C., Green, E. D., Fischbeck, K. H. & Goldfarb, L. G. 2005 Phenotypic spectrum of disorders associated with glycyl-tRNA synthetase mutations. *Brain* **128**, 2304-14.

Skre, H. 1974 Genetic and clinical aspects of Charcot-Marie-Tooth's disease. *Clin Genet* **6**, 98-118.

Smithies, O. 1993 Animal models of human genetic diseases. *Trends Genet* **9**, 112-6.

Steward, O. & Schuman, E. M. 2003 Compartmentalized synthesis and degradation of proteins in neurons. *Neuron* **40**, 347-59.

Suter, U. & Scherer, S. S. 2003 Disease mechanisms in inherited neuropathies. *Nat Rev Neurosci* **4**, 714-26.

Swerdlow, N. R., Braff, D. L., Masten, V. L. & Geyer, M. A. 1990 Schizophrenic-like sensorimotor gating abnormalities in rats following dopamine infusion into the nucleus accumbens. *Psychopharmacology (Berl)* **101**, 414-20.

Swerdlow, N. R., Shoemaker, J. M., Kuczenski, R., Bongiovanni, M. J., Neary, A. C., Tochen, L. S. & Saint Marie, R. L. 2006 Forebrain D1 function and sensorimotor gating in rats: effects of D1 blockade, frontal lesions and dopamine denervation. *Neurosci Lett* **402**, 40-5.
Szigeti, K., Nelis, E. & Lupski, J. R. 2006 Molecular diagnostics of Charcot-Marie-Tooth disease and related peripheral neuropathies. *Neuromolecular Med* **8**, 243-54.

Thaung, C., West, K., Clark, B. J., McKie, L., Morgan, J. E., Arnold, K., Nolan, P. M., Peters, J., Hunter, A. J., Brown, S. D., Jackson, I. J. & Cross, S. H. 2002 Novel ENU-induced eye mutations in the mouse: models for human eye disease. *Hum Mol Genet* **11**, 755-67.

Thomas, P. K., King, R. H., Small, J. R. & Robertson, A. M. 1996 The pathology of charcot-marie-tooth disease and related disorders. *Neuropathol Appl Neurobiol* **22**, 269-84.

Thornton, C. E., Brown, S. D. & Glenister, P. H. 1999 Large numbers of mice established by in vitro fertilization with cryopreserved spermatozoa: implications and applications for genetic resource banks, mutagenesis screens, and mouse backcrosses. *Mamm Genome* **10**, 987-92.

Topilko, P., Schneider-Maunoury, S., Levi, G., Baron-Van Evercooren, A., Chennoufi, A. B., Seitanidou, T., Babinet, C. & Charnay, P. 1994 Krox-20 controls myelination in the peripheral nervous system. *Nature* **371**, 796-9.

Tsai, H., Hardisty, R. E., Rhodes, C., Kiernan, A. E., Roby, P., Tymowska-Lalanne, Z., Mburu, P., Rastan, S., Hunter, A. J., Brown, S. D. & Steel, K. P. 2001 The mouse slalom mutant demonstrates a role for Jagged1 in neuroepithelial patterning in the organ of Corti. *Hum Mol Genet* **10**, 507-12.

Tucci, V., Achilli, F., Blanco, G., Lad, H. V., Wells, S., Godinho, S. & Nolan, P. M. 2007 Reaching and grasping phenotypes in the mouse (Mus musculus): a characterization of inbred strains and mutant lines. *Neuroscience* **147**, 573-82.

Tzima, E. & Schimmel, P. 2006 Inhibition of tumor angiogenesis by a natural fragment of a tRNA synthetase. *Trends Biochem Sci* **31**, 7-10.

Vandenberghe, N., Upadhyaya, M., Gatignol, A., Boutrand, L., Boucherat, M., Chazot, G., Vandenberghe, A. & Latour, P. 2002 Frequency of mutations in the early growth response 2 gene associated with peripheral demyelinating neuropathies. *J Med Genet* **39**, e81.

Venter, J. C., Adams, M. D., Myers, E. W., Li, P. W., Mural, R. J., Sutton, G. G., Smith, H. O., Yandell, M., Evans, C. A., Holt, R. A., Gocayne, J. D., Amanatides, P., Ballew, R. M., Huson, D. H., Wortman, J. R., Zhang, Q., Kodira, C. D., Zheng, X. H., Chen, L., Skupski, M., Subramanian, G., Thomas, P. D., Zhang, J., Gabor Miklos, G. L., Nelson, C., Broder, S., Clark, A. G., Nadeau, J., McKusick, V. A., Zinder, N., Levine, A. J., Roberts, R. J., Simon, M., Slayman, C., Hunkapiller, M., Bolanos, R., Delcher, A., Dew, I., Fasulo, D., Flanigan, M., Florea, L., Halpern, A., Hannenhalli, S., Kravitz, S., Levy, S., Mobarry, C., Reinert, K., Remington, K., Abu-Threideh, J., Beasley, E., Biddick, K., Bonazzi, V., Brandon, R., Cargill, M., Chandramouliswaran, I., Charlab, R., Chaturvedi, K., Deng, Z., Di Francesco, V., Dunn, P., Eilbeck, K., Evangelista, C., Gabrielian, A. E., Gan, W., Ge, W., Gong, F., Gu, Z., Guan, P., Heiman, T. J., Higgins, M. E., Ji, R. R., Ke, Z., Ketchum, K. A., Lai, Z., Lei, Y., Li, Z., Li, J., Liang, Y., Lin, X., Lu, F., Merkulov, G. V., Milshina, N., Moore, H. M., Naik, A. K., Narayan, V. A., Neelam, B., Nusskern, D., Rusch, D. B., Salzberg, S., Shao, W., Shue, B., Sun, J., Wang, Z., Wang, A., Wang, X., Wang, J., Wei, M., Wides, R., Xiao, C.,

Yan, C., et al. 2001 The sequence of the human genome. *Science* **291**, 1304-51.

Vitaterna, M. H., King, D. P., Chang, A. M., Kornhauser, J. M., Lowrey, P. L.,

McDonald, J. D., Dove, W. F., Pinto, L. H., Turek, F. W. & Takahashi, J. S. 1994 Mutagenesis and mapping of a mouse gene, Clock, essential for circadian behavior.*Science* **264**, 719-25.

Wakasugi, K. & Schimmel, P. 1999 Highly differentiated motifs responsible for two cytokine activities of a split human tRNA synthetase. *J Biol Chem* **274**, 23155-9.

Wang, H. Q., Nakaya, Y., Du, Z., Yamane, T., Shirane, M., Kudo, T., Takeda, M., Takebayashi, K., Noda, Y., Nakayama, K. I. & Nishimura, M. 2005 Interaction of presenilins with FKBP38 promotes apoptosis by reducing mitochondrial Bcl-2. *Hum Mol Genet* **14**, 1889-902.

Warner, L. E., Hilz, M. J., Appel, S. H., Killian, J. M., Kolodry, E. H., Karpati, G., Carpenter, S., Watters, G. V., Wheeler, C., Witt, D., Bodell, A., Nelis, E., Van Broeckhoven, C. & Lupski, J. R. 1996 Clinical phenotypes of different MPZ (P0) mutations may include Charcot-Marie-Tooth type 1B, Dejerine-Sottas, and congenital hypomyelination. *Neuron* **17**, 451-60.

Waterston, R. H., Lindblad-Toh, K., Birney, E., Rogers, J., Abril, J. F., Agarwal, P., Agarwala, R., Ainscough, R., Alexandersson, M., An, P., Antonarakis, S. E., Attwood, J., Baertsch, R., Bailey, J., Barlow, K., Beck, S., Berry, E., Birren, B., Bloom, T., Bork, P., Botcherby, M., Bray, N., Brent, M. R., Brown, D. G., Brown, S. D., Bult, C., Burton, J., Butler, J., Campbell, R. D., Carninci, P., Cawley, S., Chiaromonte, F., Chinwalla, A. T., Church, D. M., Clamp, M., Clee, C., Collins, F. S., Cook, L. L., Copley, R. R., Coulson, A., Couronne, O., Cuff, J., Curwen, V., Cutts, T., Daly, M., David, R., Davies, J., Delehaunty, K. D., Deri, J., Dermitzakis, E. T., Dewey, C., Dickens, N. J., Diekhans, M., Dodge, S., Dubchak, I., Dunn, D. M., Eddy, S. R., Elnitski, L., Emes, R. D., Eswara, P., Eyras, E., Felsenfeld, A., Fewell, G. A., Flicek, P., Foley, K., Frankel, W. N., Fulton, L. A., Fulton, R. S., Furey, T. S., Gage, D., Gibbs, R. A., Glusman, G., Gnerre, S., Goldman, N., Goodstadt, L., Grafham, D., Graves, T. A., Green, E. D., Gregory, S., Guigo, R., Guyer, M., Hardison, R. C., Haussler, D., Hayashizaki, Y., Hillier, L. W., Hinrichs, A., Hlavina, W., Holzer, T., Hsu, F., Hua, A., Hubbard, T., Hunt, A., Jackson, I., Jaffe, D. B., Johnson, L. S., Jones, M., Jones, T. A., Joy, A., Kamal, M., Karlsson, E. K., et al. 2002 Initial sequencing and comparative analysis of the mouse genome. *Nature* **420**, 520-62.

Winkler, C., Eggert, C., Gradl, D., Meister, G., Giegerich, M., Wedlich, D., Laggerbauer, B. & Fischer, U. 2005 Reduced U snRNP assembly causes motor axon degeneration in an animal model for spinal muscular atrophy. *Genes Dev* **19**, 2320-30.

Yoshikawa, H., Nishimura, T., Nakatsuji, Y., Fujimura, H., Himoro, M., Hayasaka, K., Sakoda, S. & Yanagihara, T. 1994 Elevated expression of messenger RNA for peripheral myelin protein 22 in biopsied peripheral nerves of patients with Charcot-Marie-Tooth disease type 1A. *Ann Neurol* **35**, 445-50.

Zhao, C., Takita, J., Tanaka, Y., Setou, M., Nakagawa, T., Takeda, S., Yang, H. W., Terada, S., Nakata, T., Takei, Y., Saito, M., Tsuji, S., Hayashi, Y. & Hirokawa, N. 2001 Charcot-Marie-Tooth disease type 2A caused by mutation in a microtubule motor KIF1Bbeta. *Cell* **105**, 587-97.

Zuchner, S., Mersiyanova, I. V., Muglia, M., Bissar-Tadmouri, N., Rochelle, J., Dadali, E. L., Zappia, M., Nelis, E., Patitucci, A., Senderek, J., Parman, Y., Evgrafov, O., Jonghe, P. D., Takahashi, Y., Tsuji, S., Pericak-Vance, M. A., Quattrone, A., Battaloglu, E., Polyakov, A. V., Timmerman, V., Schroder, J. M. & Vance, J. M. 2004 Mutations in the mitochondrial GTPase mitofusin 2 cause Charcot-Marie-Tooth neuropathy type 2A. *Nat Genet* **36**, 449-51.

Appendix 1 72 markers used for the GENA 201 and 202 and Moonwalker genome scan

SNPs_C3H_C57BL/6_ BALB/cAnN _for genome scan						
Chromosome	**Position**	**For/Rev**	**C3H**	**C57BL/6**	**BALB/cAnN**	**NCBI SNP reference**
1	11		A	G	G	rs4222150
1	36		T	C	C	rs3088581
1	73		A	G	G	rs4222426
1	93	Rev	T	C	C	rs3022829
1	135	Rev	G	A	A	rs4222662
1	150	Rev	A	G	G	rs3023658
1	170	Rev	T	C	C	rs3022851
1	193		T	G/T	G	rs4222922
2	38	Rev	G	T	T	rs3022883
2	72		G	A	A	rs4223216
2	99	Rev	T	C	C	rs3089575
2	130		G	A	A	rs4223477
2	181	Rev	T	C	C	rs3022944
3	26		G	A	A	rs3022950
3	88		C	A	A	rs4224044
3	105	Rev	C	T	T	rs4224158
3	132		A	G	G	rs4224218
4	14		G	G	A	rs3090919
4	32		A	G	G	rs4224427
4	80	Rev	C	C	T	rs4224562
4	133	Rev	G	C	C	rs4224824
4	145		C	G	G	rs4224944
5	23	Rev	T	G	G	rs3023038
5	51	Rev	T	C	C	rs3023044
5	76		G	A	A	rs4225300
5	104		T	C	C	rs3023049
5	137		C	T	T	rs4225539
6	22		A	C	C	rs3088527
6	52		G	T	T	rs3023069
6	84	Rev	A	A	G	rs4226024
6	114	Rev	G	A	A	rs4226196
6	146		T	G	G	rs3023100
7	11		G	T	T	rs4226424
7	54		C	A	A	rs4226656
7	72	Rev	A	G	G	rs3023147
7	102	Rev	G	A	A	rs3023155
8	26		A	T	T	rs3090663
8	65	Rev	G	A	A	rs4227194
8	95		T	C	C	rs4227350

8	123	Rev	A	G	G	rs4227432
9	57		A	G	G	rs4227685
9	62		T	C	C	rs4227704
10	28		A	G	G	rs3023233
10	56		C	T	T	rs3089794
10	89		C	C	T	rs3089366
10	105	Rev	T	T	C	rs3088857
11	22		A	C	C	rs4228622
11	54		C	A	A	rs3023258
11	117		C	T	T	rs3024036
12	12		T	C	C	rs3090133
12	68		A	T	T	rs3021895
12	114	Rev	T	C	C	rs3023547
13	4	Rev	G	G	A	rs3023640
13	59		C	C	T	rs3023383
13	93		A	G	G	rs3023390
14	3	Rev	C	T	T	rs4230157
14	16		A	G	G	rs4230209
14	59		T	G	G	rs3089070
15	5		T	C	C	rs4230638
15	52	Rev	T	C	C	rs3023676
15	103	Rev	A	T	T	rs4231032
16	10		T	A	A	rs3023432
16	59	Rev	A	G	G	rs3023244
16	88	Rev	T	T	A	rs3023436
17	19		G	T	T	rs3023727
17	31		A	G	G	rs4231428
17	71		C	T	T	rs3023668
18	62		G	G	T	rs4231898
18	80	Rev	G	G	T	rs4231968
19	19	Rev	A	C	C	rs3023480
19	56		T	C	C	rs3023497

Appendix 2 Additional markers used to refine the haplotypes of GENA 201 and 202 and Moonwalker

Name	Left	Right	Length	Chr	Pos (cM)	C57BL/6	C3H	BALB/c	Mb
D6Mit273	TAACATC CTCTAAT GCCTTTG TATG	TTTCCAGA CCCAATAC TGGC	124	Chr6	9.8	128	128	112	46
D6Mit183	TTCTCAA TGAACAC TAGAACA TTCG	AAAACACA GGTAGAAA ACATACAT ACA	104	Chr6	13.1	104	98	162	53
D6Mit384	AATGCTT TATATGC AAACTAC TCTCTC	GAATATAG CAAGACAA GGGAGAC A	125	Chr6	15.3	126	148	142	55
D6Mit175	GTTAGTG AGATCCA AAGCCAC C	GCCACCAT CTCAACCC TG	200	Chr6	18.6	201	195	201	65
D6Mit186	GGTTTAT AACTCCA GTTCCTG GG	ATGAGAAA ACAGACAC TCATTGTA GG	185	Chr6	20.8	182	184	172	73
D6Mit188	CTTTAGT CATTATT AGGATTG CCTATG	TGGGATA GCATTGGA AACGT	128	Chr6	32.5	130	155	147	75

Name	Left	Right	Length	Chr	Pos (cM)	C3H	BALB/c	Mb
D3Mit90	AGTTAAA TTTCTTT GGTAATT GACACA	GTCTCTA ATAACCA AAAATGT TTCAA	144	Chr3	4.6	145	139	12
D3Mit328	ATTTATT GGTACA GCCCCC C	CTCTGAC CTCCACA CATGTAC TG	125	Chr3	5.6	130	124	19
D3Mit93	TCAATCA GTTTCAT GTGCTG TG	TTTTTGC CTTCAAA GGATTTA T	164	Chr3	13.8	174	164	29

Appendix 3 Sequence of *Gars* (5' upstream and 3' downstream sequence in pink, non-coding sequence in green, coding sequence in black and flanking intronic sequence in blue)

5'upstream sequence.....atttcatcatgcaccgggcgggccgcgccgcttccgtagccgccctgc

Exon 1(214bp) GCACCGCCTAGGCGGCGTGCTCATGCCCTGTCTGCTCCCCTCGCTGCTCAGAGCCACCCG
CGCCGCGCTGCCGCTCCTGTCGCCGCCCCGAGTGGTCGCAGCGTCCGCGTCTCAGCGGCT
CCTCAGCGCTCCCGCGCAGCCCGCCGCCTCCCGGAGCAGCATGGACAGCGCGGAGGAGCT
GCTGGCCCCACTGCGGCTAGCCGTGCGCCAGCAG

Intron1-2(8180bp) gtaccgacccctgcccgcagccgcg.....tgattgtagcttgtttgttggccag

Exon 2 (102bp) GGAGACTTTGTACGGAAGTTAAAAGAAGATAAAGCCCCACAAGTGGATGTGGACAGAGCA
GTAGCTGAGCTCAAGGCCCGGAAGAGGGTTCTGGAAGCAAAG

Intron2-3(1551) gtaagtcttaggatgctaaggcaga.....actctcttcttgtttgctcttatag

Exon 3 (103bp) GAGCTGGCATTGCAGCCCAAAGATGACATCGTAGATAGAGCAAAAATGGAAGATACGTTG
AAGAGGAGGTTTTTCTACGATCAGGCTTTTGCTATTTATGGAG

Intron3-4(2150bp) gtaggggtgaatgaagccacagtg.....ccacgtttacctctctcctcacag

Exon 4 (142bp) GTGTCAGTGGATTGTATGACTTCGGGCCGGTAGGATGTGCTTTGAAGAACAATATCATCC
AGGCCTGGAGGCAGCACTTTATCCAAGAGGAGCAGATCCTGGAGATTGACTGCACCATGC
TCACCCCTGAGCCAGTTTTAAA

Intron4-5(1714bp) gtgagcttctgcttcggtgggagag.....cttgttggtttgcttgttcacttag

Exon 5 (89bp) GACCTCTGGCCACGTAGACAAATTTGCTGACTTCATGGTGAAGGACGTGAAGAACGGAGA
GTGCTTCCGAGCAGACCACCTGTTGAAAG

Intron5-6(864bp) gtatgcgtctgcatctttcttgtac.....tcgcttaccagcactgttgttctag

Exon 6 (77bp) CTCATTTACAGAAACTGATGTCAGATAAGAAGTGCTCTGCTGAGAAGAAGTCAGAGATGG
AAAGTGTCTTGGCCCAG

Intron6-7(2544bp) gtgagcagtcgggagacacatcaga.....attatcttctctctgtgccccttag

Exon 7 (146bp) CTTGATAACTATGGACAACAAGAACTTGCGGATCTTTTTGTGAACTATAATGTAAAATCT
CCCACCACTGGCAATGACCTGTCCCCTCCGGTACCTTTTAACTTAATGTTCCAGACCTTC
ATTGGGCCTGGAGGAAATATGCCTGG

Intron7-8(5013bp) gtacgtattgtttttcatttatttg.....tagactggtttatttaattttatag

Exon 8 (150bp) ATATCTGAGACCAGAAACTGCACAGGGAATTTTCCTGAATTTCAAACGACTTTTGGAATT
CAACCAAGGGAAATTGCCTTTTGCTGCTGCCCAGATTGGAAACTCCTTCAGAAATGAGAT
CTCACCTCGGTCTGGACTGATCCGAGTCAG

Intron8-9(2032bp) gtactcactgttggtgtcgggatgg.....attttgatcttgtttttccttccag

Exon 9 (163bp) GGAGTTTACAATGGCAGAGATTGAGCACTTTGTAGATCCCACTGAGAAAGACCATCCCAA
GTTCCAAAGTGTGGCCGACCTCTGCCTTTATTTGTACTCAGCAAAAGCCCAGGTCACTGG
ACAGTCTGCTCGGAAGATGCGTCTGGGAGATGCTGTTGAACAG

Intron9-10(2194bp) gtaaggttctcagggagctgatgaa.....ctttgctgctcttctatttgttcag

Exon 10 (165bp) GGTGTGATTAACAACTCAGTATTAGGCTATTTTATTGGCCGCATCTACCTCTACCTCACG
AAGGTTGGAATATCTCCTGATAAACTCCGCTTCCGGCAGCATATGGAGAATGAGATGGCC
CATTATGCCTGCGACTGCTGGGATGCCGAGTCCAAAACGTCCTAT

Intron10-11(2448bp) gtgagtagcccgcagtaatgctttta.....gactttgttagttctgttttcctag

Exon 11 (108bp) GGCTGGATTGAGATTGTTGGATGTGCTGACCGTTCCTGCTACGACCTCTCCTGTCATGCT
CGAGCCACCAAAGTTCCACTAGTAGCTGAGAAACCTCTGAAAGAACCC

Intron11-12(5bp) atatc

Exon 12 (4bp) CTTT

Intron12-13(1170bp) gtggccactccaaaattaaggctaa.....tccttgactgtttcatacaaaacag

Exon 13 (139bp) TTAACGTTGTACAGTTTGAGCCCAACAAGGGCGCCGTGGGCAAGGCGTACAAGAAGGATG
CAAAGCTAGTGCTGGAGTATCTCAGCGCCTGTGATGAGTGCTACATTTCAGAGATGGAGC
TGCTGCTGAGTGAGAAAGG

Intron13-14(3852bp) gtaagcgtctccctcaggctctgag.....ttttgtctttttttctctgtttgtag

Exon 14 (86bp) GGAATTCACTATTGAAACTGAAGGAAAAACATTTCAGTTAACGAAAGACATGGTCAGTGT
GAAGAGATTCCAGAAAACACTGCATG

Intron14-15(1957bp) gtaatttattagatcaataaagaaa.....ctaaattgtctactttttttgcag

Exon 15 (110bp) TGGAAGAAGTTGTTCCGAGTGTAATTGAGCCCTCCTTTGGCTTGGGCAGGATCATGTATA
CCATATTGGAACATACATTCCATGTCCGAGAGGGAGATGAACAGAGAACG

Intron15-16(1463bp)	gtgagctgccccgaaatgagtgctt.....atttctttctttaaaaccatctag
Exon 16 (94bp)	TTCTTCAGTTTCCCTGCTGTGGTTGCTCCATTCAAATGTTCTGTCCTTCCACTGAGCCAG
	AACCAAGAGTTTATGCCATTTGTCAAGGAATTAT
Intron16-17(534bp)	gtaagcaaatccagttgggtgatct.....ctctgcctcactttgttttgaatag
Exon 17 (191bp)	CCGAAGCTCTGACCAGGAACGGCGTGTCTCATAAAGTCGATGACTCCTCTGGGTCTATTG
	GAAGGCGCTATGCAAGAACTGATGAGATTGGCGTGGCTTTCGGCATCACTATTGACTTTG
	ATACAGTGAACAAGACGCCCCACACTGCAACTCTGAGGGACCGAGACTCCATGAGACAGA
	TAAGGGCAGAG
Intron17-18(1446bp)	gtgactgccttctcacacagttact.....gcttgcacttcttttctcttcccag
Exon 18 (281bp)	GTCTCTGAGCTGCCCAATGTGGTCCGCGATCTGGCCAACGGCAACATTACCTGGGCTGAT
	GTGGAGGCCAGGTACCCACTCTTTGAAGGGCAAGAGACTGGCAAGAAGGAGACAGTAGAG
	GAATGAGAACAGCTGGCAGCTTATGACCATCGTGCTAATAAATAACTCATCATGTCCACT
3'downstream	ACACAGAGCATTGTGACTGCATCCAGGGACGGTTTTTCCTCAGTGGCTGCTTGGTTTTAC
	TCCCACAATTAAAGTTGAAGGAATTCTGAACACATTTATAA
	tccatctgttgtgtttccatttttttttttttttttttagcaaagactttt.....

Appendix 4 GENA 201 and 202 genome scan results

Legend:	
1=	C3H/HeJ
2=	C3H/HeJ+BALB/c/cJ
BC=	BALB/cJ
F=	Failed

SNP_Mb	11	36	73	93	135	150	170	193
C3H	A	T	A	T	G	A	T	T
BALB/c	G	C	G	C	A	G	C	G
Sample 1	1	F	1	1	1	1	1	1
2	1	1	1	1	1	1	1	1
3	1	1	1	1	1	1	1	1
4	1	1	1	1	1	1	1	1
5	1	1	1	1	1	1	1	1
6	1	1	1	1	1	1	1	1
7	1	1	1	1	1	1	1	1
8	1	1	1	1	1	1	1	1
9	1	1	1	1	1	1	1	1
10	1	1	1	1	1	1	1	1
11	1	1	1	1	1	1	1	1
12	1	1	1	1	1	1	1	1
13	1	1	1	1	1	1	1	1

CHROMOSOME 2					
SNP_Mb	38	72	99	130	181
C3H	G	G	T	G	T
BALB/c	T	A	C	A	C
Sample 1	1	F	1	1	1
2	1	1	1	1	1
3	1	1	1	1	1
4	1	1	1	1	1
5	1	1	1	F	1
6	F	1	1	1	1
7	1	1	1	F	1
8	F	1	1	1	1
9	F	1	1	1	1
10	F	1	1	1	1
11	F	1	1	1	1
12	F	1	1	1	1
13	F	1	1	1	1

CHROMOSOME 3				
SNP_Mb	26	88	105	132
C3H	G	C	C	A
BALB/c	A	A	T	G
Sample 1	1	1	1	1
2	1	1	1	1
3	1	1	1	1
4	1	1	1	1
5	1	1	1	1
6	1	1	1	1
7	1	1	1	1
8	1	1	1	1
9	1	1	1	1
10	1	1	1	1
11	1	1	1	1
12	F	1	1	1
13	1	1	1	1

CHROMOSOME 4					
SNP_Mb	14	32	80	133	145
C3H	G	A	C	G	C
BALB/c	A	G	T	C	G
Sample 1	1	1	1	1	1
2	1	1	1	1	1
3	1	1	1	1	1
4	1	1	1	1	1
5	1	1	1	1	1
6	1	1	1	1	1
7	1	1	1	1	1
8	1	1	1	1	1
9	1	1	1	1	1
10	1	1	1	1	1
11	1	1	1	1	1
12	1	1	1	1	1
13	1	1	1	1	1
CHROMOSOME 5					
SNP_Mb	23	51	76	104	137
C3H	T	T	G	T	C
BALB/c	G	C	A	C	T
Sample 1	1	1	1	1	1
2	1	1	2	2	1
3	1	1	2	2	1
4	1	1	1	1	1
5	1	1	1	1	1
6	1	1	1	1	1
7	1	1	1	1	1
8	1	1	1	1	1
9	1	1	1	1	1
10	1	1	1	1	1
11	1	1	1	1	1
12	1	1	1	1	1
13	1	1	1	1	1

CHROMOSOME 6					
SNP_Mb	22	52	84	114	146
C3H	A	G	A	G	T
BALB/c	C	T	G	A	G
Sample 1	1	2	2	1	F
2	1	2	2	1	2
3	1	2	2	1	2
4	1	2	2	1	2
5	1	2	2	1	1
6	F	2	2	1	1
7	1	2	2	1	1
8	1	2	2	1	1
9	1	2	2	1	1
10	1	2	1	1	1
11	1	2	2	1	1
12	1	2	2	1	1
13	1	2	1	1	1

CHROMOSOME 7				
SNP_Mb	11	54	72	102
C3H	G	C	A	G
BALB/c	T	A	G	A
Sample 1	1	1	1	1
2	F	1	1	1
3	F	1	1	1
4	1	1	1	1
5	F	1	1	1
6	F	1	1	1
7	1	1	1	1
8	F	1	1	1
9	1	1	1	1
10	1	1	1	1
11	F	1	1	1
12	F	1	1	1
13	F	1	1	1

CHROMOSOME 8				
SNP_Mb	26	65	95	123
C3H	A	G	T	A
BALB/c	T	A	C	G
Sample 1	1	1	NP	1
2	1	1	NP	2
3	1	1	NP	F
4	1	1	NP	1
5	1	F	NP	F
6	1	1	NP	2
7	1	1	NP	1
8	1	1	NP	2
9	1	1	NP	2
10	F	1	NP	1
11	1	1	NP	2
12	1	1	NP	F
13	1	F	NP	F

CHROMOSOME 9		
SNP_Mb	57	62
C3H	A	T
BALB/c	G	C
Sample 1	1	1
2	1	1
3	1	1
4	1	1
5	F	F
6	1	1
7	1	1
8	1	1
9	1	1
10	1	1
11	1	1
12	1	1
13	1	1

CHROMOSOME 10				
SNP_Mb	28	56	89	105
C3H	A	C	C	T
BALB/c	G	T	T	C
Sample 1	1	1	1	1
2	F	1	F	1
3	F	1	1	1
4	1	1	1	1
5	F	1	1	1
6	F	1	1	1
7	1	1	1	1
8	F	1	1	1
9	1	1	1	1
10	F	1	1	1
11	1	1	1	1
12	F	1	1	1
13	1	1	1	1

CHROMOSOME 11			
SNP_Mb	22	54	117
C3H	A	C	C
BALB/c	C	A	T
Sample 1	1	1	1
2	1	1	1
3	1	1	1
4	1	1	1
5	1	1	1
6	1	1	1
7	1	1	1
8	1	1	1
9	1	1	1
10	1	1	1
11	1	1	1
12	1	1	1
13	1	1	1

CHROMOSOME 12			
SNP_Mb	12	68	114
C3H	T	A	T
BALB/c	C	T	C
Sample 1	1	1	1
2	1	1	1
3	1	1	1
4	1	1	1
5	1	1	1
6	1	1	1
7	1	1	1
8	1	1	1
9	1	1	1
10	1	1	1
11	1	1	1
12	1	1	1
13	1	1	1

CHROMOSOME 13			
SNP_Mb	4	59	93
C3H	G	C	A
BALB/c	A	T	G
Sample 1	F	1	1
2	F	1	1
3	F	1	1
4	F	1	1
5	1	1	1
6	F	1	1
7	F	1	1
8	F	1	1
9	F	1	1
10	F	1	1
11	F	1	1
12	F	1	1
13	1	1	1

CHROMOSOME 14				
SNP_Mb	3	16	59	99
C3H	C	A	T	D14Mit170
BALB/c	T	G	G	
Sample 1	1	1	1	1
2	F	1	F	1
3	F	1	1	1
4	1	1	1	1
5	F	1	1	1
6	F	1	1	1
7	1	1	1	1
8	F	1	1	1
9	1	1	1	1
10	F	1	1	1
11	1	1	1	1
12	F	1	1	1
13	1	1	1	1

CHROMOSOME 15				
SNP_Mb	5	52	89	103
C3H	T	T	D15Mit159	A
BALB/c	C	C		T
Sample 1	1	1	F	1
2	1	1	F	1
3	1	1	1	1
4	1	1	F	1
5	1	1	F	1
6	1	1	1	1
7	1	1	F	1
8	1	1	1	2
9	1	1	F	2
10	1	1	F	1
11	1	1	F	2
12	1	1	F	1
13	1	1	1	2

CHROMOSOME 16			
SNP_Mb	10	59	88
C3H	T	A	T
BALB/c	A	G	A
Sample 1	1	1	1
2	1	1	1
3	1	1	1
4	1	1	1
5	1	1	1
6	1	1	1
7	1	1	1
8	1	1	1
9	1	1	1
10	1	1	1
11	1	1	1
12	1	1	1
13	1	1	1

CHROMOSOME 17			
SNP_Mb	19	31	71
C3H	G	A	C
BALB/c	T	G	T
Sample 1	1	1	1
2	1	1	1
3	1	1	F
4	1	F	F
5	1	1	F
6	1	1	F
7	1	1	F
8	1	1	F
9	1	1	F
10	1	1	F
11	1	1	F
12	1	1	1
13	1	1	F

CHROMOSOME 18			
SNP_Mb	48	62	80
C3H	C	G	G
BALB/c	T	T	T
Sample 1	F	1	1
2	F	1	1
3	F	1	F
4	F	F	F
5	F	F	F
6	F	F	F
7	F	F	F
8	F	F	F
9	F	F	F
10	F	F	F
11	F	F	F
12	1	1	1
13	1	1	F

CHROMOSOME 19		
SNP_Mb	19	56
C3H	A	T
BALB/c	C	C
Sample 1	1	F
2	F	F
3	F	F
4	F	F
5	F	F
6	F	F
7	F	F
8	F	F
9	F	F
10	F	F
11	F	F
12	F	F
13	1	F

Appendix 5 Aminoacylation activity raw data and statistics.

Aminoacylation activity with no preincubation on 3 month of age *Gars*$^{C201R/+}$ on C3H background

Wild types Samples	**^{3}H-glycine pmole/mg/min**	**Heterozygotes Samples**	**^{3}H-glycine pmole/mg/min**
	12.681939		6.5032819
	8.7581982		10.542162
	10.720069		12.059595
mean	10.720069		9.7016795
SD	1.9618704		2.8719264
Student t test between the means p value	>0.05		

Aminoacylation activity with preincubation on 3 month of age *Gars*$^{C201R/+}$ on C3H background

Wild types Samples	**^{3}H-glycine pmole/mg/min**	**Heterozygotes Samples**	**^{3}H-glycine pmole/mg/min**
	8.2981338		10.278443
	12.004054		9.0306306
	8.4324324		8.1061776
	6.768018		7.2930073
	6.7990138		6.4804805
	8.9216645		7.1248391
mean	8.5372195		8.052263
SD	1.9176191		1.4016469
Student t test between the means p value	>0.05		

Aminoacylation activity with no preincubation compared to aminoacylation activity with preincubation on 3 month of age *Gars*$^{C201R/+}$ on C3H background							
No preincubation				**Pre incubation**			
Wild types Samples	**^{3}H-glycine pmole/ mg/ min**	**Wild types Samples**	**^{3}H-glycine pmole/ mg/ min**	**Heterozygotes Samples**	**^{3}H-glycine pmole/ mg/ min**	**Heterozygotes Samples**	**^{3}H-glycine pmole/ mg/ min**
	12.68193908		8.298134		6.503282		10.27844
	8.758198198		12.00405		10.54216		9.030631
	10.72006864		8.432432		12.05959		8.106178
			6.768018				7.293007
			6.799014				6.48048
			8.921665				7.124839
mean	10.72006864		8.537219		9.70168		8.052263
SD	1.961870442		1.917619		2.871926		1.401647
Student t test between the wild type means and between the heterozygote means p value	>0.05				>0.05		

Aminoacylation activity with preincubation on 3 month of age *Gars*$^{C201R/+}$ on C3H background

Wild types	^{3}H-glycine pmole/mg/min	Heterozygotes	^{3}H-glycine pmole/mg/min
Samples		**Samples**	
	8.2981338		10.278443
	12.004054		9.0306306
	8.4324324		8.1061776
	6.768018		7.2930073
	6.7990138		6.4804805
	8.9216645		7.1248391
mean	8.5372195		8.052263
SD	1.9176191		1.4016469
Student t test between the means p value	>0.05		

Aminoacylation activity with preincubation on 3 month of age *Gars*$^{C201R/+}$ on C3H background

Wild types	^{3}H-tryptophan pmole/mg/min	Heterozygotes	^{3}H-tryptophan pmole/mg/min
Samples		**Samples**	
	63.28882132		60.70207958
	67.28198198		60.25468468
	40.4828668		54.38226834
	41.65600064		62.07356785
	50.57664323		58.46567353
mean	52.65713415		59.17565409
SD	12.252		2.973752274
Student t test between the means p value	>0.05		

Aminoacylation activity with preincubation on 3 month of age *Gars*$^{C201R/+}$ on C57BL/6 background

Wild types	**^{3}H-glycine pmole/mg/min**	**Heterozygotes**	**^{3}H-glycine pmole/mg/min**
Samples		**Samples**	
	3.7906542		5.3320824
	5.7029723		4.2732329
	5.6362528		5.7335274
	8.2042744		7.7977776
	6.7044616		7.4145431
	7.3094595		5.5319498
mean	6.2246791		6.0138522
SD	1.5406906		1.3378866
Student t test between the means p value	>0.05		

Aminoacylation activity with preincubation on 3 month of age *Gars*$^{C201R/+}$ on C57BL/6 background

Wild types	**^{3}H-tryptophan pmole/mg/min**	**Heterozygotes**	**^{3}H- tryptophan pmole/mg/min**
Samples		**Samples**	
1	20.19313981		30.52747748
2	15.54083466		13.93693694
3	17.91271271		16.81908075
4	11.1282299		13.29387721
5	23.64734		18.65678
mean	16.08438341		18.65107447
SD	3.364330331		6.987999169
Student t test between the means p value	>0.05		

Aminoacylation activity with preincubation compared no preincubatio n on 3 month of age *Gars*$^{C201R/+}$ on a C3H background compared to C57BL/6 background

C3H wild types	^{3}H-glycine pmole/mg /min	C5BL/6 wild types	^{3}H-glycine pmole/mg/m in	C3H heterozyg otes	^{3}H-glycine pmole/mg /min	C5BL/6 heteroz ygotes	^{3}H-glycine pmole/mg/ min
	8.2981338		3.7906542		10.27844		5.332082412
	12.004054		5.7029723		9.030631		4.273232874
	8.4324324		5.6362528		8.106178		5.733527412
	6.768018		8.2042744		7.293007		7.7977776
	6.7990138		6.7044616		6.48048		7.414543115
	8.9216645		7.3094595		7.124839		5.531949807
mean	8.5372195		6.2246791		8.052263		6.013852203
SD	1.9176191		1.5406906		1.401647		1.3378866
Student t test between the wild type means and between the heterozygotes means the p value	0.0440457				0.027565		

Aminoacylation activity with preincubation on 15 day of age *Gars*$^{C201R/+}$ on C3H background

Wild types	^{3}H-glycine pmole/mg/min	Heterozygotes	^{3}H-glycine pmole/mg/min	Homozygotes	^{3}H-glycine pmole/mg/min
	8.3126022		9.184763		2.440319
	9.2298637		5.3690801		2.690526
	8.0107698		6.3995568		5.034206
mean	8.5177452		6.9844666		3.38835
SD	0.6349096		1.9739424		1.430833
Anova	0.012784				

Aminoacylation activity with preincubation on 15 day of age *Gars*$^{C201R/+}$ on C3H background

Wild types	^{3}H-tryptophan pmole/mg/min	Heterozygotes	^{3}H-tryptophan pmole/mg/min	Homozygotes	^{3}H-tryptophan pmole/mg/min
	53.55494		54.456674		37.13083
	45.561862		44.072228		49.09085
	46.64573		31.300622		50.74746
mean	48.587511		43.276508		45.65638
SD	4.3359207		11.598515		7.429661
Anova	>0.05				

Appendix 6 Moonwalker genome scan results

Legend:	
1=	C3H/HeJ
2=	C3H/HeJ+BALB/c/cJ
BC=	BALB/cJ
F=	Failed

CHROMOSOME 1								
SNP_MB	11	36	73	93	135	150	170	193
C3H	A	T	A	T	G	A	T	T
BALB/c	G	C	G	C	A	G	C	G
Sample 1	2	2	2	1	1	1	1 F	
2	1	1	1	1	1	1	1	1
3	1	1	1	1	1	1	1	1
4	1	1	1	1	1	1	1	1
5	1	1	1	1	1	1	1	1
6	1	1	1	1	1	1	1	1
7	1	1	1	1	1	1	1	2
8	1	1	1	1	1	1	1	2
9	1	1	1	1	1	1	1	1
10	1	1	1	1	1	1 F		1
11	1	1	1 F	F		1 F		2
12	1	1	1 F	F		1 F		1
13	1	1	1	1	1	1 F		1

CHROMOSOME 2					
SNP_MB	38	72	99	130	181
C3H	G	G	T	G	T
BALB/c	T	A	C	A	C
Sample 1	F	2	1	1	1
2	1	1	1	1	2
3	1	1	1	1	1
4	1	1	1	1	1
5	1	1	1 F		1
6	2	1	1	1	1
7	1	2	2 F		1
8	1	2	2	1	1
9	1	2	2	1	2
10	2	2	1	1 F	
11	F	2	1	1 F	
12	1 F		1	1 F	
13	1	1	1	1 F	

CHROMOSOME 3								
SNP_MB	26		88		105		132	
C3H	G		C		C		A	
BALB/c	A		A		T		G	
Sample 1	2		2		2		2	
2	2		2		2		1	
3	2		2		2		2	
4	2		1		1		1	
5	2		2		1		1	
6	2		2		2		2	
7	2		1		1		1	
8	2		1		1		1	
9	2	F			2		2	
10	2		1		1		1	
11	2		1		1		1	
12	1	F			1	F		
13	2	F			1		1	

CHROMOSOME 4										
SNP_MB	14		32		80		133		145	
C3H	G		A		C		G		C	
BALB/c	A		G		T		C		G	
Sample 1	1		1	F			1	F		
2	2		2		2	F		F		
3	1		1		1		1		1	
4	1		1		1		1		1	
5	2		2		1		2		2	
6	1		1		1		1		1	
7	1		1		1		1		1	
8	1		1		1		1		1	
9	2		2	F			2		2	
10	1		1	F		F			1	
11	F		1	F		F		F		
12	F	F		F			1	F		
13	F	F		F		F		F		

CHROMOSOME 5						
SNP_MB	23	51	76	104	124	137
C3H	T	T	G	T	A	C
BALB/c	G	C	A	C	G	T
Sample 1	1	1	1	2	2	2
2	1	1	1	1	2	2
3	1	1	1	2	2	2
4	2	2	2	2	2	2
5	2	2	2	1	1	1
6	2	2	2	2	2	2
7	2	2	2	2	2	2
8	2	2	2	2	2	2
9	2	2	2	2	2	F
10	2	2	2	2	2	2
11	2	2	2	2	2	F
12	2	2	F	2	2	2
13	2	2	2	2	2	1
14	1	1	1	2	2	1
15	1	2	2	2	2	2
16	1	1	2	2	2	2
17	1	1	2	2	1	1
18	1	1	1	1	1	1
19	2	2	1	1	1	1
20			1	1	1	
21			1	1	1	

CHROMOSOME 6					
SNP_MB	22	52	84	114	146
C3H	A	G	A	G	T
BALB/c	C	T	G	A	G
Sample 1	1	1	1	1	2
2	1	1	1	1	1
3	1	1	2	2	1
4	1	1	1	1	1
5	1	1	1	1	1
6	1	1	1	1	1
7	1	1	1	1	1
8	1	1	1	1	1
9	1	1	1	1	1
10	2	2	2	1	1
11	F	F	F	F	1
12	F	F	F	F	F
13	F	F	F	1	1

CHROMOSOME 7								
SNP_MB		11		54		72		102
C3H		G		C		A		G
BALB/c		T		A		G		A
Sample 1	F			2		2		2
2		1		1		1		2
3		1		1		1		2
4		1		1		1		1
5		1		1		1		1
6		1		1		1		1
7		1		1		2	F	
8		1	F			1		1
9		1		1		1		1
10		2		2		2		1
11		2	F			2		1
12	F		F		F		F	
13	F		F		F			2

CHROMOSOME 8								
SNP_MB		26		65		95		123
C3H		A		G		T		A
BALB/c		T		A		C		G
Sample 1		2		2		2		1
2		1		1		1		2
3		1		1		1		2
4		1		1		1		1
5		1		1		1		1
6		1		1		1		1
7		1		1		1		1
8		1		1		1		2
9		1		1		1		1
10		1		2		2		1
11		1		2		2		1
12	F		F		F		F	
13	F			2		1		1

CHROMOSOME 9				
SNP_MB		57		62
C3H		A		T
BALB/c		G		C
Sample 1		1		1
2		1		1
3		1		1
4		1		1
5	F		F	
6		1		1
7		1		1
8		1		1
9		1		1
10		1		1
11		1		1
12		1		1
13		1		1

CHROMOSOME 10								
SNP_MB		28		56		89		105
C3H		A		C		C		T
BALB/c		G		T		T		C
Sample 1	F		F			2		2
2		1		1		1		1
3		1		1		1		1
4		1		1		1		1
5		1		1		1		1
6		1		1		1		2
7		1		1		1		1
8		1		1		1		1
9		2		1		1		1
10		1		1		1		1
11	F			1	F			1
12	F		F		F		F	
13	F			1	F		F	

CHROMOSOME 11						
SNP_MB		22		54		117
C3H		A		C		C
BALB/c		C		A		T
Sample 1		2		2		1
2		1		1		2
3		1		1		2
4		1		1		1
5		1		1		2
6		1		1		1
7		1		1		1
8		1		1		1
9		1		1		2
10		1		1		2
11		1		1	F	
12	F			1	F	
13	F			1	F	

CHROMOSOME 12						
SNP_MB		12		68		114
C3H		T		A		T
BALB/c		C		T		C
Sample 1		1	F		F	
2		1		1		2
3		1	F			1
4		1	F			1
5		1	F			2
6		1	F			1
7		1	F			1
8		1	F			1
9		1	F			2
10		1	F			2
11	F		F		F	
12	F		F		F	
13	F		F		F	

CHROMOSOME 13						
SNP_MB		4		59		93
C3H		G		C		A
BALB/c		A		T		G
Sample 1	F		F			1
2	F			2		2
3	F			2		1
4	F			1		1
5	F			2	F	
6	F			1		1
7	F			1		1
8	F			1		1
9	F			2		1
10	F			2		2
11	F		F			2
12	F		F		F	
13	F		F		F	

CHROMOSOME 14									
SNP_MB	3			16		59		99	
C3H	C			A		T		D14Mit170	
BALB/c	T			G		G			
Sample 1		1			1		1		
2		2			2		2		
3		1			2		2		
4		1			1		1		
5		1			2		2		
6		1			2		2		
7		1			1		1		
8		1			1		1		
9		1			1		1		
10		1			1		1		
11		1			1		1		
12		1	F			F			
13	F		F				1		

CHROMOSOME 15									
SNP_MB	5		52		89		103		
C3H	T		T		D15Mit159		A		
BALB/c	C		C				T		
Sample 1	2		1					1	
2	1		1					1	
3	1		1				F		
4	2		2				F		
5	1		1					1	
6	1		1				F		
7	1		1				F		
8	2		2					1	
9	1		1					2	
10	1		2				F		
11	F	F					F		
12	F		1				F		
13	1		1				F		

CHROMOSOME 16									
SNP_MB	10			59			88		
C3H	T			A			T		
BALB/c	A			G			A		
Sample 1		1			1			1	
2		1	F					1	
3		1	F					1	
4		1			1			1	
5		1			1			1	
6		1	F			F			
7		1	F			F			
8		2	F					1	
9		1	F			F			
10		1	F			F			
11		1	F			F			
12		2			2			2	
13		1			1			1	

CHROMOSOME 17						
SNP_MB		19		31		71
C3H		G		A		C
BALB/c		T		G		T
Sample 1	F					1
2		2				1
3	F					1
4		2				1
5		2				1
6	F					1
7		2				1
8	F					1
9		2				1
10		1				1
11		1				1
12	F				F	
13		2				1

CHROMOSOME 18						
SNP_MB		48		62		80
C3H		C		G		G
BALB/c		T		T		T
Sample 1				1		1
2			F			1
3				2		1
4				1		1
5				1	F	
6				1		1
7				1		1
8				1		1
9				1		1
10				2		2
11				2		2
12				2	F	
13				2	F	

CHROMOSOME 19				
SNP_MB		19		56
C3H		A		T
BALB/c		C		C
Sample 1		2		1
2		1		1
3		1		1
4		2		1
5		1		1
6		1		1
7	F		F	
8		1		1
9	F		F	
10	F			2
11		1	F	
12		1		1
13		1		1